

Grid-Aware Real-Time Control of Electric Vehicles

Présentée le 19 janvier 2022

Faculté informatique et communications
Laboratoire pour les communications informatiques et leurs applications 2
Programme doctoral en informatique et communications

pour l'obtention du grade de Docteur ès Sciences

par

Roman RUDNIK

Acceptée sur proposition du jury

Prof. M. Grossglauser, président du jury
Prof. J.-Y. Le Boudec, directeur de thèse
Prof. J. Peças Lopes, rapporteur
Dr A. Bernstein, rapporteur
Dr R. Cherkaoui, rapporteur

*Life is and will ever remain an equation incapable of solution,
but it contains certain known factors.*
— Nikola Tesla

To my mother...

Acknowledgements

First and foremost, I am very grateful to my thesis director, Prof. Jean-Yves Le Boudec, for his supervision, guidance, patience and motivation, not only scientifically but also on the personal level. I will miss our meetings and discussions. He was always available when I was stuck at some problem or when I hesitated about whether the research direction was correct. His way of working and his views have influenced me far beyond my professional life. I am very proud to have been his student and will always remember this experience.

I would like to express my deepest gratitude to Prof. Mario Paolone, my unofficial co-supervisor. It was a real pleasure to work with him, his positive energy and vision were very helpful during my PhD journey. Also, I would like to thank Professor Lorenzo Reyes. He is an amazing person to work with and was always my tutorial for questions about electric grids.

I would also like to thank Prof. Matthias Grossglauser, Prof. João Peças Lopes, Dr. Rachid Cherkaoui, and Dr. Andrey Bernstein for being part of my PhD jury and for their valuable comments and interesting discussions about my work. Special thanks go to Andrey for his advice at the beginning of my long PhD path.

Throughout my PhD work, I was lucky to meet and work with many brilliant people. Tech was my first office mate, and Marco helped me a lot with my first project. Nadia was my best mentor during my internship, her support and guiding helped me to get hired in the lab and survive my first days at EPFL. My friends Aleksei, Wajeb, and Maaz were with me through all the ups and downs of my PhD life, and they also actively participated in our outside-the-office life. Our trips and hikes were amazing. I guess Alex and I are famous people in Inglewood and the Bruxelles cafe in Lausanne. Ehsan joined the lab toward the end of my thesis experience, and he was very helpful during the last parts of my PhD research. I am very happy to have these guys in my life and hope we will all stay in touch.

My most complicated and longest paper would not have been possible without Cong and his strong theoretical background. Sherif helped me to prepare experiments and make theory work in reality.

I was very lucky to be a member of the LCA2 lab. I am very thankful to my colleagues: Miroslav, Tech, Maaz, Wajeb, Cong, Ehsan, Stephan, Ludovic, Elena, and Hossein for the TCP/IP teaching-assistance sessions that had a huge amount of questions from

Acknowledgements

students and for our outings. They have been like a second family to me during the course of my PhD experience.

Life at EPFL would not have been as smooth and enjoyable without support of our secretaries, Patricia and Angela, our system administrators, Marc-André and Yves, and our best editor, Holly, who read all my papers and thesis with carefulness and patience.

I would like to thank all my friends in Switzerland: Sergey, Gleb, Panayiotis, Marija, Araz, Igor, Lina, Clémence, and Priyanka for a great number of unforgettable and joyful moments. An exceptional mention goes to Kim for making special my last year of PhD life.

I also owe thanks to my best friends outside Switzerland. There were not physically with me, however I felt their help. Thank you Dmitry, Stas, Sergey, Ksenia, Artem, Zohaib and Konstantin for your friendship and support.

Last, but not least, I am enormously grateful to my mother Alla, who supported me through all this time, not only during my PhD adventure, but also on my way to being admitted to it. Without her love, support, and trust, I would not be able to successfully pursue a PhD degree at EPFL. Thank you for always believing in me.

Lausanne, January 19th, 2022

R. R.

Abstract

Electric vehicles (EVs) are already part of today's reality and their number is expected to grow rapidly in the near future. A large-scale penetration of EVs will increase the power consumption during charging periods. Hence, the uncoordinated and random charging activities could stress the grid hence severely impact the quality and continuity of the power supply. In particular, excessive power flows can cause overloads of the grid, which can lead to severe grid damages and blackouts. Due to the aforementioned issues, there is a need for intelligent control methods of the electric-vehicle charging stations (CS). In this respect, we focus on the problem of optimal grid-aware real-time charging/discharging control of EV CSs.

First, we propose a grid-aware real-time control method of EVs charging. The purpose of the proposed method is to provide flexibility for EVs connected to CSs for the grid by following an aggregated power-setpoint from a main grid controller while minimizing the EVs' battery-wear and keeping the charging balance between EVs. The aggregated power-setpoint might exhibit rapid variations due to other volatile resources of the local distribution grid. Naive allocations can transfer such variations to the EVs' batteries thus increasing EV battery-wear. One of the challenges is to allocate powers such that the fluctuation of the aggregated power-setpoint does not cause power jumps and mini-cycles of the charging power of the EVs. The method uses a realistic model for the battery charging-power and takes into account a non-ideal behaviour of EVs. For example, the charging power cannot be arbitrarily small. If not appropriately handled, the rapid fluctuations of the aggregated power-setpoint could lead to frequent disconnections and re-connections, which should be avoided. We also handle a non-ideal response of EVs to the control power-setpoints due to implementation and reaction delays and inaccuracies. Another challenge is that the power allocation should keep the charging balance among EVs hence the information about future arrivals and departures could be unavailable. To address these issues, we cast the problem as a repeated online optimization. This leads to a mixed-integer quadratic problem; to solve it in real-time, we develop a heuristic that reduces the number of integer variables. Then, we implement and validate the method in a real field experiment, i.e., on real-scale microgrid with real commercial EVs.

Second, we focus on vehicle-to-grid (V2G) technology. In order to minimize global operational costs, to take into account grid constraints, and to minimize EVs battery wear, we suggest combining an optimal scheduler that takes care of charging/discharg-

ing EVs and minimizing the global operational costs with a real-time controller that reacts to grid-aware external setpoints. The scheduler computes optimal powers for EVs; it considers forecasts of future arrivals, departures, and operations of other energy resources, i.e., other loads and photo-voltaic panels (PVs). The real-time controller, in turn, follows an aggregated power-setpoint from a main controller of the local distribution grid, thus minimizing the EV battery-wear while following the scheduler's decisions. We validate our method by simulations and compare it with benchmark real-time algorithms. We show that our method presents lower operational costs and EV battery-wear when compared with benchmark algorithms.

Third, we focus on the side effects of CS integration into grid control-systems. In particular, we address two issues that should be handled by grid control. One important issue is sudden power-steps caused by a disconnection of a huge load, e.g., an EV that directly affects the decisions of the grid controller that aims to avoid voltage or line-ampacity violations that can cause large sub-optimality of the grid operation. We propose a method by which a real-time grid control can handle large power steps by permitting and controlling temporary voltage and current violations in order to remain within the limits imposed by standards and safe operation. This brings more flexibility to the grid operation, which can lead to better operational results such as increased self-consumption or higher EV charging rates.

We also address the occasional losses of messages between the grid controller and grid resources; this can be caused by, for example, network delays, controller crashes, and reboots. As a controller performs real-time control at a sub-second scale, such losses increase the uncertainty in the operation of the controller and deteriorate the controller's ability to maintain a feasible control over the grid resources. We present a method for real-time power-grid control that is robust in non-ideal network conditions. In this method, resources send information that is valid for long-term horizons, as well as short-term horizons, and we use long-term information when message loss occurs.

Keywords: Electric vehicles, real-time control, vehicle-to-grid, model predictive control, mixed-integer programming, fairness, battery protection, software agents, power steps, microgrid, explicit power-setpoints, soft operational-constraints, grid-aware control, decentralized algorithms.

Résumé

Les véhicules électriques (VE) font déjà partie de notre quotidien, et leur nombre devrait augmenter très rapidement dans les années à venir. Leur utilisation à grande échelle augmentera considérablement la consommation d'énergie du fait des périodes de charge. Les rechargements non coordonnés et aléatoires pourraient stresser le réseau et grandement dégrader la qualité et la continuité de l'approvisionnement en énergie. En particulier, les flux de puissance excessifs peuvent surcharger le réseau, ce qui peut conduire à des importantes dégradations et des pannes. Les méthodes de contrôle intelligentes des stations de recharge électriques (SR) deviennent donc nécessaires, c'est pourquoi nous étudions dans cette thèse le problème de contrôle optimal en temps-réel sur le réseau de la charge/décharge d'une SR de VEs.

Premièrement, nous proposons une méthode de contrôle temps-réel sur le réseau pour la recharge des VEs. L'objectif de la méthode proposée est de fournir une flexibilité au réseau pour les VEs connectés aux SRs en suivant un ensemble de points de puissance explicites du contrôleur réseau principal tout en minimisant l'usure de la batterie et en maintenant un équilibre de charge entre les VEs. L'ensemble des points de puissance explicites doit mettre en avant les variations rapides dues aux autres ressources variables du réseau de distribution local. Des allocations naïves peuvent transférer ces variations directement à la batterie des VEs, entraînant une usure importante de cette dernière. L'objectif est donc d'allouer la puissance afin que la variation de l'ensemble des points de puissance n'entraîne pas des sauts de puissance et des mini-cycles de la puissance de charge des VEs. Notre méthode utilise un modèle réaliste pour la puissance de charge des batteries et prend en compte un comportement non-idéal des VEs. Par exemple, la puissance de charge ne peut pas être arbitrairement petite. Si elles ne sont pas traitées de manière appropriée, les variations rapides des points de puissance explicites pourraient conduire à de fréquentes connexions et déconnexions, ce qui doit être absolument évité. Nous prenons aussi en compte les réponses non-idéales des VEs au contrôle de points de puissance explicites en raison de l'implémentation, des délais de réaction et des inexactitudes. Un autre point important est que l'allocation de puissance doit conserver un équilibre de charge entre les VEs, même si les informations sur les arrivées et départs futurs sont indisponibles. Pour ce faire, nous avons modélisé le problème comme une optimisation en-ligne répétée, qui est quadratique mixte linéaire. Pour le résoudre en temps-réel, on développe une heuristique qui réduit le nombre de variables entières. Ensuite, cette méthode a été

implémentée et validée sur un cas réel : un micro-réseau à échelle réelle avec de vrais véhicules électriques commerciaux.

Deuxièmement, nous étudions la technologie véhicule-réseau (V2G). Pour minimiser les coûts opérationnels globaux en prenant en compte les contraintes réseaux et en minimisant l'usure de la batterie, on propose de combiner un ordonnanceur optimal qui prend en compte la charge/décharge des VEs tout en minimisant le coût opérationnel global avec un contrôleur temps-réel qui réagit à l'ensemble des points externes du réseau. L'ordonnanceur calcule les puissances optimales pour les VEs : Il considère les prévisions des arrivées et départs futurs, et des opérations des autres ressources d'énergie (i.e. autre charges et PVs). Le contrôleur temps-réel, en retour, suit l'ensemble des points de puissance du contrôleur principal du réseau de distribution local, et ainsi minimise l'usure de la batterie des VEs tout en suivant les décisions de l'ordonnanceur. Nous validons notre méthode avec des simulations et les comparons avec des algorithmes temps-réel de référence. Par comparaison avec les algorithmes existants, nous montrons que notre méthode présente des coûts opérationnels plus faibles et une moindre usure de batterie du VE.

Troisièmement, nous étudions les effets secondaires de l'intégration des SRs dans un système contrôle réseau. En particulier, nous abordons deux problèmes qui devraient être traités par le contrôle du réseau. Le premier problème concerne les sauts de puissance soudains causés par la déconnexion d'une charge importante, par exemple un VE, qui affecte directement les décisions du contrôleur réseau dont le but est d'éviter les violations de tension ou de courant permanent admissible qui peuvent entraîner une sous-optimalité importante du fonctionnement du réseau. Nous proposons une méthode avec laquelle le contrôleur réseau temps-réel peut gérer des grand pas de puissance en acceptant et contrôlant les violations temporaires de courant et de tensions tout en restant à l'intérieur des limites imposées par les standards et en maintenant un fonctionnement sûr. Cela apporte plus de flexibilité au fonctionnement du réseau, et peut conduire à de meilleurs résultats opérationnels, tels qu'une autoconsommation accrue ou des taux de charge de VE plus élevés.

Pour finir, nous analysons les pertes occasionnelles de messages entre le contrôleur réseau et les ressources du réseau; cela peut être dû par exemple à des délais sur le réseau, des accidents du contrôleur, ou des redémarrages. Lorsqu'un contrôleur effectue un contrôle en temps-réel à une échelle inférieure à la seconde, de telles pertes augmentent l'incertitude dans le fonctionnement du contrôleur et détériorent la capacité du contrôleur à maintenir un contrôle réalisable sur les ressources du réseau. Nous introduisons une méthode de contrôle du réseau électrique temp-réel robuste dans des conditions de réseau non-idéal. Dans cette méthode, les ressources envoient des informations valides pour des horizons long-terme, ainsi que des horizons court terme, et nous utilisons les informations long-terme quand des pertes de message ont lieu.

Mots clés : Véhicules électriques, contrôle temps-réel, véhicule-réseau, commande

prédictive (MPC), optimisation linéaire MILP, équité, protection de batterie, agents logiciels, pas de puissance, micro-réseau, points de puissance explicites, contraintes opérationnelles souples, contrôle de réseau électrique, algorithmes décentralisés.

List of Abbreviations

| | |
|------|--------------------------------------|
| BESS | Battery-Energy Storage System (BESS) |
| CO | Community Operator |
| CS | Charging Station |
| DER | Distributed Energy Resource |
| DR | Demand Response |
| DSO | Distributed System Operator |
| EDF | Earliest Deadline First |
| EV | Electric Vehicle |
| GA | Grid Agent |
| GCP | Grid Connection-Point |
| LLF | Least Laxity First |
| MPC | Model Predictive Control |
| PCC | Point of Common Coupling |
| PV | Photo-Voltaic |
| RA | Resource Agent |
| RMSE | Root Mean Square Error |
| SE | State Estimation |
| SoC | State-of-Charge |
| TSO | Transmission System Operator |
| V2G | Vehicle-to-Grid |
| VPP | Virtual Power Plant |

List of Notations

Real-time control problem notations

| | |
|-----------------------|---|
| k | discretized index of a time interval |
| $\Gamma[k]$ | collection of EVs that are connected to CS at time k |
| $\mathcal{C}[k]$ | collection of EVs that are unlocked at time k |
| $\mathcal{L}[k]$ | collection of EVs that are locked at time k |
| $P^{\text{req}}[k]$ | aggregated power-setpoint at time k |
| $P_i[k]$ | power setpoint of EV i at time k |
| $\hat{P}_i[k]$ | measured charging power of EV i at time k |
| $\mathbf{P}[k]$ | collection of power setpoints $P_i[k]$ for all EVs in $\mathcal{C}[k]$ |
| $\hat{\mathbf{P}}[k]$ | collection of measured powers $\hat{P}_i[k]$ for all EVs in $\Gamma[k]$ |
| $\omega_i[k]$ | on/off decisions for EV i at time k |
| $\mathbf{\Omega}[k]$ | collection of on/off decisions for all EVs in $\mathcal{C}[k]$ |
| $P_i^{\text{ref}}[k]$ | reference powers for all EVs in $\Gamma[k]$ |

Scheduling problem notations

| | |
|-----------------|--|
| H | scheduling horizon |
| \mathcal{P}^+ | collection of scheduled charging powers |
| \mathcal{P}^- | collection of scheduled discharging powers |
| \mathcal{P}_G | collection of scheduled powers bought from the main grid |
| w_m | weight of the scenario m |
| \mathcal{I} | matrix that stores the identifiers of connected EVs |

Contents

| | |
|--|--------------|
| Acknowledgements | i |
| Abstracts (English and French) | v |
| List of Abbreviations | xiii |
| List of Notations | xv |
| List of Figures | xxiii |
| List of Tables | xxvii |
| 1 Introduction | 1 |
| 1.1 Motivation | 1 |
| 1.2 Overview | 4 |
| 1.3 Contributions | 7 |
| 1.4 Dissertation Outline | 8 |
| 2 State of the Art | 11 |
| 2.1 Overview of Control Architectures | 11 |
| 2.2 Provision of Grid Services | 13 |
| 2.2.1 Voltage Control | 13 |
| 2.2.2 Congestion Management | 14 |
| 2.2.3 Power-system Losses | 15 |
| 2.2.4 Frequency Regulation and Spinning Reserve | 16 |
| 2.3 EV-users Mobility and Incentives | 16 |
| 2.4 VPP and EVs | 18 |
| 3 Real-Time Control of an Electric-Vehicle Charging Station | 21 |
| 3.1 Introduction | 22 |
| 3.2 Problem Statement | 23 |
| 3.2.1 Charging-Station Model | 23 |
| 3.2.2 Constraints of the EVs | 24 |
| 3.2.3 Power Allocation to EVs | 25 |
| 3.3 Control Scheme at the CS | 25 |

xvii

Contents

| | | |
|----------|---|-----------|
| 3.3.1 | Aggregated Power-Setpoint Tracking | 26 |
| 3.3.2 | Battery Wear | 27 |
| 3.3.3 | Fair Allocation of Charging Power | 29 |
| 3.3.4 | Full Formulation | 31 |
| 3.4 | Real-Time Implementation Aspects | 31 |
| 3.4.1 | Reducing the Number of Integer Variables | 31 |
| 3.5 | Validation | 36 |
| 3.5.1 | Simulation Setup | 36 |
| 3.5.2 | Model of the Grid Controller | 38 |
| 3.5.3 | Performance Evaluation Metrics | 39 |
| 3.5.4 | Congestion Indication | 40 |
| 3.5.5 | Results for the Default Weight Combination | 40 |
| 3.5.6 | Results for the Different Weight Combinations | 41 |
| 3.6 | Conclusions | 46 |
| 4 | Experimental Validation of the Real-Time Control of an Electric-Vehicle Charging Station | 47 |
| 4.1 | Introduction | 47 |
| 4.2 | Summary of the EV charging station control architecture | 49 |
| 4.2.1 | Charging-Station Control | 49 |
| 4.2.2 | Charging-Power Computation | 50 |
| 4.3 | Experimental Setup | 51 |
| 4.3.1 | Microgrid Control Framework | 51 |
| 4.3.2 | Real-Scale Microgrid and EVs | 52 |
| 4.3.3 | Charging Station Agent | 52 |
| 4.4 | Experimental Results | 55 |
| 4.4.1 | Self-consumption Scenarios | 56 |
| 4.4.2 | Line Congestion Scenario | 57 |
| 4.5 | Conclusions | 60 |
| 5 | Combined Grid-Aware Control and Optimal Scheduling of Electric Vehicle Charging Stations with V2G Capabilities | 61 |
| 5.1 | Introduction | 61 |
| 5.2 | Problem Statement | 63 |
| 5.3 | Scheduling Problem | 66 |
| 5.3.1 | Definitions | 66 |
| 5.3.2 | Formulation | 67 |
| 5.3.3 | Scenario Generation | 69 |
| 5.4 | Real-Time Problem | 72 |
| 5.5 | Validation | 74 |
| 5.5.1 | Benchmarks | 74 |
| 5.5.2 | Performance Evaluation Metrics | 74 |
| 5.5.3 | Simulation Setup | 75 |

| | | |
|----------|--|------------|
| 5.5.4 | EV-related Hypotheses | 75 |
| 5.5.5 | Real-Time Control Evaluation | 76 |
| 5.5.6 | Comparison against Benchmarks | 77 |
| 5.5.7 | Results for Different Grid-Price Traces | 79 |
| 5.5.8 | Robustness Evaluation | 80 |
| 5.6 | Conclusions | 83 |
| 6 | Handling Large Power Steps in Real-Time Microgrid Control via Explicit Power Setpoints | 85 |
| 6.1 | Introduction | 85 |
| 6.2 | The Commelec Framework | 86 |
| 6.3 | Penalty Functions in the Grid Agent | 87 |
| 6.3.1 | Modification to the Voltage Penalty-Function | 88 |
| 6.3.2 | Modification to the Current Penalty-Function | 91 |
| 6.4 | Validation | 93 |
| 6.4.1 | Simulation Scenario | 93 |
| 6.4.2 | Simulation Results: Voltage Violation | 94 |
| 6.4.3 | Simulation Results: Current Violation | 94 |
| 6.4.4 | Experimental Setup | 95 |
| 6.4.5 | Experimental Results: Voltage Violation | 95 |
| 6.4.6 | Experimental Results: Current Violation | 96 |
| 6.5 | Conclusions | 99 |
| 7 | Robust Real-Time Control of Power Grids in the Presence of Communication Network Non-Idealities | 101 |
| 7.1 | Introduction | 101 |
| 7.1.1 | Background | 101 |
| 7.1.2 | Contributions | 103 |
| 7.2 | Method | 104 |
| 7.2.1 | Properties of Long-term Fields of an Advertisement | 105 |
| 7.2.2 | Constructing Long-term Fields | 105 |
| 7.3 | Experimental Setup | 108 |
| 7.4 | Results | 110 |
| 7.4.1 | Frequency Support with Non-binding Grid Constraints | 110 |
| 7.4.2 | Tracking a Power Profile with Binding Grid Constraints | 111 |
| 7.4.3 | Validation | 112 |
| 7.5 | Conclusions | 114 |
| 8 | Conclusions and Directions for Future Work | 115 |
| | Bibliography | 119 |
| | List of Publications | 135 |

Contents

| | |
|------------------|-----|
| Curriculum Vitae | 137 |
|------------------|-----|

List of Figures

| | | |
|------|---|----|
| 1.1 | Transmission and distribution grids. Blue arrows is traditional power flow, red arrows are flows when there are renewable resources in the grid. | 2 |
| 1.2 | General architecture of grid control with several CSs. | 3 |
| 2.1 | Schematic representation of centralized and decentralized control architectures. CC - central controller, LC - local controller. | 12 |
| 2.2 | General overview of VPP elements. | 18 |
| 3.1 | General setup of the considered charging station. | 24 |
| 3.2 | Evolution of $\lambda_i[k]$. | 28 |
| 3.3 | Result of the water-filling algorithm for 5 EVs. EVs 1, 4 and 5 are fully filled, whereas 2 and 3 have reference powers of $h\zeta_2$ and $h\zeta_3$, respectively. The reference powers $P_1^{\text{ref}}, P_2^{\text{ref}}, P_3^{\text{ref}}, P_4^{\text{ref}}, P_5^{\text{ref}}$ are in kW. | 30 |
| 3.4 | Proof of statement (S4). | 35 |
| 3.5 | Structure of the grid. The arrows show the positive directions of the corresponding active-power flows. | 36 |
| 3.6 | PV production scenarios and the number of EVs. | 43 |
| 3.7 | Metrics for the regular production. | 44 |
| 3.8 | Metrics for the fluctuating production. | 44 |
| 3.9 | Metrics for the sharp jump. | 44 |
| 3.10 | Fluctuating production, $c_0 = 1, c_1 = 10$. This illustrates that CS can opportunistically use the fluctuated PV power production while respecting the transformer limit. | 45 |
| 3.11 | Fluctuating production, $c_0 = 1, c_1 = 10$. Power setpoints change for EVs from group A (red curve) and group B (blue curve). | 45 |
| 4.1 | The experimental microgrid. All elements used in the experiments of this chapter are shown in black. | 52 |
| 4.2 | Tesla and Renault charging patterns. | 53 |
| 4.3 | Overall architecture of the system. | 54 |
| 4.4 | Scenario 1 experimental results. | 57 |
| 4.5 | Scenario 2 experimental results. | 58 |
| 4.6 | Line congestion experimental results. | 59 |

List of Figures

| | | |
|------|--|-----|
| 4.7 | Cumulative distributions of the CS processing-times measured from the instant when the GA aggregated power-setpoint is sent to the CS. . . . | 60 |
| 5.1 | Schematic representation of the energy community. | 64 |
| 5.2 | Scheduling and real-time problems interaction. | 66 |
| 5.3 | Load consumption realisation vs upper and lower traces of all scenarios. . . | 70 |
| 5.4 | PV production realisation vs upper and lower traces of all scenarios. . . | 70 |
| 5.5 | Our method and scenario-based MPC without real-time control 24-hours simulation. | 77 |
| 5.6 | Our method and scenario-based MPC without real-time control zoom on 15 minutes window. | 77 |
| 5.7 | Our method and scenario-based MPC without real-time control 24-hours simulation. | 78 |
| 5.8 | Our method and scenario-based MPC without real-time control zoom on 15 minutes window. | 78 |
| 5.9 | Non-satisfied demand metric for our method, EDF and LLF during congested period. | 79 |
| 5.10 | Battery-wear metric for our method, EDF and LLF congested period. . . | 79 |
| 5.11 | Non-satisfied demand metric for our method, EDF and LLF non-congested period. | 80 |
| 5.12 | Battery-wear metric for our method, EDF and LLF during non-congested period. | 80 |
| 5.13 | Grid price traces for different cases. | 81 |
| 5.14 | Non-satisfied demand metric for the oracle and our method. | 82 |
| 5.15 | Battery-wear metric for the oracle and our method. | 82 |
| 5.16 | Robustness simulation results. | 82 |
| 6.1 | States transitions per bus. $\mathcal{F} = [V^{nom} - \beta, V^{nom} + \beta]$ represents the voltage feasible state. In brackets we describe the condition under which the transition will occur. In red we describe the action associated with the transition. In green we describe the properties of the state. | 89 |
| 6.2 | Functions $J_{A,k}(V)$ and $J_{B,k}(V)$, $\alpha = 10^4$ and $V_k^{nom} = 1$ | 89 |
| 6.3 | Voltage trajectory with time period dynamics. | 92 |
| 6.4 | Simulation results for the voltage violation case. | 95 |
| 6.5 | Simulation results for the current violation case. | 96 |
| 6.6 | The experimental microgrid. In black all elements participating in this work's experiments. Location of measurement devices for state estimation (PMUs) are also indicated. | 97 |
| 6.7 | Experimental results for the voltage violation case. | 97 |
| 6.8 | Experimental results for the current violation case. The plots in the lower part refer to line L01 of Fig.6.6. | 98 |
| 7.1 | COMMELEC Architecture | 102 |

| | | |
|-----|--|-----|
| 7.2 | CIGRÉ low-voltage benchmark microgrid. The resources not used for our experiments are greyed-out. | 109 |
| 7.3 | Frequency signal imposed by the main grid used to provide frequency support. | 110 |
| 7.4 | Root mean square error (in Watts) between the real power at the slack bus and the requested tracking signal, for a 10-minute interval | 111 |
| 7.5 | Tracking experiment of <i>Only-long</i> GA with binding grid conditions and a 2% loss rate | 112 |
| 7.6 | Tracking experiment of <i>Robust</i> GA with binding grid conditions and a 2% loss rate | 112 |
| 7.7 | 24-hour frequency support <i>Robust</i> experiment with a 2% link loss rate. The power at the slack is not visible since it is below the reference (tracking). | 113 |
| 7.8 | Battery state-of-charge (SoC) during the 24-hour experiment | 113 |

List of Tables

| | | |
|-----|--|-----|
| 5.1 | Parameters of EV users behavior | 76 |
| 5.2 | Energy bought from the grid and from V2G EVs, for different price cases. | 80 |
| 7.1 | Root mean square error (in Watts) between the real power at the slack bus and the requested tracking signal, for a 10-minute interval | 110 |

1 Introduction

All of science is nothing more than the refinement of everyday thinking.
— Albert Einstein

1.1 Motivation

Electric Vehicles (EVs) are expected to have a significant increase in market share in the next decade. Countries all over the world are supporting and promoting EVs for their energy efficiency and for their potential to reduce CO₂ emission in the transportation sector, in contrast with the conventional fuel-based vehicles [1, 2]. For example, given an expected growth in sales of 20%, there will be more than four million EVs in the USA by 2024 [3]. Similar growth is expected, proportionally, in most of the countries in Europe [4]. This will affect the planning and operation of electrical grids, with a particular emphasis on distribution networks. Indeed, uncoordinated and random EV-charging can severely impact the quality and continuity of the power supply. Furthermore, power flows and voltage-quality patterns throughout the grid will be affected considerably [5] and might increase the risk of local blackouts due to overloads. The authors in [6, 7, 8, 9, 10] show how an uncontrolled charging of EVs can jeopardize the operation of the power grid, causing voltage deviations, increasing power-system losses, and cable or transformer overloading [11, 12, 13, 14]. A possible solution is grid reinforcement that is often very expensive [15], especially in urban areas. An alternative solution is to dynamically control the power consumed by charging stations and to keep the grid in safe operating conditions [16]. In other words, it is possible to use electric vehicles as flexible resources rather than passive ones, which can enhance the grid operation (e.g., [17, 18, 19]).

Electric-power delivery systems are divided in two parts: transmission grids and distribution grids. Transmission grids are responsible for delivering electric power from centralized power-plants. The power is transmitted at a high voltage and long

Chapter 1. Introduction

distances from the power plants. Distribution grids, in turn, carry electric power from the transmission grids to individual consumers. The voltage level in these grids is lower than in transmission grids. Traditionally, the power flows between transmission and distribution grids are unidirectional; this means that the power generated by power plants goes through transmission grids to the distribution grids and then to the end consumers.

Today, a growing penetration of renewable energy resources, such as batteries, photo-voltaic plants (PVs) [20] and wind turbines [21], makes it possible to have energy production available at the distribution-grid level. However, local power consumption is also increasing. One of the important factors is an emergence of electric-vehicle charging stations [22, 23, 24] (see Fig. 1.1). These loads could represent one of the largest loads for the grid. Hence, local power-generation, together with the local power-consumption, can create excessive power flows, compared to the dimension of the grid. This excess causes grid overloads and safety issues such as transformer over-rating, line congestions, and over/under-voltages [25, 26]. Although, grid overloads can be compensated by a renewable generation, there are still issues due to high volatility and low inertia of renewable generation.

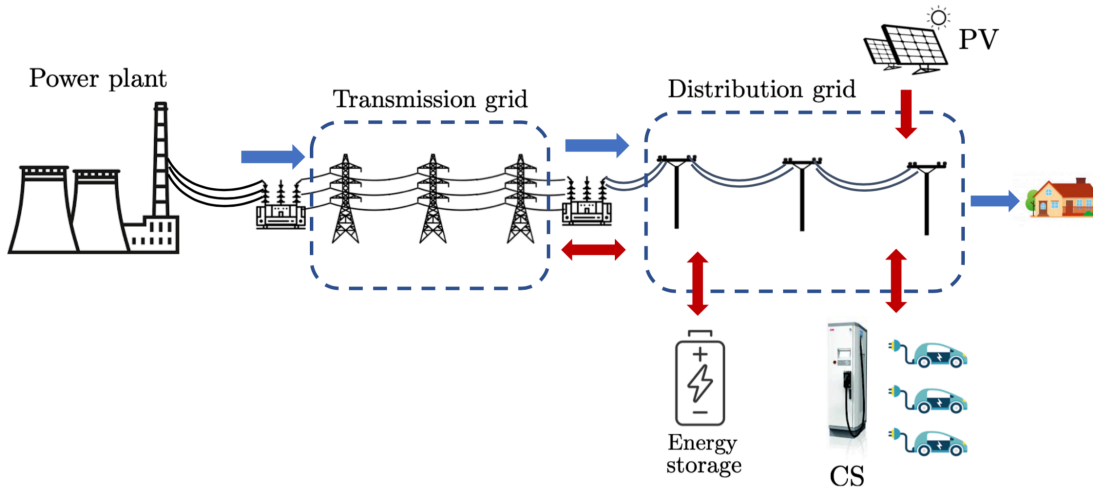


Figure 1.1 – Transmission and distribution grids. Blue arrows is traditional power flow, red arrows are flows when there are renewable resources in the grid.

For an example of transformer over-rating, we consider a situation of a distribution network that contains local generation (e.g., PV panels) and an EV CS, both connected to the main grid through a transformer. When EVs that are connected to CSs are charged mostly by the PV production (i.e., during sunny days), there can be a rapid PV power-drop that can be caused by a passing cloud and can reach up to 60% of the rated power in a few seconds [27]. This power drop, due to the low inertia of the PV production, will suddenly increase the power flow through the transformer. This could cause the transformer to exceed its rated power and create a risk of overloading it.

Alternatively, the CS can reduce its charging power to compensate for the solar drop. However, given external conditions, this requires the CS to constantly update the maximum charging-power it can consume. To solve this issue, the naive approach would be for the CS to know the exact amount of PV injected-power and of the transformer rated-power. In the literature, this problem is typically formulated as a cost-driven demand-response optimization (DR, e.g., [28]), where the forecast of arrivals and departures and of the electricity price is usually fundamental. However, these solutions are not scalable for different setups due to the complexity of the problem. This is where real-time control can help. Indeed, the optimal decision should be taken by an entity (grid controller) that has a broader view of the system operation (e.g., [29]) given by a state estimation process (SE, e.g., [30, 31, 32, 33]). If all flexible devices in the grid could be manipulated by a grid controller, their flexibility could be used to keep the grid in a feasible state of operation in terms of line ampacity limits and voltage magnitudes. The grid controller can also minimise global operational costs of the entire grid and provide ancillary services, for example, tracking a dispatch plan [34] (i.e., acting as a virtual power plant to an upper-level grid), thus providing primary [35] and secondary frequency control [36], etc. In this case, the grid controller computes an *aggregated power-setpoint* for an entire CS and considers it as a single resource. The CS, in turn, allocates an aggregated power-setpoint among connected EVs and advertises an abstract representation of its internal state and an estimation of their behavior in the time horizon when the aggregated power-setpoint is expected to be implemented. Similarly, if we have several CSs, the grid controller computes an aggregated power-setpoint per CS. This provides scalability to the system, as the grid controller has no detailed information about the CS and connected EVs: arrivals/departures, amount of connected EVs, their energy demand and staying times, etc. (see Fig. 1.2).

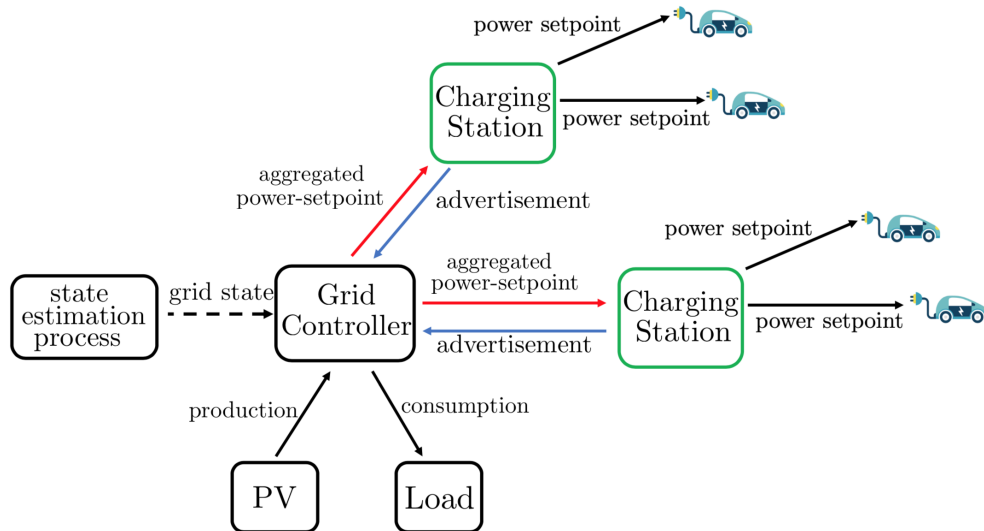


Figure 1.2 – General architecture of grid control with several CSs.

1.2 Overview

The integration of EVs in existing power grids and their real-time control will make for a number of challenges. Taking advantage of the available flexibility means that CSs are required to frequently change their charging/discharging powers to adapt to quickly changing grid conditions that can be caused by volatile renewable resources (e.g., solar and wind generation). One of the main concerns associated with such a behavior is EV battery-wear, i.e., directly transferring the changes from the CS to the connected EVs can accelerate the battery wear in terms of capacity loading and losses increase [37, 38]. Therefore, one of the requirements of real-time control is to minimize the battery wear and to keep the battery in a safe state of operation. Such a requirement must be maintained even during periods of substantial changes of the grid conditions.

Another concern is about the power-allocation strategy among EVs. As every EV has its own *energy demand* (amount of energy that user needs for next trip) and *staying time* (time that user would like to spend at CS). Both the heterogeneous-energy demand and staying time define the *charging priority* of an EV. For example, if the energy demand of EV *A* is lower than the energy demand of EV *B* and the staying time of *A* is higher than *B*, then *A* has a lower charging priority than *B* and can be charged at lower power. In this case, we can decrease the consumption of EV *A* if there is a need for the grid service. However, why would a user of EV *A* to stay longer if they can just require it to charge as fast as possible and declare a small staying time? The user should have an economic incentive to stay longer at a CS: for example, a user that stays longer (EV *A*, in our case) will pay less for the energy, compared to those who require faster charging (EV *B*). In this thesis, we do not study in detail the pricing schemes (e.g., [39, 40]) that define incentives for users to provide the flexibility to the grid, as this is out of the scope of the current research. We focus on the development of the charging method by assuming that users are properly encouraged. In this case, the method should incorporate a heterogeneity of users' energy demands, staying times and incentives for preserving a *charging balance* between EVs. On one hand, charging of *A* should not starve the charging of *B*. On the other hand, *B* should not delay the charge of *A*. Instead, *B* (who requires rapid charging) should be prioritised over *A*, but not at the expense of *A*'s satisfaction.

According to the architecture described in Section 1.1, the task of a CS is to maintain charging/discharging of its connected EVs while tracking aggregated power-setpoints from the grid controller. The aggregated power-setpoint can exhibit rapid variations due to other volatile resources of the local distribution grid. The allocation of power to EVs is a difficult task because an aggregated power-setpoint can change dramatically in only a few seconds. The naive power allocation, which would transfer these variations directly to the EVs, could increase their battery wear by creating large power-jumps, mini-cycles, and frequent on-off switching of the EVs. Furthermore, in order to keep a

charging balance, the power should be allocated fairly, considering that each EV has its own energy demand and departure time because the aggregated power-setpoint might not be enough to satisfy the demand of all EVs. As there is no traditional definition of a fair charging of EVs, we propose to use definitions that are widely used in resource sharing and networking: weighted-proportional and weighted-max-min fairnesses [41]. Weights in this case represents the priority of an EV to be charged and computed as a function of energy demand and staying time. Both allocation strategies are Pareto optimal [42], and it is often difficult to choose between the two. In this thesis, we prove that, in our specific setting, both allocations are identical. As a result, the development of the method that takes into account all objectives listed above remains to be done, i.e., the method that provides the flexibility of EVs to the grid by fairly allocating the aggregated power-setpoints among connected EVs while minimizing the battery-wear. Although the state-of-the-art assumes that EV charging behavior is ideal, we consider the impact of non-idealities on both the EV and grid operations. To this end, we implement a number of features that account for the realistic behaviour of EVs by incorporating results of the measurements on real-field deployment. In particular, our method considers a non-ideal response, due to internal reaction and implementation delays, of an EV to a charging power change. The change of a charging power from 0kW to maximum charging power (depends on the EV type, for example, for Renault Zoe it is 22kW [43]) can take more than 10s in reality, which is a long time-period when we talk about real-time control. Moreover, an EV might not be able to implement a requested power-setpoint, due to its internal state (i.e., internal temperature, state-of-charge, etc.). Furthermore, EVs have a non-zero minimum charging power, i.e., an EV can be either switched off and consume no power, or charge at a power that lies between non-zero bounds, where the minimum charging-power cannot be arbitrarily small. Consequently, the CS should decide which EVs should be switched on and which should be switched off. This leads to a mixed-integer variables in the optimization problem. In order to solve this efficiently in real time, we developed a heuristic that limits the number of integer variables and that enables us to solve the optimization problem in real time.

Vehicle-to-grid (V2G) is the ability of EVs to discharge their batteries and to deliver energy back to the grid (e.g., [44, 45]). This technology has the potential to further increase the flexibility and safety of the grid operation [46, 47, 48], thus further expanding a grid-aware operation of the EVs and increasing the hosting capacity of the combination of EVs and distributed generation, such as PVs (e.g., [49]).

The V2G operation requires that users have incentives to discharge their batteries back to the grid, which is different from a charging-only case. As batteries are the most expensive components of EVs, their users need to have clear incentives to permit the V2G operation. The discharging of the battery will accelerate its degradation process by increasing the number of full-equivalent cycles [50], [51]. The main challenge in this case is to decide when it is more economically convenient for V2G EVs to discharge.

One possible approach is to discharge EVs whenever there is power deficit caused by the charging of other EVs or other load consumptions. However, this can be sub-optimal as the decision is taken based only on current-time information. Indeed, as V2G EVs can act as storage devices, it could be more beneficial to temporarily keep the available energy and use it in the future only when, for example, the energy cost from the grid is high. Such decisions are long-term in the sense that, in order to make them, the future events in the grid should be anticipated, i.e., arrivals/departure of EVs, energy demand of charging EVs, staying times, amount of energy that V2G could provide, PVs production and consumption of loads (e.g., domestic buildings). The standard technique for these kind of tasks is model predictive control (MPC, [52]). Adding grid constraints in the scheduling problem significantly increases its complexity and makes it impractical in the real-time operation of the grid, due to high number of variables and non-convex grid constraints. To solve this issue, we suggest to combine the scheduling that performs long-term decisions without grid constraints with a real-time controller that reacts to grid-aware external setpoints and takes into account long-term decisions of scheduling.

As was mentioned in Section 1.1, the CS is a part of the grid control-system. However, there are side effects to this integration. In particular, there are two issues that must be taken into account by the grid controller itself. First, the sudden EVs (or other huge loads) disconnections can cause line congestions and voltage violations. When trying to completely avoid these violations, the control-systems typically have predefined large safety bounds, which means that integration forces the grid operation to be more restricted, which can lead to large sub-optimality. However, temporary violations of the steady-state bounds are permitted by grid standards (e.g., [53, 54, 55]) and could enable the exploitation of the flexibility of other resources to better control the system's state. We propose a method by which such temporary violations are controlled so that they remain within the limits imposed by grid standards and safe operations.

The second issue is message losses between the grid controller and the CS; they are caused by the inherent uncertainties and non-idealities of communication networks and processes. In a real-time control system, occasional message losses are usually handled by a reliability protocol such as TCP [56]. However, there can still be occasional message losses due to crashes/reboots of the processes or failures of the communication nodes or excessive delays in reliable protocols. An occasional loss of one or more messages can render the controller incapable of issuing valid setpoints, especially when the control action is taken at a sub-second time-scale. We address this issue by having the resources send information about their state that is valid for the long-term, in addition to the short-term information originally sent. This long-term information is stored by a grid controller and used to compute valid setpoints, in cases when there are message losses from a resource.

Taking into account the aforementioned challenges, in this thesis, we focus on the

design concepts and applications of real-time control algorithms for electric-vehicle charging and discharging. We then test our proposed methods through real-field deployments on a real-scale CIGRÉ low-voltage benchmark [57] with real EVs.

1.3 Contributions

A detailed list of the contributions of this thesis can be found below.

1. We develop a method for real-time control charging of EVs. The proposed method meets the following objectives: (i) to follow an aggregated power-setpoint, (ii) to minimize the battery wear of each EV, and (iii) to fairly allocate the power proportional to the EVs needs. In order to achieve these objectives, we define novel metrics and use them to construct a dedicated optimization problem. Our method enables us to combine the optimal charge of EVs and satisfy dynamic-grid constraints. As the charging power is discontinuous (the minimum charging power is not arbitrarily small), our optimization problem is a mixed integer one.
2. In order to solve the mixed-integer problem in real-time, we propose a heuristic for reducing the number of integer variables, thus reducing the complexity of the problem. As a result, our method can solve the mixed-integer problem in real-time in less than 20 ms.
3. We prove that our method is able to account for an EV's energy demand and staying time heterogeneity and that it provides a charging balance between different EVs.
4. We assess the performance of the proposed control method in a real-field setup and show that the method works in the field, i.e., the method can control the charge of commercial EVs that are connected through a CS to a real CIGRÉ low-voltage benchmark microgrid. We verify the real-time capabilities of the method and show how it handles the non-ideal response of the EVs to the control power-setpoints, due to implementation and reaction delays, and inaccuracies.
5. We design and implement a method for taking advantage of the available flexibility of regular and V2G EVs in a community setting, by minimising the community energy-cost and by reducing the effect of modifying the charging and discharging powers in the battery wear. The method is designed as a combination of a scheduling problem and a real-time problem. In this sense, the method is aware of the grid operation and takes into account the decisions of the scheduler, thus satisfying the EV energy-needs and minimizing the EV battery-wear.
6. We compare our method from item five against benchmark real-time methods, earliest deadline first (EDF) [58] and least laxity first (LLF) [59], and we show

that our method presents significantly better performance. We also study the robustness of our method. We simulate the case when the forecasts of EV-users behaviour are incorrect. Then, we compare the performance of the method to the oracle that knows the future. The results show that our method performs close to the oracle, even with inaccurate forecasts.

7. We propose a method that enables a real-time grid controller to continuously provide optimal control by relaxing the pre-defined hard constraints and that permits temporary voltage and current violations caused by load (e.g., EV) disconnections or load in-rushes. The method improves the performance of the grid controller, making it less conservative and enabling it to opportunistically use available resources.
8. We address the possible communication network non-idealities and propose a method that enables a grid controller to compute and issue setpoints with partial information from the resources. Using this method, the grid controller guarantees that grid safety is maintained despite missing advertisements from resources.

1.4 Dissertation Outline

This thesis is organized as follows.

In Chapter 2, we provide the context. Specifically we evaluate the literature on real-time control of EVs charging, V2G operation and scheduling, highlighting the drawbacks and limitations of existing solutions.

In Chapter 3, we introduce the real-time charging control method for CS that follows an aggregated power-setpoint in real time. This method is two-fold: from one side it serves the grid quality by following aggregated power-setpoints sent by a grid controller, and from other side it optimally charges EVs by minimizing the battery-wear and by preserving fairness of charge. We introduce weighted-max-min and weighted-proportional fairness and prove their equivalence in our case. Then, we formulate a mixed-integer optimization problem to combine all objectives of the method. Subsequently, we develop a heuristic for reducing the amount of integer variables that enable us to solve optimization problems in real time. Finally, we evaluate our method in a stressed situation when the charging station does not have enough power to charge all EVs at maximum, and we show the performance of the method.

In Chapter 4, we present a real-field validation of the charging control-method presented in Chapter 3. We perform several field experiments with different PV productions, and EV energy needs and staying times. We show that the method is able to provide a real-time control (i.e., at sub-second scale) for charging commercial EVs. We

also study the charging patterns of commercial EVs.

In Chapter 5, we propose grid-aware control and an optimal scheduling of EV CSs that can provide V2G. First, we present the scheduler that makes long-term decisions for EVs' charging/discharging powers based on grid energy-prices, the forecasts of PV production, load consumption, EV arrivals/departures, the amount of energy that EVs want to charge/discharge, and their energy prices. This scheduler is formulated as a scenario-based model predictive control (MPC) problem. Second, we describe scenario generation and scenario selection techniques. Third, we formulate a real-time problem that follows an aggregated power-setpoint (i.e., provides grid quality-service), and we take into account the decisions of the scheduler and minimize the EV-battery wear. Fourth, we compare our method against benchmark real-time methods, EDF and LLF. Finally, we study the robustness of our method. That is to say, we simulate the case when the forecasts of EV-users behavior are incorrect, and these forecasts do not represent the real behaviour of users. We compare the performance of the method to the oracle that knows the future. The results show that our method performs close to the oracle, even with inaccurate forecasts.

In Chapter 6, we move from the charging control and focus on the real-time grid control itself. We describe, in particular, a method by which a grid real-time control can handle large power steps by permitting and controlling temporary voltage and current violations so that they remain within the limits imposed by standards and safe operation.

In Chapter 7, we go one step forward in real-time grid control. We address the network non-idealities issue. Mainly, we present a method for real-time grid control that is robust in non-ideal network conditions.

Finally, in Chapter 8, we conclude this thesis with a summary of the main findings and possible directions for future work.

2 State of the Art

The EV control-methods presented in the literature can be classified based on several aspects. In this thesis, we consider the classification based on control architecture (centralized, distributed and decentralized) and grid awareness (grid-aware and non-grid-aware). Grid-aware methods are those that take into account grid constraints (e.g., overload control constraints, nodal voltage constraints, ampacity limits constraints), whereas non-grid-aware methods ignore them. In this chapter, we survey the state of the art on charging/discharging control of EVs, their integration into the distribution grids, and possible services that EVs can provide to the power grids. Also, we discuss the possibility of EVs integrating and participating in the electricity market. This is addressed by the concept called virtual power-plant (VPP).

2.1 Overview of Control Architectures

In the literature, control architecture, in which EVs are integrated as controllable resources, are generally clustered in three categories: *centralized* [60, 61], *decentralized* [62, 63] and *distributed* [64].

Centralized control strategies require a centralized infrastructure to collect information from all the EVs and to centrally optimize their charging profiles. In this case, a central controller has information about its resources and their particular nature. Using this information, the central controller computes a global optimal solution for each resource individually. As a result, the controller achieves optimal charging powers for each EV. Given all the necessary input, the centralized control can guarantee an optimal solution. The drawback, however, is that the size of centralized optimization increases with the number of EVs hence causes issues for the scalability of the system. Additionally, such an architecture requires strong communication network, as all resources should receive the decisions of a central controller. Yet, a single point of failure at the central controller could potentially collapse the whole system. In order to pre-

vent this, the duplication strategy (e.g., hot standby, backup, etc) is required. Typically, centralized control methods are used as benchmarks for the analysis of decentralized and distributed methods.

With a distributed control, in contrast to a central control, the decisions are made by local controllers that interact with each other. Every local controller reacts locally by exchanging information with other controllers, hence each controller needs to solve its own small-scale problems. In this case, there is a collection of local decisions that are implemented locally by controllers and that leads to the optimal global solution. Such architecture is highly scalable, however, the design of a distributed algorithm is a non-trivial task. Also, the convergence time could be considerably larger than in centralized algorithms and involves communication between controllers.

Decentralized control is also known as hierarchical control. Usually, the hierarchy is aligned with the physical hierarchical structure of a distribution grid. In this case, there is an upper-level controller that takes global decisions based on information given by local controllers. Local controllers, in turn, receive global decisions from an upper-level controller (or central controller) and make local decisions based on local information without requiring permission from the central controller. In other words, local controllers operate on local information in order to accomplish global goals. Therefore, decentralized architecture is more scalable than centralized control as it decreases the need for data exchange, i.e., the local low-level goals are hidden from the upper levels, where global decisions are made. Similar to centralized control, decentralized control suffers from a single point of failure and requires strategies to prevent it.

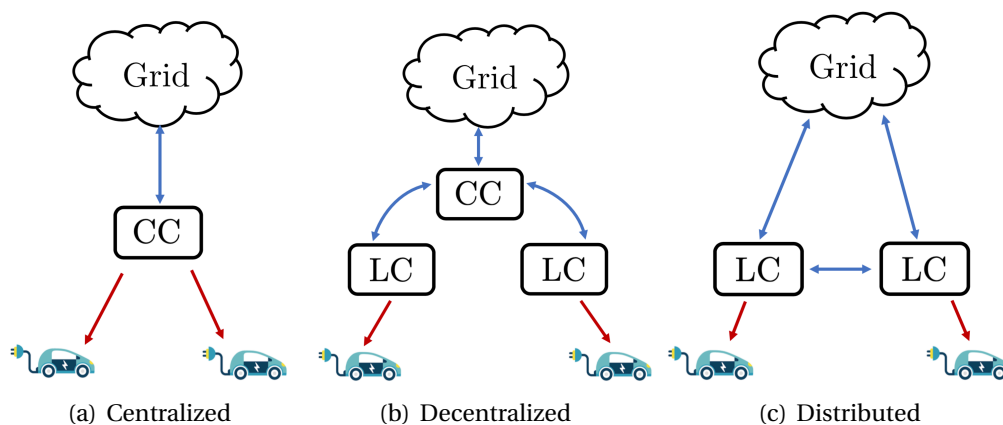


Figure 2.1 – Schematic representation of centralized and decentralized control architectures. CC - central controller, LC - local controller.

2.2 Provision of Grid Services

In Chapter 1, we propose that EVs can bring more flexibility and help a grid controller to keep a grid quality of service. In the literature, there are a number of services that EVs can provide: voltage control, congestion management, loss reduction, frequency regulation, spinning reserve, etc.

In this chapter, we present the literature overview of the methods for charging/dis-charging control of EVs that provide services for the grid by using architectures presented in Section 2.1.

2.2.1 Voltage Control

Voltage control requires maintaining the voltage deviations within predetermined limits. For example, standard [65] describes the main voltage parameters and their allowed deviations: according to the guide, the voltage should remain within $\pm 10\%$ of the nominal value. These deviations are a result of many factors such as overall grid load, generation schedule, etc. Traditionally, the voltage control is associated with reactive power-control, which assumes the decoupling of the active and reactive power [66]. This is true in the case of transmission grids or grids where resistance is much smaller than reactance (hence the resistive part is neglected). However, this assumption is usually true for transmissions grids but is not for distribution ones. Therefore, the influence of the active power is significant and should be taken into account. In this respect, authors in [67] developed a decentralized grid-aware real-time voltage control method, taking into account both active and reactive power injections. In [68], an emergency real-time voltage-control algorithm is proposed. Under this method, software agents locally control generators and controllable loads, based on local measurements and until their control resources saturate, in which case they start exchange information with peer agents for assistance.

Concerning EV charging control, different schemes for the charging control of EVs are proposed in the literature. In [69], the authors propose a centralized grid-aware load-management control strategy for improving the voltage profile and for minimizing the power losses during peak hours by assuming that EVs are scheduled in three different types of charging periods and do not violate the voltage limits. In [6], the authors present a centralized heuristic method for avoiding lines and transformer congestions and for improving voltage profiles by using an intelligent charging algorithm. Periodically (on an hour time-scale), the algorithm computes power flows and checks whether the operating conditions are suitable. If conditions are not suitable, then the algorithm recognizes whether the problem is due to voltage deviations or to the congestion in the grid; then, it stops charging a predefined percentage of EVs and adds them to a waiting list. When the grid conditions are suitable, the charge of the

affected EVs is restarted. A heuristic approach is also used in [70], the method also checks voltage deviations and congestions. The charging powers are computed such that power losses are minimized. In [71], the authors propose a scheduling method for dealing with active and reactive management of a distribution network with EVs in order to improve the voltage profile and to minimize operation costs. Although research in [6, 69, 70] takes care of the grid constraints, the user satisfaction is not taken into account. In [71], it is assumed that users commit in advance their amount of energy that allows to travel with EVs for the next day which could be unrealistic requirement.

Decentralized methods that take into account user demand can be found in [72, 73]. In [72], a novel method is proposed; it uses historical information of the local voltage magnitudes at each node to maintain the operational limits of the distribution grid and coordinate charging of EVs. The authors in [73] design independent fuzzy-logic controllers to keep the voltage and energy storage SoC (state-of-charge) within appropriate ranges, as well as to keep the power balance among charging stations. The authors in [74, 75] propose a shrunken primal–dual sub-gradient algorithm to minimize load variance and to regulate nodal voltage magnitudes. The grid controller (or operator) controls EVs by broadcasting the dual variable linked to voltage magnitudes and to the Lagrange gradient that is computed based on previous charging profiles of EVs.

Distributed approaches can be found in [76, 77, 78]. The authors in [76] propose a droop-based method for reducing voltage imbalances by modulating the EVs' charging current by using local voltage measurements. However, the users' charging demands are not taken into account. Another decentralized droop-based method can be found in [77], where their method also relies only on local measurements. Their method prevents voltage issues, however, it dramatically increases charging time. The authors in [78] develop a decentralized algorithm for reducing energy costs and to control the voltage profile.

2.2.2 Congestion Management

The issues of congestion in distribution grids typically appears in situations when the generation or demand exceeds the grid capacities (e.g., lines, transformer and other equipment). As a result, the risk of overloading and power losses increases. The solution to these issues is congestion management. Overloading issues can be incorporated into the control by taking into account capacity constraints of the grid equipment (e.g., transformer limits and line-ampacity limits) or adding it into an objective function of the control problem.

In [79], the authors propose a decentralized congestion management method that relies on the Alternating Direction Method of Multipliers (ADMM). The optimization

problem is formulated as a quadratic programming problem with linear capacity constraints. A centralized approach, with similar constraints, can be found in [80]. However, these approaches require extensive information/visibility of the network (e.g., voltages and currents) and the state-of-charge (SoC) of the EVs. The authors in [81] present an online heuristic-based controlled charging-method that takes into account transformer limits, nodal voltage deviations, and EV user preferences. In [82], the authors offer a decentralized framework that minimizes the total cost of energy for the users while preventing a thermal overload of transformers and cables. A similar approach can be found in [83], which is extended to a V2G operation. A multi-agent market-based system for congestion management with a non-V2G integration of EVs is proposed in [84]. The EV charging limit is computed based on market price signals. A distributed approach that exploits a V2G capability can be found in [85]. The authors use V2G EVs to minimize the variation of the grid load, however they do not take into account the EV-user preferences; whereas, the approaches in [84, 85] are highly dependant on a forecast accuracy.

2.2.3 Power-system Losses

In addition to the voltage control and congestion management, EVs can be used to minimize power losses. Power losses are dependant on various factors such as length of the cables, size of conductors, and transformer installations. As losses typically increase with demand and depend on the current flows through the lines [86, 87], various strategies were developed to minimize power losses.

In [88], the authors compare three intelligent centralized-charging algorithms that minimize the effects of EV charging on the distribution grid. First, the algorithm minimizes power losses; second, it minimizes the load variance; and third, it maximizes the load factor. It is shown that using the load variance or the load factor as the objective function is better because they have less computation time and complexity, which is a crucial factor for real-time control applications. However, centralized architectures require obtaining information from all EVs, which could be problematic in reality. The authors in [89] also address load variance by developing a double-layer decentralized optimal-charging control method that exploits the V2G capabilities of EVs. However, incentives and battery safety are not taken into account. Several centralized meta-heuristic algorithms, where global operational costs take into consideration the grid constraints and user satisfaction, are proposed in [90]. The authors in [91] developed a distributed algorithm for power-loss minimisation during EV charging, taking into account grid constraints. But, a specific initialization procedure during each EV charging cycle is needed. A similar distributed approach that accounts for power losses can be found in [92].

2.2.4 Frequency Regulation and Spinning Reserve

Frequency regulation is a reserve service that aims to establish an instantaneous balance between the generation and the demand. This service is divided into three types: primary, secondary and tertiary. Typically, it is a service that provides for TSO; however, there are works that consider such a service for DSO for the near future. This service, in particular, could be interesting for microgrids [93, 94] in order to improve their stability during islanded (when a grid is disconnected from the main grid) operations [95].

A substantial amount of the literature focuses on the usage of battery-energy storage systems (BESS) for providing frequency support. In this regard, the authors in [96, 97] developed control methods for a BESS to provide a primary frequency and other ancillary services to the grid in the presence of uncertainties caused by renewable production. As a V2G EV can be considered an energy storage that is temporarily connected to a grid, a huge amount of research is addressed to the possibility of a provision for a frequency regulation on a grid.

The authors in [98] propose a non-grid-aware centralized V2G scheduling for EVs in order to provide a frequency regulation service. In [99], a decentralized droop-based V2G control scheme is proposed, considering the charging demands of EV users. In this case, however, the grid constraints are not taken into account. In [100], a dynamic programming non-grid-aware method for V2G is used to achieve an optimized frequency regulation with V2G. The aggregator maximizes the revenue of EVs that participate in frequency regulation, but the battery degradation is not taken into account. A heuristic scheduling method for providing frequency support, which also omits the degradation of batteries, can be found in [101]. The charging of EVs is based on EDF policy.

The spinning reserve is a generating capacity available to the grid in order to dynamically balance a system load. The authors in [102] propose a non-grid-aware method where an aggregator controls the charging/discharging of the EVs and participates in the energy market by sending price signals for EVs. The authors in [103] propose a V2G decentralized game approach for providing a distributed spinning reserve to customers with different reliability levels.

2.3 EV-users Mobility and Incentives

One of the main differences of EVs, compared to typical loads (e.g., domestic buildings), is their mobility. Furthermore, real arrivals, departures, user energy-demands and bids, and the staying times are uncertain.

As mentioned above, the charging/discharging control of EVs is extensively exploited in the literature. However, user mobility is not always taken into account. The

authors in [104, 105] propose a distributed scheduling method that treat EVs as static loads with fixed parameters. Such assumptions could be unrealistic, as a scheduling method should adapt to various temporal variations, such as random arrivals, unexpected departures, and different energy demands. Therefore, in order to handle the random behaviors of EV users, many scheduling methods perform re-scheduling at every time slot, with updated information. For example, to minimize the total cost of the supply of electricity, the authors in [106] adapt to the environment by repeatedly (every 15 minutes) performing three steps of the developed algorithm. However, grid constraints in this case are not taken into account. This work was further extended to handle the arrivals and departures that occur within one time interval by using an event-driven mechanism [107]. Similarly, the authors in [108] propose an event-driven approach that activates the scheduling process EV is plugs-in EVs plugs-out. In [109], the authors propose to formulate the scheduling problem as an infinite-horizon dynamic program by introducing its state space, admissible action set, transition probabilities, stage costs, and average-cost objective function. In [110], the EV charging control problem is formulated as a Markov decision process to handle the randomness of EV arrivals and the departures and charging demands. Another approach, which tackles EV users and is the most popular, is called model predictive control (MPC, e.g., [52]). This method finds charging schedules for a finite-time horizon in the rolling-horizon fashion and takes into account the forecasts of the future state of the grid (i.e., PV production, load consumption, EVs arrivals/departures, etc.). At each iteration, an MPC performs a rescheduling of EVs charging/discharging powers, taking into account the current state of the grid, i.e., it provides feedback control thus adapting for the possible forecast deviations (e.g., [111]).

EV users should be encouraged to participate in grid services described in Chapter 2.2 and to provide their EVs' flexibility to the grid and permit the modulation of their EVs charging/discharging power. For example, the incentive for users can be to minimize the EV charging cost. These minimizing methods depend on the corresponding electricity market and perform the scheduling to shift charging of EVs in low-electricity-price times and to prevent the congestion in the grid. However, typically these methods do not take into account grid constraints [106, 109, 112, 113]. As a result, the schedules can be infeasible and unsafe for the operation of the grid. The authors in [114, 115] use MPC-based approaches to incorporate voltage constraints into the charging-schedule problem. Even though in this case grid constraints are taken into account, the methods do not see the fast inter-period power fluctuations, as scheduling is performed on a minute-based scale. In Chapter 5 of this thesis, we show that such fluctuations can result in severe violations of the grid constraints, and we propose a two-layer approach to effectively take into account grid constraints and to adapt to the grid state in real time.

2.4 VPP and EVs

A VPP is as a cluster of generator units, controllable loads, and storage systems that is geographically dispersed and aggregated in order to operate as a single power plant [116, 117] see Fig. 2.2. Thus, VPP represents a single entity for a Distributed System Operator (DSO) and a Transmission System Operator (TSO). It should be noted that VPPs are non-grid-aware. These systems can react quickly to changing customer-load conditions, compared to the fossil central station power plants. VPPs can potentially replace conventional power plants while providing higher efficiency and more flexibility. Although, more flexibility enables the system to react better to fluctuating energy needs, the complicated structure of VPPs requires complicated controlling and monitoring techniques.

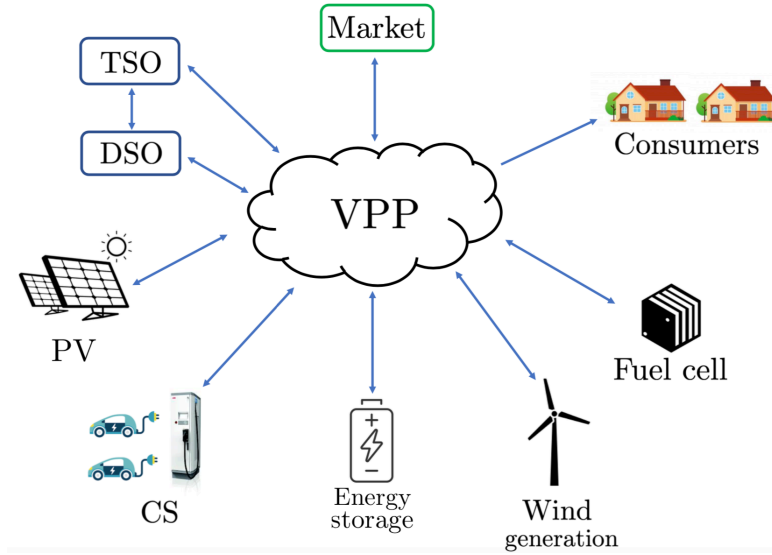


Figure 2.2 – General overview of VPP elements.

In the context of a VPP, group of EVs can be seen as distributed energy resources (DERs) that can provide their flexibility to the power system. The V2G concept adjusts an ability to use EVs as distributed storage batteries and to utilise their energy when needed. Due to their fast response times, EVs become suitable candidates to help utilities solve grid balancing problems. Therefore, EVs can be controlled by VPPs to participate in energy markets [118].

In the literature, typically hierarchical (decentralized) architecture is used. EVs are controlled via aggregators that are considered to be the intermediary level between EVs and VPPs. In [119], the present optimal scheduling of EVs takes into account the fluctuation of renewable energy. The authors in [120] propose an agent-based method for VPPs, which consists of wind generation and EVs, in order to address the highly volatile behaviour of wind-power generation. In this setup, when the price of electricity

is low, the energy generated by wind is stored in EV batteries, and when the price is high, it is sold. Day-ahead scheduling is done to maximize VPPs' profits, and receding horizon optimisation is done to take into account wind behaviour.

In this thesis, we do not focus on the non-grid-aware control of EVs. The methods and techniques presented in the thesis can, however, be potentially used for the integration of EVs into VPPs. For example, in Chapter 3 and Chapter 5, we present hierarchical methods for controlling EV CSs that follow aggregated power-setpoints as a single entity. These methods can be used for controlling EVs under VPPs.

3 Real-Time Control of an Electric-Vehicle Charging Station

As highlighted in Chapter 2, the progressive penetration of EVs and distributed energy resources in the distribution grids significantly influences its planning and operation. In order to avoid grid reinforcement caused by a such penetration, in this chapter we propose to use smart charging stations that adapt the charging power of EVs to the instantaneous capability of the grid. More precisely, we consider the problem of controlling the charging of electric vehicles (EVs) connected to a single charging station that follows an aggregated power-setpoint from a main controller of the local distribution grid. To cope with volatile resources such as load or distributed generation, this controller manages in real time the flexibility of the energy resources in the distribution grid and uses the charging station to adapt its power consumption. The aggregated power-setpoint could exhibit rapid variations due to other volatile resources of the local distribution grid. However, large power jumps and mini-cycles could increase the EV-battery wear. Hence, our first challenge is to properly allocate the powers to EVs so that such fluctuations are not directly absorbed by EV-batteries. We assume that EVs are used as flexible loads and that they do not supply the grid. As the EVs have a minimum charging power that cannot be arbitrarily small, and as the rapid fluctuations of the aggregated power-setpoint could lead to frequent disconnections and re-connections, the second challenge is to avoid these disconnections and re-connections. The third challenge is to fairly allocate the power in absence of the information about future EVs arrivals and departures, as this information might be unavailable in practice. To address these challenges, we formulate an online optimization problem and repeatedly solve it by using a mixed-integer-quadratic program. To do so in real-time, we develop a heuristic that reduces the number of integer variables. We validate our method by simulations with real-world data.

3.1 Introduction

The allocation of power to EVs is a challenging task because, as previously mentioned in Chapter 1, an aggregated power-setpoint can change substantially in a few seconds. The naive power-allocation, which would transfer these variations directly to the EVs, could increase their battery ageing by creating large power-jumps, mini-cycles, and frequent on-off switching of EVs. Furthermore, the power should be allocated fairly considering that each EV has its own energy demand and departure time. Indeed, the aggregated power-setpoint might not be enough to satisfy the demand of all EVs. The authors in [102] minimize the battery-degradation cost associated with additional cycling, assuming that there is sufficient amount of power to satisfy the EVs demand, and fairness issues are not addressed. Whereas, studies in [112, 121, 122], propose charging schemes that consider fairness of the power allocation among EVs, but without accounting for battery wear. The authors in [123] use an on-off strategy stating that a constant power minimizes the battery wear. However, the large power jump, from no charge to maximum charge, could represent a significant impact on the battery's lifetime. In our formulation we penalize the on/off transition and the power change, so that the charge smoothness is guaranteed. We develop a method that considers both battery wear and fair-demand satisfaction and that tracks the aggregated power-setpoint. Also, the battery size, charging rate, initial state-of-energy, and desired state-of-energy at departure, can be different for every EV.

The authors in [69] propose a load-management control strategy for minimizing the power losses and for improving the voltage profile during peak hours by assuming that EVs are scheduled in three different types of charging periods. The authors in [124] develop a decentralized control-scheme, using concepts from non-cooperative games, showing optimality when the EVs characteristics are identical (same departure time, energy demand and maximum charging-power) and all charging schedules are agreed upon with the CS one-day ahead. [125] proposes an online charging-algorithm, assuming that no EVs will arrive when a charging schedule is made. In [126], a chance-constrained optimization problem is formulated to minimize the charging cost. However, the problem is computationally heavy and might not be applicable in actual real time. We propose to take a different approach without the need for scenarios but only with updated information, thus significantly reducing the computational burden and using the minimum amount of information to represent historical and future events in the decision taken at each time-step. Studies [5, 127, 128] assume that all the EVs have the same charging rate. But, such assumptions do not hold in practice. In contrast, our method considers the EVs heterogeneity. We do not have any information about future arrivals and departures, nor can we know the real amount of time any charging will take; we can only estimate it.

A common assumption in the literature is that the charging power of an EV is a continuous value between 0 and the maximum power (e.g., [112, 127, 128]). However,

in reality, this is not the case because an EV can be either switched off and consume no power, or charge at a power that lies between non-zero bounds, where the minimum charging-power cannot be arbitrarily small. The authors in [129] developed a distributed control-scheme that supports on-off states, but it is limited to a constant power when on. Whereas, we consider both switch on and off possibilities and not arbitrarily small minimum charging-power.

The proposed method has the following objectives: (i) follow an aggregated power-setpoint, (ii) minimize the battery degradation of each EV, and (iii) fairly allocate the power proportional to the EVs needs. In order to achieve these objectives, we define novel metrics and use them to construct a dedicated optimization problem. As the charging power is discontinuous (the minimum charging power is not arbitrarily small), our optimization problem is mixed integer. As a mixed-integer optimization problem is difficult to perform in real time, we propose a heuristic for reducing the number of integer variables, thus reducing the complexity of the problem.

Our main contributions are the following:

- We assume that the control scheme has no internal information about battery charging (e.g., ramping rates, current state-of-energy), nor about actual departure time of EVs. This is more realistic, as modern charging stations are myopic to this kind of parameters.
- Our method provides sub-second-scale control. Whereas most of the existing methods work on a minute scale, ours enables the CS to react faster to changes in the grid.
- We use a realistic model for the battery charging-power, i.e., an EV is either switched off (charging power is 0 W), or its power lies within non-zero bounds.
- We minimize the battery wear by avoiding large power jumps and by reducing the number of cycles.

3.2 Problem Statement

3.2.1 Charging-Station Model

We consider a charging station (CS) that can host N EVs. Time is discretized in constant interval, indexed by k . The CS keeps track of the number of connected EVs at every step k . A newly arrived EV cannot begin charging before being instructed by the CS. Each EV, say i , upon its arrival, is assumed to inform the CS of (i) charging-power bounds P_i^{\min} and P_i^{\max} , (ii) energy demand E_i^{dem} , and (iii) expected departure time k_i^{dep} . Information about future arrivals, future expected departures, and future demands is unknown.

Also, the CS has access to the measured power $\hat{P}_i[k]$ of EV i at every time k . The CS is able to control the charging power of an EV by sending the setpoint $P_i[k]$ to EV i at time k (see Fig. 3.1). As the CS is connected to a three-phase system, we assume that the EV charging power is evenly balanced on the three-phases, and we do not target phase-balancing. The CS receives an aggregated setpoint $P^{\text{req}}[k]$ from the grid controller. In return, it sends its updated status (see Section 3.5 for details).

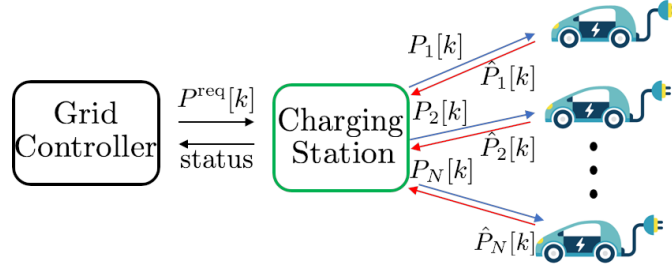


Figure 3.1 – General setup of the considered charging station.

3.2.2 Constraints of the EVs

We assume that the CS has the ability to stop the charge of an EV. The individual power flexibility of EV i is defined by the set $\{0\} \cup [P_i^{\min}, P_i^{\max}]$. We denote the *on/off decision* for EV i at time k by $\omega_i[k]$. Specifically, $\omega_i[k] = 1$ (respectively, 0) means that we decide to switch on (respectively, off) EV i at time k . We assume that an EV is initially switched off, upon arrival.

When receiving new setpoints from the CS, the EVs cannot immediately change their charging power due to delays:

- *reaction* delay is the time an EV takes to start modifying its power after receiving a new setpoint,
- *implementation* delay is the time an EV takes to reach a new setpoint, which depends on the EV charger ramping-rate.

We say that an EV is *locked* if it is in the process of reacting or implementing a setpoint. As the specific delays are usually different for every type of EV, it is difficult to know their exact values. Therefore, we take a conservative upper bound T^L (20s in this work). Specifically, we consider that, after receiving a setpoint, any EV will be locked for the *locking period* T^L .

Note that the locking of the EVs temporarily shrinks the flexibility of the CS as the amount of EVs that can change power varies from one control cycle to another. Thus, this information is supposed to be constantly sent to the grid controller. As the

ramping rates and delays are unknown, it is impossible to know a-priori exactly how the charging power will change when an EV is locked.

3.2.3 Power Allocation to EVs

The CS needs to allocate the time-varying aggregated power-setpoint to the connected EVs. The purpose of the power-allocation strategy is to allocate the consumed power in such a way that the satisfaction of the EV demands are maximized and that their batteries are subjected to minimal wear. In particular, it might not be possible to satisfy all EV demands if the power capacity is not sufficient. In such a case, power should be allocated fairly. Furthermore, fast variations of the aggregated setpoint should be smoothed, otherwise its direct implementation can degrade the EV batteries. In summary, the objectives of the allocation strategy are

1. track the aggregated setpoint from a grid operator,
2. minimize the wear of EV batteries,
3. maximize the EVs energy-demand satisfaction, while maintaining fairness,
4. minimize the number of times the charging station stops the charging of an EV, while it is plugged-in.

In this work, we consider all four objectives together. In the next section, we formulate a specific mixed-integer program and show how we solve it in real-time.

3.3 Control Scheme at the CS

The CS computes setpoints for all EVs that are not locked at time k . At each time k , the CS has the following inputs, states, and outputs.

- Inputs (as introduced in Section 3.2):
 - aggregated power-setpoint $P^{\text{req}}[k]$,
 - measured powers $\hat{P}_i[k]$ for every EV i ,
 - on/off decisions $\omega_i[k-1]$ for every EV i .
- States (will be detailed Section 3.3.2):
 - history of charging power changes $\lambda_i[k]$,
 - the desire of an EV to be charged $\rho_i[k]$
- Outputs (as introduced in Section 3.2):

- the power-setpoints $P_i[k]$,
- on/off decisions $\omega_i[k]$

According to the objectives described in Section 3.2.3, the CS solves the following optimization problem

$$\min_{\mathbf{P}[k], \mathbf{\Omega}[k]} c_0 f_0(\mathbf{P}[k], P^{\text{req}}[k]) + c_1 (f_1(\mathbf{P}[k], \mathbf{\Lambda}[k]) + f_2(\mathbf{\Omega}[k], \mathbf{R}[k], \hat{\mathbf{P}}[k]) + f_3(\mathbf{P}[k])) \quad (3.1)$$

$$\text{s.t. } P_i^{\min} \omega_i[k] \leq P_i[k] \leq P_i^{\max} \omega_i[k] \quad (3.2)$$

$$\omega_i[k] \in \{0, 1\}, \forall i \in \mathcal{C}[k] \quad (3.3)$$

where

- $\mathcal{C}[k]$ is the collection of EVs that are unlocked at time k (just before starting a new computation of setpoints),
- $\mathbf{P}[k]$ is the collection of setpoints $P_i[k]$ that will be computed for each EV in $\mathcal{C}[k]$,
- $\hat{\mathbf{P}}[k]$ collects measured powers $\hat{P}_i[k]$ for all EVs,
- $\mathbf{\Omega}[k]$ is the collection of on/off decisions that will be computed for each EV in $\mathcal{C}[k]$,
- $\mathbf{\Lambda}[k] = (\lambda_i[k])_{i=1,2..}$ and $\mathbf{R}[k] = (\rho_i[k])_{i=1,2..}$,
- functions f_0, f_1, f_2, f_3 , and parameters $c_0, c_1 > 0$ will be described in next subsections.

Note that this optimization is a mixed-integer problem due to the presence of the collection of binary control variables $\mathbf{\Omega}[k]$. In addition, this problem is online, with $\lambda_i[k]$ and $\rho_i[k]$ being the proxies for the history and future, respectively.

3.3.1 Aggregated Power-Setpoint Tracking

The first term in (3.1) is responsible for tracking the aggregated power-setpoint $P^{\text{req}}[k]$. As the locked EVs either react to or implement a previous setpoint, they cannot follow a setpoint and should be removed from the aggregated setpoint, i.e. $\tilde{P}^{\text{req}}[k] = P^{\text{req}}[k] - \sum_{i \in \mathcal{L}[k]} P_i[k]$, where $\mathcal{L}[k]$ collects all the locked EVs. In this case, $P_i[k]$ represents the

very last setpoint that a locked EV has received. This impedes the CS from reallocating the same power in the unlocked EVs. Finally, f_0 can be expressed as

$$f_0(\mathbf{P}[k], P^{\text{req}}[k]) = \left(\tilde{P}^{\text{req}}[k] - \sum_{i \in \mathbf{C}[k]} P_i[k] \right)^2 \quad (3.4)$$

Note that, in this case, the aggregated setpoint might not be followed exactly, due to the delays mentioned in Section 3.2.2. However, such uncertainty can be informed to the grid controller, in order to use it in its setpoint-computation process. In Section 3.5, we explain how this uncertainty is computed.

3.3.2 Battery Wear

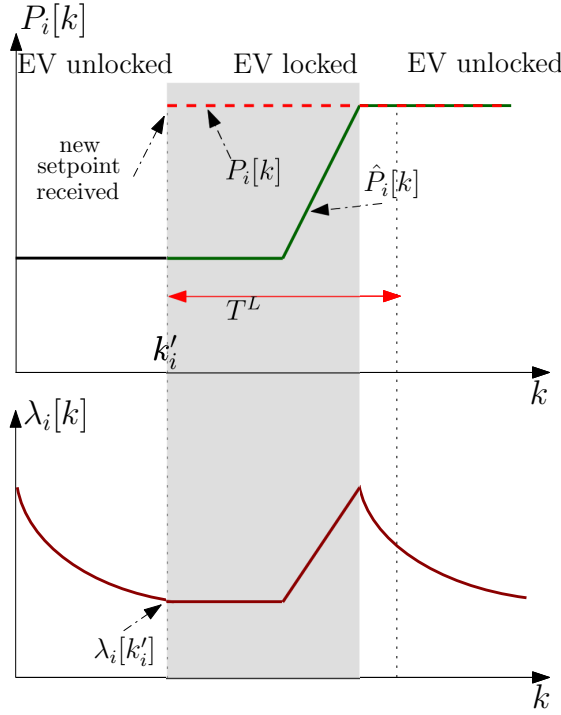
In order to minimize the impact of changing power in the EV batteries, we use f_1 and f_2 in the objective function. f_1 penalizes the deviation between the setpoint and the measured power, together with the changes in the measured power. f_2 penalizes sudden switch off of the EVs caused by the CS. To formalize f_1 and f_2 , let us introduce new variables. As our method is online, we introduce two *non-linear* integral terms to account for (i) the past behaviour of EVs' charging power, and (ii) the desire of an EV to be charged.

The first of these terms, $\lambda_i[k] \in [0.5, 1]$ per EV i , quantifies how long ago and how large the power changes were. This is used as a priority metric: the smaller λ_i is, the more priority to change power there is. Let k'_i be the time of the most recent change of the setpoint for EV i before k (so that $P_i[\kappa] = P_i[k'_i]$ for $\kappa = k'_i, k'_i + 1, \dots, k - 1$). Note that k'_i is also a function of k but, for the ease of notation, we drop this dependency. When EV i arrives, $P_i[k'_i]$ is set to zero. Consequently, we take

$$\lambda_i[k] = \begin{cases} \lambda_i[k'_i] + \left(\frac{|\hat{P}_i[k] - \hat{P}_i[k'_i]|}{P_i^{\text{max}}} \right) (1 - \lambda_i[k'_i]), \\ \quad \text{if } |\hat{P}_i[k] - \hat{P}_i[k'_i]| > \epsilon \text{ and } k - k'_i < T^L \\ (\lambda_i[k - 1] - 0.5)\delta + 0.5, \text{ otherwise.} \end{cases} \quad (3.5)$$

The first case of Eq. (3.5) occurs when EV i is locked and the setpoint is not yet implemented¹. In this case, $\lambda_i[k]$ increases linearly with respect to the implemented power change (grey area on Fig. 3.2). It is defined by the following conditions: (i) if $\hat{P}_i[k] = \hat{P}_i[k'_i]$, then $\lambda_i[k] = \lambda_i[k'_i]$, and (ii) if $|\hat{P}_i[k] - \hat{P}_i[k'_i]| = P_i^{\text{max}}$, then $\lambda_i[k] = 1$. In the second case, $\lambda_i[k]$ decreases exponentially with a decay δ (see Fig. 3.2). Observe that the right-hand side of Eq. (3.5) is always in $[0.5, 1]$.

¹ $\epsilon = 100$ W is a pertinent safety margin.


 Figure 3.2 – Evolution of $\lambda_i[k]$.

f_1 uses the term $P_i[k] - \hat{P}_i[k]$ and $f_1(\mathbf{P}[k], \mathbf{\Lambda}[k])$ as follows

$$f_1(\mathbf{P}[k], \mathbf{\Lambda}[k]) = \sum_{i \in \mathcal{C}[k]} (P_i[k] - \hat{P}_i[k])^2 \lambda_i[k]. \quad (3.6)$$

The second term, $\rho_i[k] \in [0.5, 1]$, expresses the desire of an EV i to charge. It is also used as a priority metric: the larger the ρ_i is the higher the priority to increase the power is. Note that, the CS can keep track of the remaining energy demand $\Delta E_i^{\text{dem}}[k]$ of EV i at time k , and expected remaining charging time $k_i^{\text{dep}} - k$. Therefore at time k , the CS computes the power that EV i needs to satisfy its demand as $\Delta E_i^{\text{dem}}[k]/(k_i^{\text{dep}} - k)$. And, for $k = k_i^{\text{arr}}$ this power equals $\Delta E_i^{\text{dem}}[k_i^{\text{arr}}]/(k_i^{\text{dep}} - k_i^{\text{arr}})$. With this, we compute the unit-less quantity per EV as follows

$$\zeta_i[k] = \frac{1}{P_i^{\text{max}}} H \left(\frac{\Delta E_i^{\text{dem}}[k_i^{\text{arr}}]}{k_i^{\text{dep}} - k_i^{\text{arr}}}, \frac{\Delta E_i^{\text{dem}}[k]}{k_i^{\text{dep}} - k} \right), \quad (3.7)$$

where H represents the harmonic mean. By property of the harmonic mean, $\zeta_i[k] \in \left[0, \frac{2\Delta E_i^{\text{dem}}[k_i^{\text{arr}}]}{P_i^{\text{max}}(k_i^{\text{dep}} - k_i^{\text{arr}})} \right]$, which depends on the initial state of an EV. Moreover, $\zeta_i[k]$ is monotonically increasing function of $\Delta E_i^{\text{dem}}[k]/(k_i^{\text{dep}} - k)$. Consequently,

$$\rho_i[k] = 0.5 + \zeta_i[k]/(2 \max_{i \in \mathcal{C}[k]} \zeta_i[k]). \quad (3.8)$$

f_2 , which penalises the switch off of EVs, is expressed as

$$f_2(\mathbf{\Omega}[k], \mathbf{R}[k], \hat{\mathbf{P}}[k]) = \sum_{i \in \mathcal{C}[k]} (1 - \omega_i[k]) \omega_i[k-1] \rho_i[k] \hat{P}_i^2[k]. \quad (3.9)$$

We multiply each term by $\rho_i[k]$ to enforce EVs with larger values to be switched off at last. We also multiply by $\omega_i[k-1]$ to exclude EVs that are switched off.

3.3.3 Fair Allocation of Charging Power

The aggregated power setpoint P^{req} must be allocated fairly among EVs. In order to anticipate the future information, we allocate the power by using ζ_i as a weight for EV i . To this end, at time k , we compute *reference powers*, $P_i^{\text{ref}}[k] \in [0, P_i^{\text{max}}]$ for all EVs, ideally fair such that $\sum_{i \in \mathcal{C}[k] \cup \mathcal{L}[k]} P_i^{\text{ref}}[k] = P^{\text{req}}[k]$. It should be noticed that if $P^{\text{req}} = 0$, then reference powers of all EVs are also equal to 0. Commonly used fair allocations are *weighted-proportional* and *weighted-max-min* [41]. It is sometimes difficult to choose between the two. In our specific case, we show that both are identical.

Let us first describe the weighted-max-min fair allocation. As the set of constraints is convex and compact², we know that this allocation exists and is unique [41]. In order to find such an allocation, the *water-filling* algorithm is used, which works as follows. The power of all EVs is increased at the same pace, until one or more powers reach their maximum. The powers that reach their maximum are frozen, and the others continue to increase at the same pace. The algorithm is repeated until $\sum_{i \in \mathcal{C} \cup \mathcal{L}} P_i^{\text{ref}} = P^{\text{req}}$ (henceforth, the time index k is omitted for simplicity of notation). For details, see Fig. 3.3. Here, we use again ζ_i to prioritize the EVs that need to be charged to satisfy their demand. Each EV i is represented as a water tank of width ζ_i and height $\frac{P_i^{\text{max}}}{\zeta_i}$, the volume of the tank is P_i^{max} . The volume of the water in tank is either P_i^{max} or $h\zeta_i$, where h is the common height of the non-saturated tanks. Note that the EV with $\zeta_i = 0$ is charged fully and, therefore it no longer needs to be considered in the allocation.

Another possibility is to consider weighted-proportional fairness. We find a proportionally fair allocation of power by solving the following convex optimization-problem in (A):

$$\begin{aligned} \text{(A)} \quad & \max_{P_i^{\text{ref}}} \sum_{i \in \mathcal{C} \cup \mathcal{L}} \zeta_i \log P_i^{\text{ref}} \\ & \text{s.t. } 0 < P_i^{\text{ref}} \leq P_i^{\text{max}} \end{aligned} \quad (3.10)$$

$$\sum_{i \in \mathcal{C} \cup \mathcal{L}} P_i^{\text{ref}} = P^{\text{req}} \quad (3.11)$$

²i.e., closed and bounded in Euclidean space.

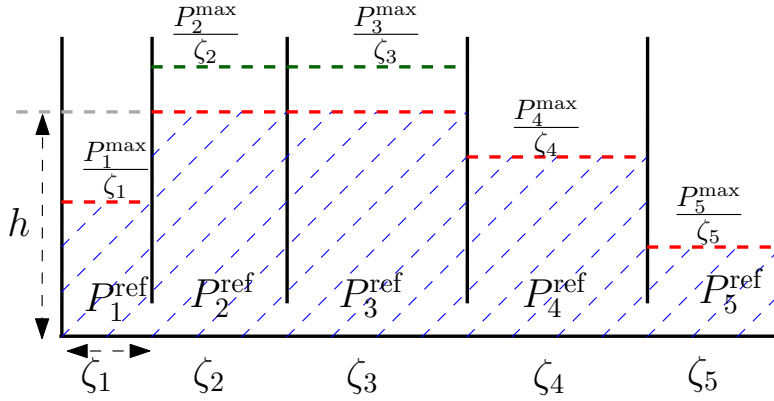


Figure 3.3 – Result of the water-filling algorithm for 5 EVs. EVs 1, 4 and 5 are fully filled, whereas 2 and 3 have reference powers of $h\zeta_2$ and $h\zeta_3$, respectively. The reference powers $P_1^{\text{ref}}, P_2^{\text{ref}}, P_3^{\text{ref}}, P_4^{\text{ref}}, P_5^{\text{ref}}$ are in kW.

We next prove that the above weighted-proportional and weighted-max-min fair allocations are equivalent. This means that it is possible to find the fair allocation by either solving the optimization problem (A) or water-filling.

Theorem 3.1. *Weighted-proportional and weighted-max-min fair allocations, as defined above, are equivalent.*

Proof. Let P_i^{ref} be a weighted-proportional fair allocation. To compute this solution, we first get the Lagrangian of (A)

$$L(x, \eta) = - \sum_{i \in \mathcal{C} \cup \mathcal{L}} \zeta_i \log P_i^{\text{ref}} + \eta \left(\sum_{i \in \mathcal{C} \cup \mathcal{L}} P_i^{\text{ref}} - P^{\text{req}} \right) \quad (3.12)$$

where $0 < P_i^{\text{ref}} \leq P_i^{\text{max}}$ and η is the Lagrange multiplier. The solution of the problem is

$$P_i^{\text{ref}} = \begin{cases} \frac{\zeta_i}{\eta} & \text{if } \frac{\zeta_i}{\eta} \in [0, P_i^{\text{max}}] \\ P_i^{\text{max}} & \text{otherwise} \end{cases} \quad (3.13)$$

Next, we show that the solution in (3.13) follows the definition of weighted-max-min fairness in [41]. Mainly, we show that increasing one component i is at the expense of decreasing other component j such that $P_j^{\text{ref}}/\zeta_j \leq P_i^{\text{ref}}/\zeta_i$. By (3.13), P_i^{ref} is either $\frac{\zeta_i}{\eta}$ or P_i^{max} . If $P_i^{\text{ref}} = P_i^{\text{max}}$, this component cannot be increased. Let us consider the case when $P_i^{\text{ref}} = \frac{\zeta_i}{\eta}$. If we increase the power of EV i , we have to decrease the power of at least one other EV, say j , to satisfy constraint (3.11). There are also two cases for EV j : either $P_j^{\text{ref}} = \frac{\zeta_j}{\eta}$ or $P_j^{\text{ref}} = P_j^{\text{max}}$.

If $P_j^{\text{ref}} = \frac{\zeta_j}{\eta}$, then $\frac{P_j^{\text{ref}}}{\zeta_j} = \frac{P_i^{\text{ref}}}{\zeta_i} = \frac{1}{\eta}$. Hence, the inequality in weighted-max-min fairness definition holds. If $P_j^{\text{ref}} = P_j^{\text{max}}$, then $P_j^{\text{ref}} \leq \frac{\zeta_j}{\eta}$. Dividing each part by ζ_j gives

that: $\frac{P_j^{\text{ref}}}{\zeta_j} \leq \frac{1}{\eta} = \frac{P_i^{\text{ref}}}{\zeta_i}$. Therefore, in both cases the inequality holds, proving that the two types of fairness give the same results. \square

Finally, after computing the fair allocation $P_i^{\text{ref}}[k]$, we construct, at every time-step k , f_3 as follows:

$$f_3(\mathbf{P}[k]) = \sum_{i \in \mathcal{C}[k]} (P_i[k] - P_i^{\text{ref}}[k])^2. \quad (3.14)$$

3.3.4 Full Formulation

By combining (3.1), (3.4), (3.6), (3.9), (3.14) with constraints (3.2), (3.3), the optimization problem to be solved, at each time k , is

$$\begin{aligned}
 (\mathbf{P}) \quad & \min_{P_i[k], \omega_i[k]} \quad c_0 \left(\tilde{P}^{\text{req}}[k] - \sum_{i \in \mathcal{C}[k]} P_i[k] \right)^2 \rightarrow \text{reference tracking} \\
 & \text{battery wear} \leftarrow \begin{cases} +c_1 \left(\sum_{i \in \mathcal{C}[k]} (P_i[k] - \hat{P}_i[k])^2 \lambda_i[k] \right. \\ \left. + \sum_{i \in \mathcal{C}[k]} (1 - \omega_i[k]) \omega_i[k-1] \rho_i[k] \hat{P}_i^2[k] \right) \\ \text{fair allocation} \leftarrow + \sum_{i \in \mathcal{C}[k]} (P_i[k] - P_i^{\text{ref}}[k])^2 \end{cases} \quad (3.15)
 \end{aligned}$$

$$\text{s.t. (3.2) -- (3.3)} \quad (3.16)$$

3.4 Real-Time Implementation Aspects

3.4.1 Reducing the Number of Integer Variables

As (\mathbf{P}) is mixed-integer, its complexity grows exponentially with the number of integer variables [130] (here ω_i). To reduce the problem complexity, we propose a heuristic that runs at every time k and limits the number of integer variables. The heuristic partitions the collection of unlocked EVs, $\mathcal{C}[k]$, into three collections: EVs that are forced to be switched (or remain) on ($\mathcal{S}^{\text{on}}[k]$), EVs that are forced to be switched (or remain) off ($\mathcal{S}^{\text{off}}[k]$), and EVs for which the on/off decision is decided by the optimization problem ($\mathcal{S}[k]$). We require that $|\mathcal{S}[k]| \leq m$, where m is fixed small number (e.g., $m \leq 10$).

In other words, we define a new problem (\mathbf{H}) that has at most m integer variables.

Chapter 3. Real-Time Control of an Electric-Vehicle Charging Station

All other $\omega_i[k]$ remain fixed.

$$(\mathbf{H}) \min_{P_i[k], \omega_i[k]} \quad (3.15)$$

s.t. (3.2), (3.3)

$$\omega_i[k] = 1, \forall i \in \mathcal{S}^{\text{on}}[k], \quad \omega_j[k] = 0, \forall j \in \mathcal{S}^{\text{off}}[k] \quad (3.17)$$

The constraints in (3.17) force the corresponding EVs to be switched on/off.

Note that, with this consideration, the flexibility that the problem (\mathbf{H}) considers is, however, smaller than that of (\mathbf{P}) . Specifically, the power to be allocated among the unlocked EVs, $\tilde{P}^{\text{req}}[k]$, might not be able to be tracked, depending on the partition of \mathcal{C} . Let us thus define the full flexibility of the CS at time k , as \mathcal{F} (see Section 3.5.2), and the reduced flexibility (the one available for (\mathbf{H})), as the interval $[P^{\text{lb}}, P^{\text{ub}}]$ with

$$P^{\text{lb}} = \sum_{i \in \mathcal{S}^{\text{on}}[k]} P_i^{\text{min}}, \quad P^{\text{ub}} = \sum_{i \in \mathcal{S}^{\text{on}}[k] \cup \mathcal{S}[k]} P_i^{\text{max}}. \quad (3.18)$$

Thus, the partition $\{\mathcal{S}[k], \mathcal{S}^{\text{on}}[k], \mathcal{S}^{\text{off}}[k]\}$ should ensure that $\tilde{P}^{\text{req}}[k] \in [P^{\text{lb}}, P^{\text{ub}}]$. Note that we compute the bounds excluding locked EVs. Their power is already defined, as explained in Section 3.3.3.

We now describe the heuristic, detailed in Alg. 1. First, we define a metric that takes into account both the past behaviour of the EVs power and their desire to be charged, as follows:

$$\mu_i[k] = \lambda_i[k] + (1 - \omega_i[k-1])(1.5 - \rho_i[k]) + \omega_i[k-1]\rho_i[k], \quad (3.19)$$

with $\mu_i[k] \in [1, 2]$, unit-less, and consisting of three parts:

- $\lambda_i[k]$ contains information about the past behaviour of the charging power. Smaller $\lambda_i[k]$ means that EV i is more prone to change its power,
- $(1 - \omega_i[k-1])(1.5 - \rho_i[k])$ identifies the propensity of a switched-off EV to switch on,
- $\omega_i[k-1]\rho_i[k]$ identifies the propensity of a switched-on EV to switch off.

Therefore, $\mu_i[k]$ quantifies the propensity of EV i to change its on/off decision and charging power. Smaller $\mu_i[k]$ indicates more propensity.

Second, we rank the EVs according to their individual operational margins. As the maximum power an EV i can consume is P_i^{max} and the minimum is 0, its positive margin is $P_i^{\text{max}} - \hat{P}_i[k]$ and its negative margin is $\hat{P}_i[k]$. By dividing these values by

Algorithm 1 Heuristic for partitioning $\mathcal{C}[k]$.

Input: $\mathcal{C}[k]$, $m \geq 1$, $0 \leq \tilde{P}^{\text{req}}[k] \leq \sum_{i \in \mathcal{C}[k]} P_i^{\text{max}}$

Output: partition $\mathcal{S}[k]$, $\mathcal{S}^{\text{on}}[k]$, $\mathcal{S}^{\text{off}}[k]$ of $\mathcal{C}[k]$, such that $|\mathcal{S}[k]| \leq m$ and $\tilde{P}^{\text{req}}[k] \in [P^{\text{lb}}, P^{\text{ub}}]$ computed in (3.18)

- 1: **if** $|\mathcal{C}[k]| \leq m$ **then**
- 2: $\mathcal{S}[k] = \mathcal{C}[k]$, $\mathcal{S}^{\text{on}}[k] = \mathcal{S}^{\text{off}}[k] = \emptyset$,
- 3: stop algorithm.
- 4: **else**
- 5: $\mathcal{S}[k] = \text{top}(\mathcal{C}[k], m)$,
- 6: $\mathcal{S}^{\text{on}}[k] = \{i \mid i \in \mathcal{R}, \omega_i[k-1] = 1\}$,
- 7: $\mathcal{S}^{\text{off}}[k] = \{i \mid i \in \mathcal{R}, \omega_i[k-1] = 0\}$,
- 8: let $\mathcal{R} = \mathcal{C}[k] \setminus \mathcal{S}[k]$.
- 9: **end if**
- 10: compute reduced flexibility bounds as in (3.18).
- 11: **while** $\tilde{P}^{\text{req}}[k] \notin [P^{\text{lb}}, P^{\text{ub}}]$ **and** $\mathcal{R} \neq \emptyset$ **do**
- 12: $i = \text{top}(\mathcal{R}, 1)$, $j = \text{top}(\mathcal{S}[k], 1)$
- 13: **if** $\tilde{P}^{\text{req}}[k] > P^{\text{ub}}$ **then**
- 14: $\mathcal{S}^{\text{on}}[k] = \mathcal{S}^{\text{on}}[k] \cup \{j\}$
- 15: **else if** $\tilde{P}^{\text{req}}[k] < P^{\text{lb}}$ **then**
- 16: $\mathcal{S}^{\text{off}}[k] = \mathcal{S}^{\text{off}}[k] \cup \{j\}$
- 17: **end if**
- 18: update $\mathcal{S}[k] = \mathcal{S}[k] \cup \{i\} \setminus \{j\}$
- 19: **if** $i \in \mathcal{S}^{\text{on}}[k]$ **then**
- 20: remove i from $\mathcal{S}^{\text{on}}[k]$
- 21: **else**
- 22: remove i from $\mathcal{S}^{\text{off}}[k]$
- 23: **end if**
- 24: recompute bounds according to (3.18)
- 25: update $\mathcal{R} = \mathcal{R} \setminus \{i\}$
- 26: **end while**

P_i^{max} , we obtain normalized margins. Therefore, we introduce the ranking metric $r_i[k]$, which combines the operational margins with $\mu_i[k]$:

$$r_i[k] = \begin{cases} \frac{\hat{P}_i[k]}{P_i^{\text{max}} \mu_i[k]} & \text{if } \Delta P^{\text{req}}[k] < 0, \\ \frac{P_i^{\text{max}} - \hat{P}_i[k]}{P_i^{\text{max}} \mu_i[k]} & \text{otherwise,} \end{cases} \quad (3.20)$$

where $\Delta P^{\text{req}}[k] = \tilde{P}^{\text{req}}[k] - \sum_{i \in \mathcal{C}[k]} \hat{P}_i[k]$. Finally, we define the function $\text{top}(\mathcal{X}, m)$ that returns the index of the m elements with the largest $r_i[k]$ metric, from a collection \mathcal{X} . In the rest of this section, for sake of clarity, we omit the time index k .

The purpose of the heuristic is to limit the number of integer variables to m . If the amount of unlocked EVs is initially less than m , then all these EVs can change their on/off decision (lines 2-3). Otherwise, we take the m EVs with the largest metric r_i (lines 5-8). This choice is sufficient in most of the cases as, according to r_i , these EVs

are the best to be selected. However, it can happen that $\tilde{P}^{\text{req}} \notin [P^{\text{lb}}, P^{\text{ub}}]$. In which case, we loop until fulfilling this constraint. If \tilde{P}^{req} lies above the bounds, we force the EV from \mathcal{S} with highest rank to be switched on and replace it with highest ranked EV in $\mathcal{R} = \mathcal{C} \setminus \mathcal{S}$ (lines 12-14, 18-19). Doing this, we automatically increase P^{ub} , eventually reaching \tilde{P}^{req} (see Theorem 3.2). Similarly, if \tilde{P}^{req} lies below the bounds, we switch off the highest ranked EV from \mathcal{S} (lines 15-17) and replace it with the highest ranked EV in \mathcal{R} .

Theorem 3.2 (Correctness of the heuristic). *Given that $m \geq 1$, Alg. 1 finds a partition $\mathcal{S}, \mathcal{S}^{\text{on}}, \mathcal{S}^{\text{off}}$ of \mathcal{C} , such that $\tilde{P}^{\text{req}} \in [P^{\text{lb}}, P^{\text{ub}}]$, $|\mathcal{S}| \leq m$. Alg. 1 takes at most $|\mathcal{C}| - m$ iterations.*

Proof. Let ℓ be the number of iterations in the while loop between lines 11-26. $\ell = 0$, when the while loop is not executed. If Alg. 1 enters the loop, we increment ℓ just before executing line 12. Denote $\mathcal{S}^{(\ell)}, \mathcal{S}^{\text{on},(\ell)}, \mathcal{S}^{\text{off},(\ell)}, \mathcal{R}^{(\ell)}$ the state of collections and $[P^{\text{lb},(\ell)}, P^{\text{ub},(\ell)}]$ the state of bounds, at the end of the ℓ -th iteration. $\mathcal{S}^{(0)}, \mathcal{S}^{\text{on},(0)}, \mathcal{S}^{\text{off},(0)}, \mathcal{R}^{(0)}, [P^{\text{lb},(0)}, P^{\text{ub},(0)}]$ are initial states of collections and bounds.

We now prove the following 5 statements (S1-S5):

(S1) For every $\ell \geq 0$

$$\mathcal{R}^{(\ell)} \subseteq \mathcal{S}^{\text{on},(\ell)} \cup \mathcal{S}^{\text{off},(\ell)}. \quad (3.21)$$

Indeed, for $\ell = 0$, (3.21) holds by lines 7, 8. Assume that (3.21) holds at $\ell - 1$. We remove one element from $\mathcal{R}^{(\ell-1)}$ and either from $\mathcal{S}^{\text{on},(\ell-1)}$ or $\mathcal{S}^{\text{off},(\ell-1)}$ (lines 20,22). Thus, (3.21) holds at ℓ .

(S2) For every $\ell \geq 0$, $\mathcal{S}^{(\ell)}, \mathcal{S}^{\text{on},(\ell)}, \mathcal{S}^{\text{off},(\ell)}$ is partition of \mathcal{C}

$$\mathcal{C} = \mathcal{S}^{(\ell)} \cup \mathcal{S}^{\text{on},(\ell)} \cup \mathcal{S}^{\text{off},(\ell)}, \quad (3.22)$$

$$\mathcal{S}^{(\ell)} \cap (\mathcal{S}^{\text{on},(\ell)} \cup \mathcal{S}^{\text{off},(\ell)}) = \emptyset, \quad (3.23)$$

$$\mathcal{S}^{\text{on},(\ell)} \cap \mathcal{S}^{\text{off},(\ell)} = \emptyset. \quad (3.24)$$

Indeed, for $\ell = 0$, $\mathcal{S}^{(0)}, \mathcal{S}^{\text{on},(0)}, \mathcal{S}^{\text{off},(0)}$ is a partition of \mathcal{C} by construction. Assume that (3.22)-(3.24) hold at $(\ell - 1)$. Then, $\mathcal{S}^{(\ell)} = \mathcal{S}^{(\ell-1)} \cup \{i\} \setminus \{j\}$ (line 18) and $\mathcal{S}^{\text{off},(\ell)} \cup \mathcal{S}^{\text{on},(\ell)} = \mathcal{S}^{\text{off},(\ell-1)} \cup \mathcal{S}^{\text{on},(\ell-1)} \cup \{j\} \setminus \{i\}$ (lines 13-17, 19-23). Since $j \in \mathcal{S}^{(\ell-1)}$ and, by (3.21), $i \in \mathcal{S}^{\text{on},(\ell-1)} \cup \mathcal{S}^{\text{off},(\ell-1)}$ (3.22) and (3.23) holds at ℓ . Also, we take j from $\mathcal{S}^{(\ell-1)}$ and move it either to $\mathcal{S}^{\text{on},(\ell-1)}$ (line 14) or $\mathcal{S}^{\text{off},(\ell-1)}$ (line 16), then (3.24) holds at ℓ .

(S3) If Alg. 1 visits line 14 at iteration ℓ , then $P^{\text{ub},(\ell-1)} \in [P^{\text{lb},(\ell)}, P^{\text{ub},(\ell)}]$ and, if it visits line 16 at iteration ℓ , then $P^{\text{lb},(\ell-1)} \in [P^{\text{lb},(\ell)}, P^{\text{ub},(\ell)}]$.

Let us show (S3) in the first case, i.e., that $P^{\text{ub},(\ell-1)} \leq P^{\text{ub},(\ell)}$ and $P^{\text{ub},(\ell-1)} \geq P^{\text{lb},(\ell)}$.

To this end, let us first check how $\mathcal{S}^{\text{on},(\ell-1)}$ and $\mathcal{S}^{(\ell-1)}$ are changed by Alg. 1. We take i from $\mathcal{R}^{(\ell-1)}$ (line 12) and add it to $\mathcal{S}^{(\ell-1)}$. Also, we move j from $\mathcal{S}^{(\ell-1)}$ to $\mathcal{S}^{\text{on},(\ell-1)}$. Then, we have two cases, since i can be either from $\mathcal{S}^{\text{on},(\ell-1)}$ or $\mathcal{S}^{\text{off},(\ell-1)}$ (see (3.21) and (3.24)). If $i \in \mathcal{S}^{\text{on},(\ell-1)}$, then $\mathcal{S}^{\text{on},(\ell)} = \mathcal{S}^{\text{on},(\ell-1)} \cup \{j\} \setminus \{i\}$ and $\mathcal{S}^{(\ell)} = \mathcal{S}^{(\ell-1)} \cup \{i\} \setminus \{j\}$, hence $\mathcal{S}^{(\ell)} \cup \mathcal{S}^{\text{on},(\ell)} = \mathcal{S}^{(\ell-1)} \cup \mathcal{S}^{\text{on},(\ell-1)}$. According to (3.18) $P^{\text{ub},(\ell-1)} = P^{\text{ub},(\ell)}$. Rewrite expressions in (3.18) for $P^{\text{ub},(\ell-1)}$ and $P^{\text{lb},(\ell)}$

$$P^{\text{ub},(\ell-1)} = \sum_{j' \in \mathcal{S}^{\text{on},(\ell-1)}} P_{j'}^{\text{max}} + \sum_{j' \in \mathcal{S}^{(\ell-1)} \setminus \{j\}} P_{j'}^{\text{max}} + P_j^{\text{max}} \quad (3.25)$$

$$P^{\text{lb},(\ell)} = \sum_{j' \in \mathcal{S}^{\text{on},(\ell-1)} \cup \{j\} \setminus \{i\}} P_{j'}^{\text{min}} = P^{\text{lb},(\ell-1)} - P_i^{\text{min}} + P_j^{\text{min}} \quad (3.26)$$

By inspecting (3.25) and (3.26) term by term, we see that each term in (3.25) is not smaller than the corresponding term in (3.26).

If $i \in \mathcal{S}^{\text{off},(\ell-1)}$ then $\mathcal{S}^{\text{on},(\ell)} = \mathcal{S}^{\text{on},(\ell-1)} \cup \{j\}$ and $\mathcal{S}^{(\ell)} \cup \mathcal{S}^{\text{on},(\ell)} = \mathcal{S}^{(\ell-1)} \cup \mathcal{S}^{\text{on},(\ell-1)} \cup \{i\}$. By (3.18) $P^{\text{ub},(\ell-1)} \leq P^{\text{ub},(\ell)}$,

$$P^{\text{lb},(\ell)} = \sum_{j' \in \mathcal{S}^{\text{on},(\ell-1)} \cup \{j\}} P_{j'}^{\text{min}} = P^{\text{lb},(\ell-1)} + P_j^{\text{min}} \quad (3.27)$$

Comparing (3.25) and (3.27), we get $P^{\text{ub},(\ell-1)} \geq P^{\text{lb},(\ell)}$, which concludes the proof. The proof is similar in the case when algorithm visits line 16.

(S4) If Alg. 1 visits line 14, it will never visit line 16 and vice versa.

Assume that Alg. 1 visits line 14 at iteration $\ell - 1$. From (S3) we know that $P^{\text{lb},(\ell-1)} \in [P^{\text{lb},(\ell)}, P^{\text{ub},(\ell)}]$. We will prove (S4) by contradiction. Assume that Alg. 1 visits line 16 at ℓ , i.e., $\tilde{P}^{\text{req}} < P^{\text{lb},(\ell)}$. Then, $P^{\text{ub},(\ell-1)} < \tilde{P}^{\text{req}} < P^{\text{lb},(\ell)}$ (see Fig. 3.4(a)). This is impossible because $P^{\text{lb},(\ell)} \leq P^{\text{ub},(\ell-1)}$ according to (S3). Similarly, the case for line 16 can be proven (Fig. 3.4(b)).

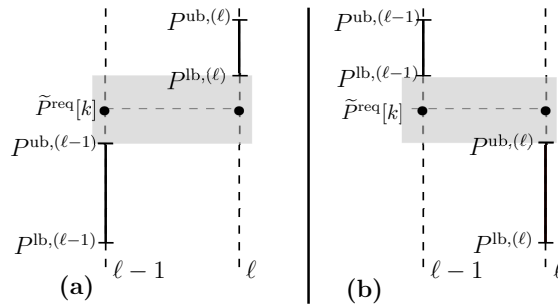


Figure 3.4 – Proof of statement (S4).

(S5) If Alg. 1 terminates with empty $\mathcal{R}^{(\ell)}$, then $\tilde{P}^{\text{req}} \in [P^{\text{lb},(\ell)}, P^{\text{ub},(\ell)}]$.

Let us prove (S5) when algorithm visits line 14 (similar for line 16). a) We show that $\mathcal{S}^{\text{off},(\ell)} \subset \mathcal{R}^{(\ell)}$ at every iteration ℓ . If $\ell = 0$ it is true by construction. Let us assume that $\mathcal{S}^{\text{off},(\ell-1)} \subset \mathcal{R}^{(\ell-1)}$ at $\ell - 1$. According to (S4), if Alg. 1 visits line 14 it will never visit line 16, so no new elements are added to $\mathcal{S}^{\text{off},(\ell-1)}$. Next, if $i \in \mathcal{S}^{\text{on},(\ell-1)}$, $\mathcal{S}^{\text{off},(\ell)} = \mathcal{S}^{\text{off},(\ell-1)}$, else (i.e., if $i \in \mathcal{S}^{\text{off},(\ell-1)}$), $\mathcal{S}^{\text{off},(\ell)} = \mathcal{S}^{\text{off},(\ell-1)} \setminus \{i\}$. Also $\mathcal{R}^{(\ell)} = \mathcal{R}^{(\ell-1)} \setminus \{i\}$. Thus, $\mathcal{S}^{\text{off},(\ell)} \subset \mathcal{R}^{(\ell)}$. Let L be the value of ℓ when Alg. 1 terminates and $\mathcal{R}^{(L)} = \emptyset$, therefore $\mathcal{S}^{\text{off},(L)} = \emptyset$, thus $\mathcal{C} = \mathcal{S}^{\text{on},(L)} \cup \mathcal{S}^{(L)}$ and $P^{\text{ub},(L)} = \sum_{i \in \mathcal{C}} P_i^{\text{max}}$. According to the input conditions $\tilde{P}^{\text{req}} \leq P^{\text{ub},(L)}$. Let us show that $\tilde{P}^{\text{req}} \geq P^{\text{lb},(L)}$. Indeed, according to (S4) Alg. 1 visited line 14 on iteration $L - 1$, therefore by (S3) $P^{\text{lb},(L)} \leq P^{\text{ub},(L-1)} < \tilde{P}^{\text{req}}$.

We can now complete the proof by observing that Alg. 1 terminates either when $\tilde{P}^{\text{req}} \in [P^{\text{lb},(\ell)}, P^{\text{ub},(\ell)}]$ or because $\mathcal{R}^\ell = \emptyset$. However, by (S5) we also have that $\tilde{P}^{\text{req}} \in [P^{\text{lb},(\ell)}, P^{\text{ub},(\ell)}]$. Moreover, Alg. 1 removes 1 element from \mathcal{R} at every iteration. The initial amount of elements in \mathcal{R} is $|\mathcal{C}| - m$, then it will terminate in at most $|\mathcal{C}| - m$ iterations. \square

After constructing $\{\mathcal{S}, \mathcal{S}^{\text{on}}, \mathcal{S}^{\text{off}}\}$, we solve problem (H) by using Branch-and-Bound [130].

3.5 Validation

3.5.1 Simulation Setup

To validate our method, we consider a grid with an existing 500 kWp PV plant connected to the distribution network through a power transformer rated $S_{\text{Tr}}^r = 500 \text{ kVA}$ ³. The CS has a power rating $P_{\text{CS}}^r = 1000 \text{ kW}$; this is a stress test for our method, as the CS has to opportunistically use all available power. The CS has 60 slots of 22 kW max.

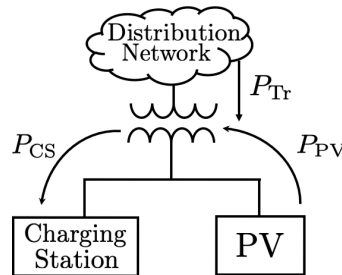


Figure 3.5 – Structure of the grid. The arrows show the positive directions of the corresponding active-power flows.

To simulate the PV production, we use real irradiance measurements taken in our

³Note that we do not consider grid constraints other than the transformer rated power.

laboratory; they are then normalized according to the PV rated power. We simulate the arrival of EVs to the CS as a homogeneous Poisson process with a rate of 30 arrivals/hour (see Fig. 3.6(d)). We assume that, upon arrival (at k_i^{arr}), EV i informs the CS of its energy-demand ΔE_i and the expected departure-time k_i^{dep} . We model the expected staying-time ($k_i^{\text{dep}} - k_i^{\text{arr}}$) to be uniformly distributed between 1.5 and 1.6 hours. This assumption has been made only for simulation purposes and serves to model the behavior of the different users. Furthermore, we consider that an EV can leave before the informed time. Thus, the real staying-time is uniformly distributed between 1.4 and 1.5 hours in our simulation. An EV will leave after the real staying-time, regardless of its level of charge. The proposed control-scheme does not have access to the information about distributions of expected staying-time and real staying-time; it uses only the exact value of expected staying-time, declared by users. Given the distributions of the arrival time and the staying time, it is highly likely that an EV will find an available slot upon arrival, otherwise this EV is ignored (as in practice this EV will leave for another charging station). In all our simulation scenarios, this property was maintained.

We consider two groups of EVs: group A with high and group B with low energy-demand. The demand is uniformly distributed between 28 and 32 kWh and between 10 and 14 kWh, respectively. Considered reaction times are also uniformly distributed between 2 and 3 s and the ramping rate is 5 kW/s⁴. We also ran simulations that consider different ramping-rates depending on each group: we set 5 kW/s for group A and 15 kW/s for group B. The obtained results show little difference to the results presented in Section 3.5.6, thus ensuring that our method is robust against the change in ramping rates. As these results are almost identical, they are not included in the work. The minimum and maximum powers of the modelled EVs are 2 kW and 22 kW.

We consider 3 scenarios, mainly defined by the PV trace, that are representative enough to show all our method features:

- *regular production*, when the PV production is smooth (see Fig. 3.6(a)),
- *fluctuating production*, when the PV production has high-frequency fluctuations (see Fig. 3.6(b)), e.g., due to clouds,
- *sharp jump*, when, for emergency reasons, part of the PV plant is suddenly disconnected (see Fig. 3.6(c)).

Finally, we analyze the influence of the combinations of weights c_0, c_1 in problem (P) on the method performance.

⁴This rate was taken according to the maximum charging power, such that the EV will reach its maximum power before the locking period finishes.

3.5.2 Model of the Grid Controller

Next, we describe the way we model the decision of the grid controller at time k . We assume that all resources are connected to the same node, thus simplifying the power-balance equation to $P_{\text{Tr}} = P_{\text{CS}} - P_{\text{PV}}$, being P_{Tr} the transformer, P_{PV} the PV plant and P_{CS} the charging station powers, respectively (see Fig. 3.5 for the powers direction convention). The control variable is P_{CS} , whereas the controlled variable is P_{Tr} . The purpose of this controller is to maximize P_{CS} , and to avoid the violation of the transformer rated-power, i.e., $|P_{\text{Tr}}| \leq S_{\text{Tr}}^r$, subject to the uncertainty produced by (i) the variation of the injected PV power and (ii) the charging of locked EVs. We focus on the case when the violation is produced by an overconsumption of the CS. The case when the violation is produced by an overproduction of the PV plant can be handled similarly. Hence, the controller's decision is computed as

$$P^{\text{req}} = P_{\text{Tr}}^r + P_{\text{PV}}^{\downarrow} - \Delta P_{\text{CS}}^{\uparrow}, \quad (3.28)$$

where $P_{\text{PV}}^{\downarrow}$ is the one-step-ahead minimum expected PV production, computed by a short-term forecasting tool [27]. $\Delta P_{\text{CS}}^{\uparrow}$ is the maximum possible consumption increment of locked EVs, i.e., the difference between their individual setpoint and their current measured power

$$\Delta P_{\text{CS}}^{\uparrow} = \sum_{i \in \mathcal{L}^{\uparrow}} P_i - \hat{P}_i, \quad \mathcal{L}^{\uparrow} = \{i \in \mathcal{L} | P_i - \hat{P}_i \geq 0\}. \quad (3.29)$$

This term accounts for the uncertainty of EVs at implementing a setpoint due to the unknown ramping properties of each EV. Finally, the computed setpoint is saturated, depending on the current flexibility of the CS, and it is computed by the CS and sent to the grid controller, represented by the interval

$$\mathcal{F} = \left[\sum_{i \in \mathcal{L}} P_i, \min \left(\sum_{i \in \mathcal{L}} P_i + \sum_{i \in \mathcal{C}} P_i^{\max}, P_{\text{CS}}^r \right) \right]. \quad (3.30)$$

It is worth noting that the flexibility is lower bounded by the locked EVs and upper bounded by the maximum power of the unlocked EVs. The flexibility is not limited by the minimum power and the handling of any setpoint below $\min_i P_i^{\min}$ is ensured by Theorem 2. Besides, the controller cannot instantly ensure that the transformer rated-power will not be violated due to the ramping mechanism of the locked EVs but, in the worst-case scenario, it will take a time T^L (locking period) to regain more flexibility, thus decreasing the consumption.

3.5.3 Performance Evaluation Metrics

As our optimization problem in (H) is multi-objective, we define the following metrics for the performance evaluation:

- *follow-request* – measures how well a CS follows the aggregated power-setpoint

$$M^{\text{fr}} = \frac{1}{K} \sum_{k=1}^K \left| P^{\text{req}}[k] - \hat{P}[k] \right|, \quad (3.31)$$

where K is the amount of discrete time-steps during the selected control period and $\hat{P}[k] = \sum_{i \in \mathcal{C}[k] \cup \mathcal{L}[k]} \hat{P}_i[k]$. This metric is lower bounded by 0. Then, the closer M^{fr} is to 0, the better the CS follows the aggregated setpoint.

- *non-satisfied demand* – measures how well the charging demand of EV i is satisfied

$$M_i^{\text{nsd}} = \Delta E_i[k_i^{\text{stop}}] / \Delta E_i[k_i^{\text{arr}}], \quad (3.32)$$

where $\Delta E_i[k_i^{\text{stop}}]$ is the energy that remains to be satisfied at departure time, and $\Delta E_i[k_i^{\text{arr}}]$ is the initial energy demand. $M_i^{\text{nsd}} \in [0, 1]$. If $M_i^{\text{nsd}} = 1$, then EV i did not charge. On contrary, EV i is fully satisfied if $M_i^{\text{nsd}} = 0$.

- *battery-wear* – measures the changes of the charge power

$$M_i^{\text{bw}} = \frac{1}{2(P_i^{\text{max}})^2} \sum_{k=1}^K (P_i[k] - P_i[k-1])^2. \quad (3.33)$$

This metric shows the effect of the control scheme into the battery life. The closer M_i^{bw} is to 0, the less effect is. If $M_i^{\text{bw}} < 1$ there was no sharp jump of charging power from 0 to P_i^{max} and back.

- *violation* – measures the maximum per-unit operating (hot-spot) temperature of the transformer

$$M^{\text{viol}} = \max_k \left\{ \frac{\theta[k]}{\theta^{\text{rated}}} \right\}, \quad (3.34)$$

where $\theta[k]$ and θ^{rated} are the hot-spot and rated hot-spot transformer temperatures⁵, and $\theta^{\text{rated}} = 160^\circ\text{C}$. As a transformer can be overloaded for short time, this metric shows how the method can exploit this flexibility by respecting the transformer physical limits.

⁵We model the dynamic behaviour of the hot-spot temperature $\theta[k]$ as a first-order dynamic system (see [131, 132]): $\theta[k+1] = \alpha\theta[k] + \beta P_{\text{Tr}}[k] + \gamma\theta^{\text{amb}}[k]$, where θ^{amb} is the ambient temperature. The parameters α , β and γ are estimated using the curves from [132].

3.5.4 Congestion Indication

As the amount of EVs connected to the CS varies in time, this influences the possibility of the CS satisfying the demand of EVs. For instance, there might be many EVs charging at the same time and that have a large energy demand (i.e., congested period). The M_i^{nsd} depends on whether CS is congested or not. If the CS is non-congested, we expect that M_i^{nsd} is close to 0 for all i . Conversely, if $M_i^{\text{nsd}} > 0$, CS is congested. In order to evaluate our method, we define a *congestion* indicator I^{con} . Specifically, I^{con} is an average non-satisfied demand, assuming that the CS is absolutely fair and attempts to charge every EV at constant power $P_i^{\text{avg}}[k] = \Delta E_i^{\text{dem}}[k_i^{\text{arr}}]/(k_i^{\text{dep}} - k_i^{\text{arr}})$. We compute I^{con} as follows

$$I^{\text{con}} = \frac{\sum_{k=1}^K (P^{\text{avg}}[k] - P^{\text{avail}}[k]) \mathbb{1}_{P^{\text{avg}}[k] \geq P^{\text{avail}}[k]}}{\sum_{k=1}^K P^{\text{avg}}[k]}, \quad (3.35)$$

where $P^{\text{avail}}[k] = P_{\text{Tr}}^r + P_{\text{PV}}[k]$ is the available power that can be consumed by the CS at time k , and $P^{\text{avg}}[k] = \sum_{i \in \mathcal{C}[k] \cup \mathcal{L}[k]} P_i^{\text{avg}}[k]$. If $I^{\text{con}} \leq 0$, there is no congestion at CS and all EVs should be satisfied. On the contrary, if I^{con} is 1, it means that there is no available power at all.

3.5.5 Results for the Default Weight Combination

In this subsection, we show the results of our method for the default weight combination ($c_0 = 1, c_1 = 1$). We show maximum battery wear ($\max_{i,A}(M_i^{\text{bw}}), \max_{i,B}(M_i^{\text{bw}})$), standard deviation ($\sigma_A(M_i^{\text{nsd}}), \sigma_B(M_i^{\text{nsd}})$) and mean value ($\mu_A(M_i^{\text{nsd}}), \mu_B(M_i^{\text{nsd}})$) of non-satisfied demand per group A and B. We also show $I^{\text{con}}, M^{\text{viol}}, M^{\text{fr}}$ and an average aggregated power-setpoint \bar{P}^{req} . The results for the scenarios are shown below:

| metrics | regular production | fluctuating production | sharp jump |
|--------------------------------------|-----------------------|---------------------------|---------------|
| $\max_{i,A}(M_i^{\text{bw}})$ (p.u.) | 0.19 | 0.34 | 0.47 |
| $\max_{i,B}(M_i^{\text{bw}})$ (p.u.) | 0.11 | 0.44 | 0.23 |
| $\mu_A(M_i^{\text{nsd}})$ (p.u.) | 0.28 | 0.14 | 0.45 |
| $\sigma_A(M_i^{\text{nsd}})$ (p.u.) | 0.03 | 0.04 | 0.03 |
| $\mu_B(M_i^{\text{nsd}})$ (p.u.) | 0.27 | 0.12 | 0.44 |
| $\sigma_B(M_i^{\text{nsd}})$ (p.u.) | 0.03 | 0.03 | 0.04 |
| I^{con} (p.u.) | 0.26 | 0.12 | 0.42 |
| M^{fr} (kW) | 0.51 | 2.61 | 0.35 |
| M^{viol} (p.u.) | 0.52 | 0.53 | 0.51 |
| \bar{P}^{req} (kW) | 607 | 709 | 369 |

We see that for all scenarios the $\mu_A(M_i^{\text{nsd}})$ and $\mu_B(M_i^{\text{nsd}})$ are close to I^{con} , $\sigma_A(M_i^{\text{nsd}})$ and $\sigma_B(M_i^{\text{nsd}})$ are less than 0.04. This means that our method efficiently and fairly allocates the power among EVs. The battery-wear is also less than 1, meaning that there were no large jumps of the charging power. Also, the CS correctly tracks an aggregated power-setpoint since M^{fr} is small compared to the \bar{P}^{req} . Finally, the M^{viol} is around 0.5 for all scenarios, i.e., we never overheat the transformer. The results show that our method has good performance in all scenarios with the default combination of weights.

3.5.6 Results for the Different Weight Combinations

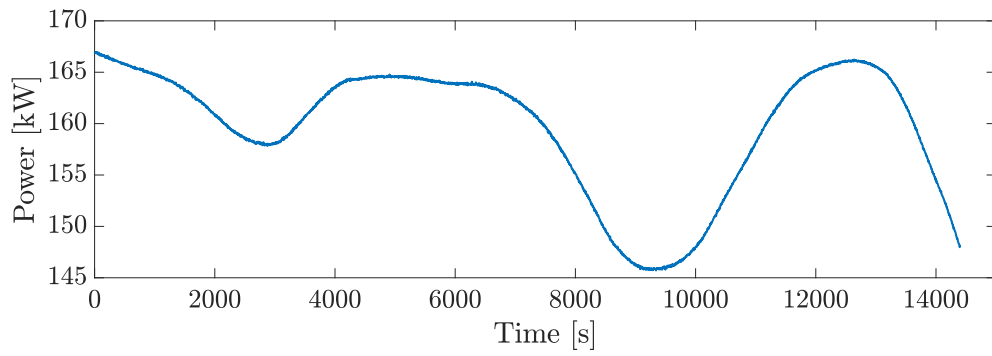
We studied the behaviour of our method for weights by taking values from the set $\{0.01, 0.1, 1, 10, 100\}$. This gives us 25 combinations, but we show only the results of nine of them, as the other combinations have significantly worse performances. For a better visualization, we show the results on eight-dimensional spider plots. We show violation M^{fr} , M^{viol} , maximum battery wear ($\max_{i,A}(M_i^{\text{bw}})$, $\max_{i,B}(M_i^{\text{bw}})$), standard deviation ($\sigma_A(M_i^{\text{nsd}})$, $\sigma_B(M_i^{\text{nsd}})$) and mean value ($\mu_A(M_i^{\text{nsd}})/I^{\text{con}}$, $\mu_B(M_i^{\text{nsd}})/I^{\text{con}}$) of non-satisfied demand per group A and B.

Fig. 3.7 shows the results for the regular production. We see that, for all combinations of weights, the power allocated fairly among EVs, as $\mu_A(M_i^{\text{nsd}})/I^{\text{con}}$ and $\mu_B(M_i^{\text{nsd}})/I^{\text{con}}$ are 1.07 and 1.03, respectively; whereas, $\sigma_A(M_i^{\text{nsd}})$ and $\sigma_B(M_i^{\text{nsd}})$ are 0.03. Our method avoids large power jumps because the battery-wear metric never exceeds 1 for any weight combination. Overall, all weight combinations have similar performance, which shows that our method is not sensitive to the weight change in case of a smooth change of the power production.

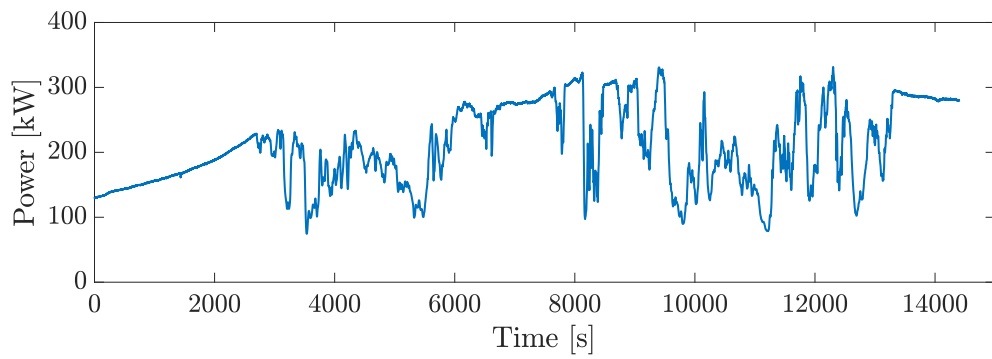
Fig. 3.8 shows the results for the fluctuating production. We observe that combinations $(c_0 = 10, c_1 = 1)$, $(c_0 = 10, c_1 = 0.1)$ and $(c_0 = 1, c_1 = 0.1)$ have the worst battery-wear performance. The combination $(c_0 = 10, c_1 = 0.1)$ has the worst non-satisfied demand for group A. Other combinations show close and good general performance in all metrics. The best combination is $(c_0 = 1, c_1 = 10)$ in this scenario.

Fig. 3.9 shows the results for the sharp jump. We see that the combination $(c_0 = 10, c_1 = 0.1)$ has the worst battery-wear performance. The rest of the combinations have close performance in all metrics, which shows that our method is not sensitive to the weights and has a good performance if there is a sharp change of the power production. The best combination is $(c_0 = 1, c_1 = 10)$ in this scenario. We also observe that, for all weight combinations, M^{viol} metric is around 0.5, i.e., we never overheat the transformer. The method potentially leads to an overshooting of the rated power of the transformer, which rapidly increases its temperature. However, as we immediately react to such overshoots, the operating temperature never exceeds the safe limit.

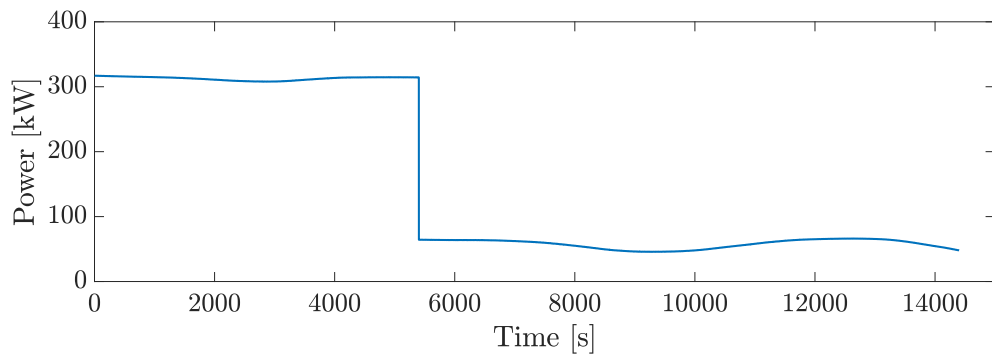
The above analysis shows that the performance of the method is largely insensitive to the weights, and that the default combination ($c_0 = 1, c_1 = 1$) works well in all scenarios. It also shows that increasing c_1 , for example with ($c_0 = 1, c_1 = 10$), leads to slightly better performance. As an example, we show in Fig. 3.10 power traces for the fluctuating production scenario for this combination. Additionally, we show the evolution of the power setpoint of two EVs: one from group A (with high energy demand) and one from group B (with low energy demand). There are no large fluctuations and mini-cycles can be seen, and the EV with higher energy demand receives more power according to the fair power allocation.



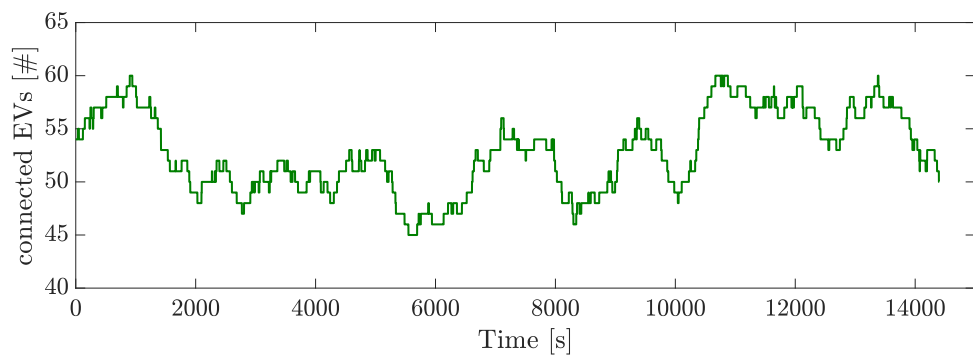
(a) PV production for regular production.



(b) PV production for fluctuating production.



(c) PV production for sharp jump.



(d) Number of connected EVs at the CS.

Figure 3.6 – PV production scenarios and the number of EVs.

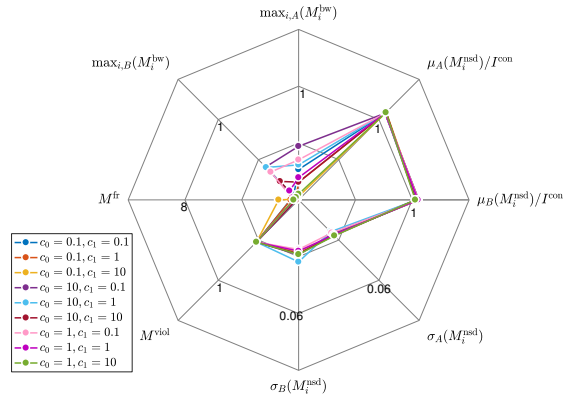


Figure 3.7 – Metrics for the regular production.

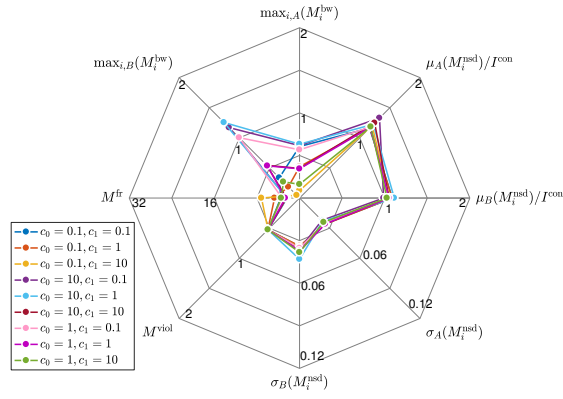


Figure 3.8 – Metrics for the fluctuating production.

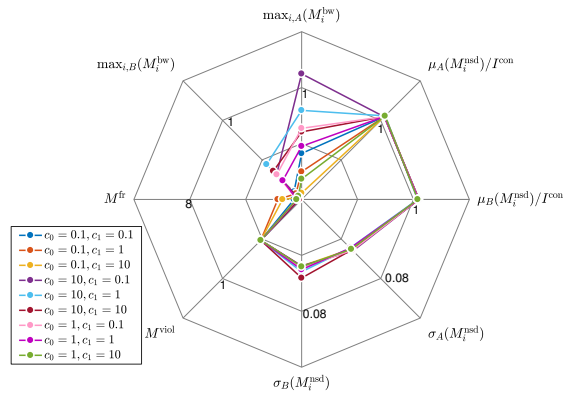


Figure 3.9 – Metrics for the sharp jump.

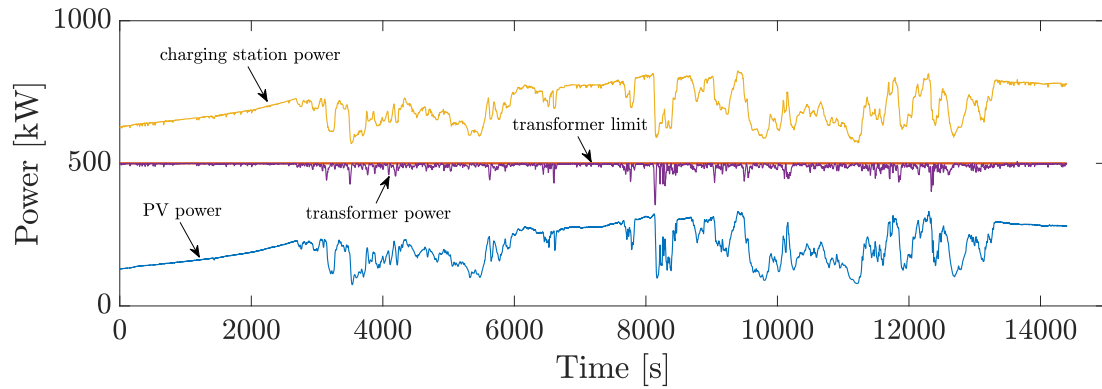


Figure 3.10 – Fluctuating production, $c_0 = 1$, $c_1 = 10$. This illustrates that CS can opportunistically use the fluctuated PV power production while respecting the transformer limit.

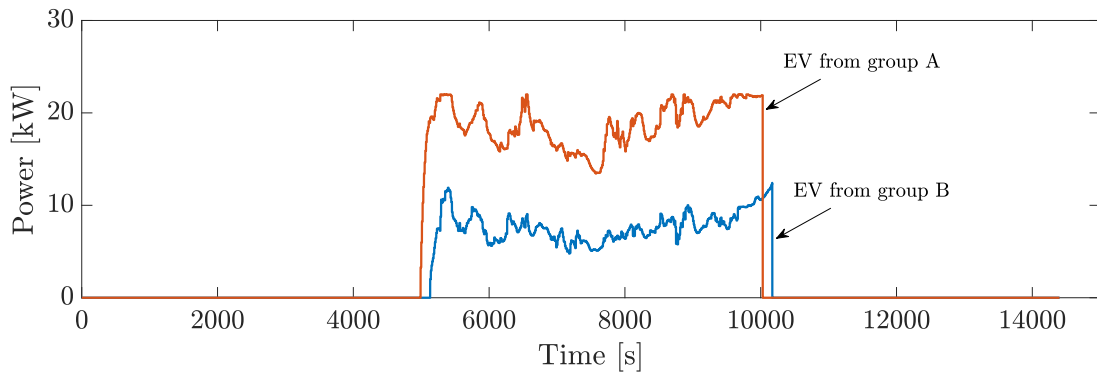


Figure 3.11 – Fluctuating production, $c_0 = 1$, $c_1 = 10$. Power setpoints change for EVs from group A (red curve) and group B (blue curve).

3.6 Conclusions

In this chapter, we have proposed a control scheme for controlling the charging of electric vehicles connected to a single charging-station that follows an aggregated power-setpoint in real time. When the charging station tracks the aggregated power-setpoint, the overall consumed power is allocated fairly among the connected EVs, and the effect on the battery life is minimized. Specifically, we have formulated a mixed-integer-quadratic program based on novel integral terms to cope with time-dependant variables such as battery wear and remaining energy-demand. To reduce the problem complexity, we have also proposed a heuristic that reduces the number of integer variables enabling it to be solved in real time. We have evaluated our method in a stressed situation when the charging station does not have enough power to charge all EVs at maximum. We have created three scenarios with different production traces and have demonstrated the performance based on rigorous metrics. The results show that the control scheme has potential for a real-world application. In this direction, in Chapter 4, we continue our work and perform real-field validation of our method. Additionally, this chapter focuses on charging control of EVs, we further investigate the possibility to discharge EVs batteries to provide more flexibility to the grid in Chapter 5.

4 Experimental Validation of the Real-Time Control of an Electric-Vehicle Charging Station

In previous chapter, we introduced real-time charging control method of EVs. This chapter focuses on real-field validation of the method. Our main goal is to show that the method works in the field, i.e., it can control the charge of commercial EVs that are connected to a real grid through a CS. The field validation has two challenges. The first one is to study the real-time capabilities of the method and by analysing how fast it computes the control power-setpoints. The second one refers to the handling of the non-ideal response of EVs to the control power-setpoints due to implementation and reaction delays and inaccuracies. The experimental results demonstrate the performance of the method and show that it can be deployed in the field.

4.1 Introduction

The charging control of EVs has been extensively exploited in the literature in order to provide ancillary services [82, 133, 134, 135]. However, the validation of most of the methods for the charging control of EVs relies on simulations. Due to its technical difficulty, the real-field experimental validation is rarely performed. The authors in [76, 136, 137] experimentally validated a droop-based charging-control method for the provision of ancillary services, such as frequency control, voltage control and congestion management. However, the EVs are controlled without accounting for their charging requirements, i.e., the energy demands and expected charging times. In this same direction, we report the field validation of the real-time EVs charging control recently proposed in [138]. The method has following features: (i) it tracks an aggregated power-setpoint dictated by a grid controller to the CS, (ii) it minimizes the battery wear of every EV and (iii) it fairly allocates the power to EVs. In order to achieve all these objectives, the problem is cast as a repeated online optimization. As

Chapter 4. Experimental Validation of the Real-Time Control of an Electric-Vehicle Charging Station

the charging power is discontinuous (the minimum charging power is not arbitrarily small), the optimization problem is mixed integer. It also does not require the CS to have precise information about the EVs ramping rates, their state-of-charge (SoC) or actual departure times. The fairness of allocation is performed using the knowledge of desired SoC and expected staying time that the user of an EV advertises upon arrival to the CS.

The main goal in this chapter is to evaluate whether the method works in a real environment. The experimental validation has two major challenges. First, we need to verify the real-time capabilities of the method. These characteristics are crucial as the grid state can change rapidly (in few seconds) due to highly volatile energy resources, such as PV plants [139]. In order to cope with this, the control method should be able to work on a sub-second scale. The main issue here is solving a mixed-integer optimization problem in real-time. In [138], a specific heuristic is proposed to reduce the amount of integer variables. Then, the problem is solved using Branch-and-Bound [130]. However, directly solving this problem can take several seconds and a commercial solver code is needed. Alternatively, in this chapter we suggest a procedure that solves several strictly convex optimization problems with fixed combinations of integer variables by using open-source software. We show that the method can compute the power setpoints for EVs at sub-second scale. Second, most of the control methods presented in the literature assume that each EV perfectly follows a power setpoint and does not take into account inaccuracies and delays in the implementation of the power setpoint. As this non-ideal behaviour could significantly influence the results, we experimentally assess how fast commercial EVs respond to changes of power setpoints. In this respect, we perform several EVs charging sessions in the presence of a rapidly fluctuating PV production. By taking into account these non-ideal behaviour, we show that the method fairly charges EVs and opportunistically use the available power, while respecting the grid operational constraints.

Our main contributions are the following:

- We experimentally validate a recently proposed charging-control method on a real-scale microgrid with real EVs and show fair allocation of a power among the EVs while tracking an aggregated power-setpoint and minimizing EV battery wear.
- We implement the method and make it compatible with real equipment and existing EV charging standards.
- We confirm that EVs charging can be controlled in real-time via time-varying power setpoints. However, the reaction time to power setpoint change and the implementation accuracy depends on the EV type. In this respect we show that the method is capable to account for these inaccuracies and compensate them.

4.2 Summary of the EV charging station control architecture

4.2.1 Charging-Station Control

In this section, we briefly describe the main principles of the control method proposed in Chapter 3 ([138]). We consider a CS that can host N EVs. Time is discretized in constant intervals, indexed by k . The CS provides, at each time step k , the measured active charging power $\hat{P}_i[k]$ and reactive power $\hat{Q}_i[k]$ for the i -th connected EV. The CS keeps track of the number of connected EVs $\Gamma[k]$ at every step k . A newly arrived EV cannot start charging before being instructed by the CS. We also assume that, upon arrival, every EV user advertises to the CS the following quantities: (i) charging-power bounds P_i^{\min} and P_i^{\max} (ii) energy demand ΔE_i^{dem} , (iii) the expected departure time k_i^{dep} . At the k -th timestep the CS also receives an aggregated power-setpoint $P^{\text{req}}[k]$ from the grid controller (see Section 4.3.1 for more details). The value of $P^{\text{req}}[k]$ accounts for the current capabilities of the various resources in the grid, (such as PVs), as well as the grid constraints.

At time step k , the problem is to decide on the collection $\mathbf{P}[k] = (P_i[k])_{i=1, \dots, \Gamma[k]}$, where $P_i[k] \in \{0\} \cup [P_i^{\min}, P_i^{\max}]$ is the charging power assigned by the CS to slot i at time k and on the collection $\mathbf{\Omega}[k] = (\omega_i[k])_{i=1, \dots, \Gamma[k]}$, where $\omega_i[k]$ is the on/off decision for EV i . Specifically, $\omega_i[k] = 1$ (respectively, 0) means that the CS decides to switch EV i on (respectively, off) at time k . We assume that an EV is initially switched off upon arrival. When receiving new setpoints from the CS, the EV cannot immediately change its charging power due to the following delays: *reaction* delay is the time an EV takes, after receiving a new setpoint, to start modifying its power, and *implementation* delay is the time an EV takes to reach a new setpoint, which depends on the EV charger ramping rate. The EV is *locked* if it is in the process of reacting to, or implementing a setpoint. Let $\mathcal{C}[k]$ be the collection of EVs that are unlocked at time k and let $\mathcal{L}[k]$ collect all locked EVs.

The implementation of the method is based on the four-step process described below. First, two non-linear integral terms are computed to account for: (i) the past behaviour of EVs' charging power, and (ii) the desire of an EV to be charged. The first of these terms, $\lambda_i[k] \in [0.5, 1]$ per EV i , quantifies how long ago and how large the power changes were. This is used as a priority metric: the smaller λ_i , the higher the priority to change power. The second term, $\rho_i[k] \in [0.5, 1]$, expresses the desire of an EV i to charge. It is also used as a priority metric: the larger ρ_i , the higher the priority to increase power. Let $\mathbf{\Lambda}[k] = (\lambda_i[k])_{i=1, \dots, \Gamma[k]}$ and $\mathbf{R}[k] = (\rho_i[k])_{i=1, \dots, \Gamma[k]}$.

Second, the method finds the power allocation that maximizes EV energy-demand satisfaction while ensuring fairness, i.e., $P^{\text{req}}[k]$ must be allocated fairly among available EVs. Commonly used fair allocations are weighted proportional and weighted max-min; in [138] it is proved that they are equivalent in our setting. Thus, the method

Chapter 4. Experimental Validation of the Real-Time Control of an Electric-Vehicle Charging Station

computes, using a water-filling algorithm, the weighted-max-min fair allocation, where the weight of an EV reflects its energy demand and its expected staying time. The result of the step is the collection $\mathbf{P}^{\text{ref}}[k]$ of *reference powers*, $P_i^{\text{ref}}[k] \in [0, P_i^{\text{max}}]$ for all EVs, ideally fair and such that $\sum_{i \in \Gamma[k]} P_i^{\text{ref}}[k] = P^{\text{req}}[k]$.

Third, in order to avoid exponential complexity, the method uses a heuristic that runs at every time k and limits the number of integer variables. The heuristic partitions the set of unlocked EVs into three subsets: EVs that are forced to be switched (or remain) on ($\mathcal{S}^{\text{on}}[k]$), EVs that are forced to be switched (or remain) off ($\mathcal{S}^{\text{off}}[k]$), and EVs for which the on/off decision is decided by the optimization problem ($\mathcal{S}[k]$). It is required that $|\mathcal{S}[k]| \leq m$, m is a fixed small number.

Fourth, the method solves the following mixed-integer optimization problem repeatedly, at every time-step:

$$\begin{aligned}
 \text{(H)} \quad & \min_{\mathbf{P}[k], \Omega[k]} f_0(\mathbf{P}[k], P^{\text{req}}[k]) + (f_1(\mathbf{P}[k], \mathbf{\Lambda}[k]) \\
 & \quad + f_2(\Omega[k], \mathbf{R}[k], \hat{\mathbf{P}}[k])) + f_3(\mathbf{P}[k], \mathbf{P}^{\text{ref}}[k]) \quad (4.1) \\
 \text{s.t.} \quad & P_i^{\text{min}} \omega_i[k] \leq P_i[k] \leq P_i^{\text{max}} \omega_i[k] \quad (4.2) \\
 & \omega_i[k] \in \{0, 1\}, \forall i \in \mathcal{C}[k] \quad (4.3) \\
 & \omega_i[k] = 1, \forall i \in \mathcal{S}^{\text{on}}[k] \quad (4.4) \\
 & \omega_j[k] = 0, \forall j \in \mathcal{S}^{\text{off}}[k] \quad (4.5)
 \end{aligned}$$

The term $f_0(\mathbf{P}[k], P^{\text{req}}[k])$ implements a soft constraint on the aggregated power-setpoint $P^{\text{req}}[k]$. The terms f_1 and f_2 minimize the wear of EV batteries. f_1 penalizes the difference between $P_i[k]$ and the measured power $\hat{P}_i[k]$, as well as changes in the measured power. Let collection $\hat{\mathbf{P}}[k] = (\hat{P}_i[k])_{i=1, \dots, \Gamma[k]}$. f_2 penalizes the EV disconnection caused by the CS (i.e., $P_i[k] = 0$). The term f_3 maximizes EV energy-demand satisfaction while ensuring fairness, by penalizing the deviation between the setpoint and the fair allocation. For more details about the method see [138].

4.2.2 Charging-Power Computation

In this subsection, we describe how we implement in real-time the solution of the mixed-integer problem (H). In [138], Branch-and-Bound is used. In this chapter, we present an alternative approach that does not need a commercial solver.

As mentioned earlier, the number of integer variables in problem (H) is less than or equal to m . Let us assume that at time k , the amount of integer variables equals $v \leq m$. Each of these v variables can be either 0 or 1. Thus, there are 2^v combinations of integer variables. For example, if $v = 2$, then the combinations are: $\{[0, 0], [1, 0], [0, 1], [1, 1]\}$. Also, if we choose any fixed combination of integer variables, the problem (H) becomes

a strictly convex quadratic problem where variables are the collection $\mathbf{P}[k]$. We then solve the problem for each fixed combination of integer variables by using the Goldfarb-Ildnani active-set dual method [140], the implementation of which is available online. After this, we evaluate the objective function of (\mathbf{H}) for every combination of integer variables and their corresponding solutions to the (\mathbf{H}) . Finally, the combination that gives a minimal objective function value is the solution to our problem.

4.3 Experimental Setup

In order to experimentally validate the charging-control method, we have integrated it into an existing experimental setup that consist of: (i) real-scale microgrid and EVs, (ii) microgrid control framework.

4.3.1 Microgrid Control Framework

The microgrid is controlled by the COMMELEC system [29]. It is a multi-agent-based framework for real-time control of power grids. It uses a hierarchy of software agents to control a power grid. Each resource is equipped with a resource agent (RA) that is adapted to the technology features of the resource. The agent responsible to control the entire grid is called the Grid Agent (GA). The GA communicates with its RAs by using a common device-independent protocol for message exchange. Each RA advertises an abstract representation (so-called advertisement) of its internal state by using the following format: (1) the PQ profile is the set in the (P, Q) plane (for active and reactive power) that the resource under the control of the RA can deploy, i.e. resource flexibility. (2) The virtual cost $CF(P, Q)$ is a function that evaluates the preference of a resource to stay in a particular zone of the PQ profile. (3) The belief function $BF(P, Q)$ is a set-valued function that accounts for the uncertainty of the resource operation. Specifically, $BF(P, Q)$ returns a convex set that contains all possible setpoints that the resource might implement when it is instructed to apply (P, Q) .

The objectives of the GA are to: (i) keep the grid in a feasible state of operation, i.e. such that nodal voltage magnitudes and line currents are in safe bounds, (ii) minimize the costs of the RAs, (iii) meet the power setpoint requested by an upper GA (for example a dispatch plan). To perform this, the GA first needs the advertisements from the resources and the current electrical state of the grid (usually given by a state estimation process). Then the GA computes optimal power setpoints by minimizing the sum of the resources cost functions, using a gradient-based method. The GA ensures that the state of the grid will be feasible by estimating the maximum variation of control by using belief functions. Finally, GA sends power setpoints to the RAs. These process is repeated every 100 ms to cope with the fastest possible variations of distributed resources (see [29] for further details).

4.3.2 Real-Scale Microgrid and EVs

We validate our method on an implementation of the CIGRÉ benchmark low-voltage microgrid [57], shown in Fig. 4.1. The microgrid interconnects various resources that, for this specific experiment, are composed of a 20 kW uncontrollable PV and CS that can simultaneously charge 2 EVs. The CS uses the IEC 61851 standard to communicate with EVs [141]. We use two commercially available EVs: a Tesla Model S 90D (90 kWh Li-Ion battery) and a Renault Zoe (54.7 kWh Li-Ion battery) both equipped with three-phase chargers.

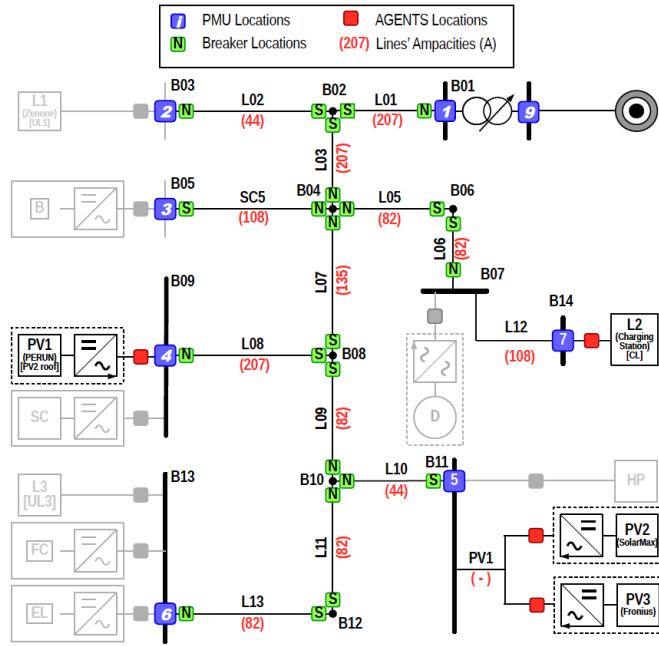


Figure 4.1 – The experimental microgrid. All elements used in the experiments of this chapter are shown in black.

4.3.3 Charging Station Agent

In our setting, the charging station is controlled by the GA. For this purpose, it must be equipped with a RA that receives the aggregated power-setpoint (P^{req}) from the GA. Then, it first allocates this power among connected EVs. In order to do so, it uses the method that computes charging powers for all connected EVs (see in Section 4.2). The CS can only control the maximum current I of and EV. Thus, we need to convert a power setpoint to a current setpoint. We experimentally discover that charging patterns for the adopted EVs are significantly different. In order to investigate such differences, we perform two independent charging sessions of both EVs. We increment the maximum charging current magnitude (I) starting from 6 A with steps equal to 0.1 A and measure implemented current and voltage fundamental frequency phasors (\hat{I} and \hat{V} respectively), active power \hat{P} and power factor $\cos \phi$ per EV. We show in Fig. 4.2

4.3. Experimental Setup

results of the experiment for Tesla and Renault. We observe that, for the Tesla EV, there is a gap between \hat{P} and $\hat{V}I$ equal to 700 W approximately. Also, $\cos \phi$ is always close to 1. For the Renault EV, we see that when charging power is more than 12 kW the behavior is similar to the Tesla EV, i.e., $\cos \phi$ is close to 1. However, when power is less than 12 kW the Renault EV reactive power is not equal to 0 due to its controller. It means that for some EV chargers, in our case the Renault EV, $\cos \phi$ can be much lower than 1. Thus, in order to provide high fidelity active power tracking, we created two lookup tables for both EVs that map the current setpoint to the corresponding consumed power. Additionally, it is visible that sometimes the Renault EV drops its charging power to 0 and goes back (for example at time close to 1000 s) these jumps take around 2 s and are caused by the internal controller of this EV.

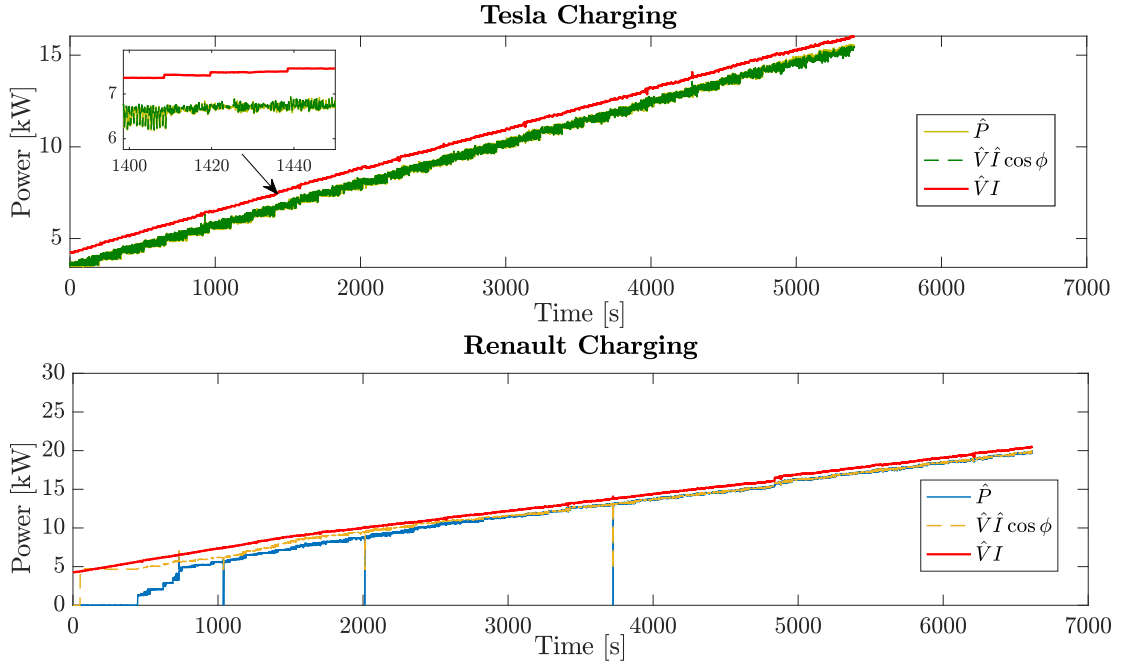


Figure 4.2 – Tesla and Renault charging patterns.

Since we are using the COMMELEC framework, the agent sends to the GA an advertisement that contains the representation of the CS internal state: (P, Q) profile, virtual cost function $CF(P, Q)$ and belief function $BF(P, Q)$ (see Fig. 4.3). The sending/receiving message cycle is repeated continuously and endlessly. As every EV has its own flexibility and uncertainty, the charging station should be able to advertise the aggregated information. The presence of delays influences the flexibility of the EV; this should be taken into account in the aggregated flexibility.

Chapter 4. Experimental Validation of the Real-Time Control of an Electric-Vehicle Charging Station

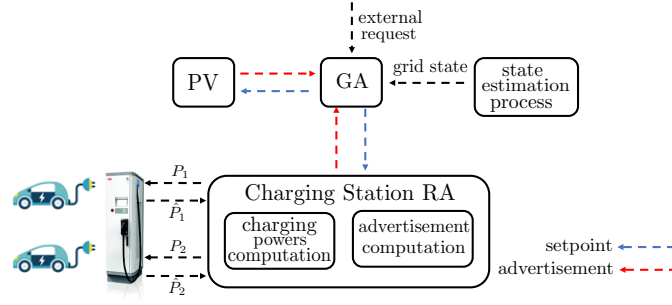


Figure 4.3 – Overall architecture of the system.

PQ Profile

The locking of EVs reduces the flexibility of the charging station, as it is not permitted to change the charging power of locked EVs. Hence, the amount of power that the charging station will consume, if we switch off all unlocked EVs, is computed as:

$$P^{lb} = \sum_{i \in \mathcal{L}[k]} P_i[k] \quad (4.6)$$

At the other extreme, the amount of power that a charging station will consume if all unlocked EVs consume their maximum power is computed as:

$$P^{ub} = \max \left(\hat{P}[k] + \sum_{i \in \mathcal{C}[k]} (P_i^{\max} - \hat{P}_i[k]), P_{CS}^{\max} \right) \quad (4.7)$$

where P_{CS}^{\max} is charging station rated power and $\hat{P}[k] = \sum_{i \in \Gamma[k]} \hat{P}_i[k]$. Hence, we compute the feasible operation set as $\mathcal{A} = \{(P, Q) | P^{lb} \leq P \leq P^{ub}, Q = \sum_{i \in \Gamma[k]} \hat{Q}_i[k]\}$.

Virtual Cost

In this work, the agent prefers to charge the EVs as fast as possible. Therefore, we define the virtual cost function as:

$$\mathcal{C}(P, Q) = \frac{1}{(P_{CS}^{\max})^2} P^2 + \frac{2}{P_{CS}^{\max}} P. \quad (4.8)$$

As we do not control the reactive power of EVs, Q does not appear in the definition of the cost.

Belief Function

One of the main sources of uncertainty is related to the EV delay on the implementation of a power setpoint, as a setpoint is not implemented immediately, due to the ramping constraints of the battery. When an EV is unlocked, the expected implemented power remains the measured power, on the contrary, when an EV is locked, the implemented power is expected to lie in the range defined by the measured power and the setpoint. Most of the time, the EV implements the instructed power setpoint accurately (see Section 4.4). However, if the battery of EV i is almost charged (this depends on the EV; in our experiments it occurs around 95% and 90% charge for the Tesla and Renault EVs respectively), it starts to decrease the maximum charging power with a rate Δr_i . The CS has no information about the EVs' SoC, also the Δr_i depends on the type of the battery and its internal conditions. Hence, Δr_i should be estimated dynamically. In this chapter, we use a Holt-Winters (double exponential weighted moving average) fitter for Δr_i estimation [142]. The computation of uncertainty bounds $\mathcal{B}_i^{\text{low}}, \mathcal{B}_i^{\text{up}}$ per EV i is detailed in Alg. 2. We detect at line 1 if the EV follows the previously computed setpoint. If not, we check if the EV itself reduces its charging power (line 2) by comparing the measured power between two consecutive time steps and update the Δr_i using Holt-Winters estimation (line 3). As a result, we compute the uncertainty bounds in lines 6 – 10. Finally, the belief function is computed as aggregated uncertainty of all EVs as $\mathcal{B}(P, Q) = \{\sum_{i \in \Gamma[k]} \mathcal{B}_i^{\text{low}} \leq P \leq \sum_{i \in \Gamma[k]} \mathcal{B}_i^{\text{up}}, Q = \sum_{i \in \Gamma[k]} \hat{Q}_i[k]\}$.

Algorithm 2 Belief function computation for EV i .

Input: $\hat{P}_i[k-1], \hat{P}_i[k], P_i[k-1], P_i[k]$
Output: $\mathcal{B}_i^{\text{low}}, \mathcal{B}_i^{\text{up}}$

```

1: if  $P_i[k-1] > \hat{P}_i[k]$  then
2:   if  $\hat{P}_i[k-1] > \hat{P}_i[k]$  then
3:      $\Delta r_i = \text{Holt} - \text{Winters}(\Delta r, \hat{P}[k-1] - \hat{P}[k])$ 
4:   end if
5: end if
6: if  $P_i[k] \geq \hat{P}_i[k-1]$  then
7:    $\mathcal{B}_i^{\text{low}} = \hat{P}_i[k] - \Delta r_i, \mathcal{B}_i^{\text{up}} = P_i[k]$ 
8: else
9:    $\mathcal{B}_i^{\text{low}} = P_i[k] - \Delta r_i, \mathcal{B}_i^{\text{up}} = \hat{P}_i[k]$ 
10: end if
```

The RA for CS is implemented in C++ and cross-compiled for embedded platform and deployed in a NI CRIO 9068.

4.4 Experimental Results

The results described in this section refer to the application of the charging control method in a real environment: real EVs and real-scale microgrid. Several scenarios

are considered in order to demonstrate the performance of the method. We use the root mean square error (RMSE) as a metric to measure how good the CS follows the PV production. For the fairness and battery wear per EV i we use metrics from [138]: (i) non-satisfied demand $M_i^{\text{nsd}} = 1 - \Delta E_i / \Delta E_i^{\text{dem}}$, where ΔE_i is the energy that EV i receives while plugged-in, (ii) battery-wear $M_i^{\text{bw}} = \frac{1}{2(P_i^{\text{max}})^2} \sum_{k=1}^K (P_i[k] - P_i[k-1])^2$, where K is the amount of discrete time-steps during the selected control period.

4.4.1 Self-consumption Scenarios

We first study the performance of the proposed method when the grid state is far from the operational limits in terms of bus voltages and line ampacity constraints. The GA is instructed to track 0 kW at the PCC, i.e. the grid should be self consuming as much as possible. In this case, the CS should follow the fluctuating PV production. In order to validate the performance of our method, we create two scenarios: (i) *Scenario 1*, where both EVs have the same expected staying time (1 h 40 min) and energy demand (15 kWh), in this case our method should charge both EVs similarly. (ii) *Scenario 2* where Renault and Tesla EVs have similar energy demand (10 kWh and 11 kWh respectively), but the Renault EV has smaller expected staying time (45 min for the Renault EV and 1 h 10 min for the Tesla EV). Additionally, the Renault EV arrives and departs while the Tesla one is plugged-in. In this case, the Renault EV should receive more power than the Tesla EV while plugged-in because it has higher priority to charge. It should be noticed that in both scenarios the PV production is not enough to satisfy EVs charging demands fully. Additionally, in both scenarios EVs depart earlier than expected, i.e. disconnection is caused by a decision of a user.

The results for Scenario 1 are shown in Fig. 4.4. It is visible that CS power perfectly follows the PV production and PCC power is always close to 0. The RMSE value between PCC target power (i.e., 0 kW) and the realized one is 254 W. Tesla and Renault EVs share PV fluctuations, charge almost at the same power due to the equal priority and receive 6.75 kWh ($M^{\text{nsd}} = 0.55$) and 6.81 kWh ($M^{\text{nsd}} = 0.55$) respectively at departure. Also, the EVs accurately follow setpoints due to implemented lookup tables that are explained in Section 4.3.3. Battery-wear metrics for both EVs are also less than 1, meaning that there were no large jumps of the charging power: 0.012 for the Tesla EV and 0.091 for the Renault EV. Finally, we observe two power jumps for the Renault EV around $t = 1800$ s and $t = 3500$ s, the possible reasons are discussed in Section 4.3.3.

The results for Scenario 2 are shown in Fig. 4.5. We observe that, first, the Tesla EV follows the PV production with high fidelity. Then, the Renault EV arrives around $t = 750$ s and start charging. After several seconds the Renault EV charges with higher power since it has more priority due to short staying time and similar energy demand. We also see that both EVs follow the PV production and share its fluctuations. The Renault EV stays around 30 min and departs at around $t = 2550$ s. Tesla and Renault

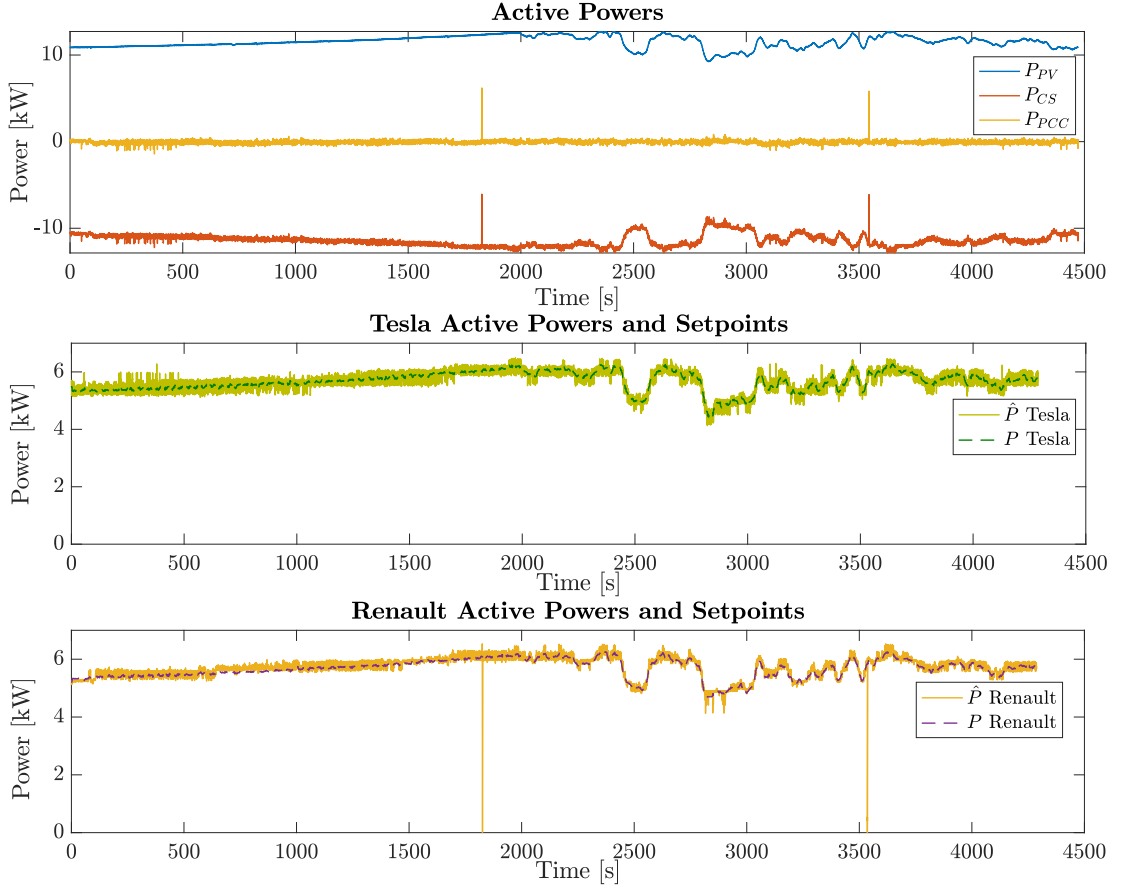


Figure 4.4 – Scenario 1 experimental results.

EVs receive 2.64 kWh ($M^{\text{nsd}} = 0.73$) and 4.14 kWh ($M^{\text{nsd}} = 0.58$) respectively during the Renault EV plugged-in time. Finally, the disconnection of the Renault EV causes a jump of the power. The reason is that, upon disconnection, the power consumed by the Renault EV suddenly goes to 0 kW, whereas the Tesla EV cannot immediately react to power change and need several seconds (around 4 s) to increase its consumption. After that, the Tesla EV follows the PV production perfectly. The final RMSE value between PCC target power (i.e., 0 kW) and the realized one is 448 W. In this experiment we also see the power jump caused by Renault internal behavior ($t = 2550$ s). Battery-wear metric 0.006 for the Tesla EV and 0.004 for the Renault EV, i.e, there were no large jumps of the charging power.

4.4.2 Line Congestion Scenario

In order to study the behavior of the method under binding-grid conditions, we consider a scenario in which the ampacity of the line connecting the CS and the grid (line L12 in Fig. 4.1) is artificially limited to 23 A. In this case, the GA main priority is to keep the grid in a feasible operation and prevent voltage and/or current violations by curtail-

Chapter 4. Experimental Validation of the Real-Time Control of an Electric-Vehicle Charging Station

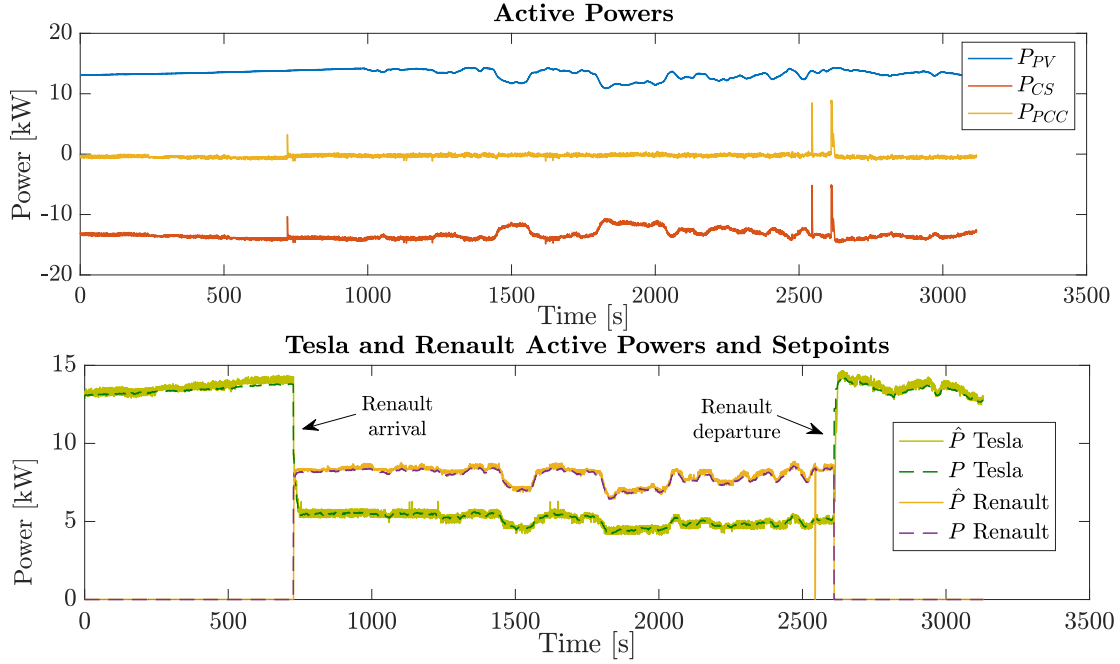


Figure 4.5 – Scenario 2 experimental results.

ing the CS consumption (see [29] for details on how the GA enforces grid constraints). In this scenario both EVs stay connected for 45 min, but the energy demand of the Tesla EV is of 15 kWh, whereas for the Renault EV is of 10 kWh.

Fig. 4.6 shows power traces, current at line L12 and EVs active power and setpoints. The line congestion management is clear around $t = 1000$ s, the CS follows increasing PV production, however, given the congestion in L12, the consumption of CS is temporarily reduced by the GA and allows CS to consume only 15 kW. We observe also that the method reduces the consumption of both EVs, while keeping priority for the Tesla. Both EVs receive 6.62 kWh ($M^{\text{nsd}} = 0.55$) and 4.37 kWh ($M^{\text{nsd}} = 0.55$) respectively. Additionally, the results show that our control method allows the GA to fully exploit the flexibility of EVs. In this experiment we also see the spurious jump of the Renault EV charging power approximately at $t = 950$ s and $t = 2750$ s.

In Fig. 4.7, we show the results of the experimental evaluation of the time latencies incurred in the involved computation processes. The curve in Fig. 4.7 shows the cumulative distribution of the latency of the CS processing-time, i.e., the time that the CS takes to perform the steps described in Section 4.2 and to construct an advertisement for the GA after receiving an aggregated power-setpoint. The median value of the processing time is 1.77 ms with a corresponding 95-th percentile of 3.44 ms. The grid controller issues aggregated power-setpoints every 100 ms. We see that the CS processing-time is ≤ 20 ms and, before a new aggregated power-setpoint is sent by the GA, the CS finishes the computation of the power setpoints for EVs. Overall, the timing performance shown here confirms the adequateness of the charging-control method

4.4. Experimental Results



Figure 4.6 – Line congestion experimental results.

for the real-time operation of the GA.

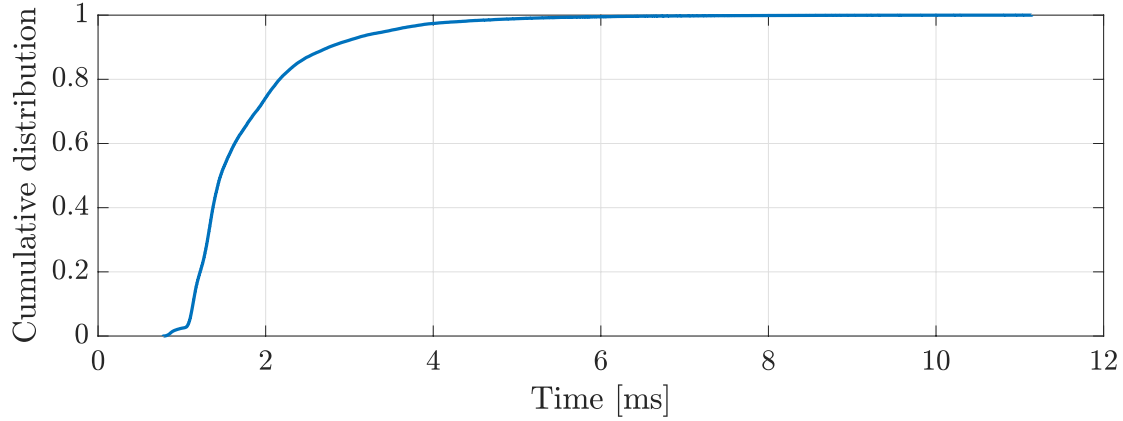


Figure 4.7 – Cumulative distributions of the CS processing-times measured from the instant when the GA aggregated power-setpoint is sent to the CS.

4.5 Conclusions

In this chapter we have experimentally validated the operation of a recently proposed real-time control method for charging EVs. We have performed field validation on a real-scale microgrid with real PV production and two commercially available EVs: a Tesla Model S 90D and a Renault Zoe. We have conducted several field experiments with different PV production, EVs energy desires and staying times. We have showed that the method is able to provide a real-time control (i.e., at sub-second scale) for charging commercial EVs. The results have also showed that the CS is able to accurately follow an aggregated power-setpoint and capable to satisfy the grid operational constraints. The method has allocated the power among EVs fairly charging an EV with higher charging priority and minimizing the battery wear. We have also studied charging patterns of EVs.

5 Combined Grid-Aware Control and Optimal Scheduling of Electric Vehicle Charging Stations with V2G Capabilities

In this chapter, we consider the problem of controlling the power of EVs that, with vehicle-to-grid (V2G) capabilities, make their batteries available to decrease the local price of electricity and to react to real-time uncertainties. The main concern with such an approach is that the constant change of charging/discharging powers could accelerate the EV battery-wear. In order to minimize global operational costs, we suggest combining an optimal scheduler that takes care of charging/discharging EVs, with a real-time controller that reacts to grid-aware external setpoints. The scheduler computes optimal powers for EVs that consider forecasts of future arrivals, departures, and operations of other energy resources (i.e., other loads and PVs). The real-time controller, in turn, follows an aggregated power-setpoint from a main controller of the local distribution grid, thus minimizing the EV battery-wear while following the scheduler's decisions. We validate our method by simulations and compare it with benchmark real-time algorithms. We show that our method presents lower operational costs and EV battery-wear when compared with benchmark algorithms.

5.1 Introduction

V2G technology (e.g., [44, 45]) has the potential to further increase the flexibility and safety of the grid operation [46, 47, 48], thus enabling a grid-aware operation of the EVs and increasing the hosting capacity of the combination of EVs and distributed generation, such as PVs (e.g., [49]). Yet, taking advantage of the available flexibility means that charging stations (CSs) are required to constantly change their charging/discharging powers. The main concern of such behaviour could be associated with EV battery-wear,

Chapter 5. Combined Grid-Aware Control and Optimal Scheduling of Electric Vehicle Charging Stations with V2G Capabilities

i.e., directly transferring the changes from the CS to the connected EVs could accelerate the battery degradation in terms of capacity loading and losses increase [38]. As batteries are the most expensive component of EVs, their users need to have clear incentives to enable the V2G operation, because this will accelerate the battery degradation process by increasing the number of full-equivalent cycles [50], [51]. For instance, a group of domestic buildings that hosts regular and V2G EVs could set up a local energy market, where V2G EVs can offer their energy. This is typically known in the literature as an *energy community* (e.g., [143, 144]). In this context, the V2G EVs can offer the energy stored in their batteries at a price that compensates for the use. However, considering the effect of the control scheme on the battery wear is a non-trivial challenge.

This flexibility enables the CS to exploit the available power and, for example, to charge faster compared to a CS with fixed constraints, thus maximizing the demand satisfaction. Systems that support such grid-aware opportunistic charging are proposed in [19, 74, 138, 145] for EVs that do not have V2G capabilities. However, the extension of these works to enable bidirectional V2G is a non-trivial task. In this direction, different control schemes were proposed in the literature. For example, the authors in [146] propose an online method that uses EVs' flexibility for peak shaving and load balance. [147] proposes a centralized control strategy for an EV fleet that provides frequency support by tracking a regulation signal. The aforementioned papers do account for operational grid-constraints but are oblivious about incentivizing users to enable the V2G operation of their EVs. The main challenge in this case is to decide when it is more economically convenient for V2G EVs to discharge. The naive approach is to discharge EVs whenever there is power deficit caused by other EVs that are charging, thus rewarding the V2G users with the payment of the charging EVs. However, this can be sub-optimal as the decision is taken based only on current-time information. Indeed, as V2G EVs act as storage devices, it might be more beneficial to temporarily keep the available energy stored and use it in the future only when, for example, the energy cost from the grid is high. In order to combine this set of requirements, we propose a two-layer approach with a scheduler that handles long-time decisions and a real-time controller that adapts to the state of the grid and to random fluctuations. The scheduler computes optimal charging/discharging powers for EVs, taking into account the forecasts of future arrivals, departures, and the operations of other energy resources (e.g., other loads, distributed generators, etc.). The real-time controller is defined such that (i) the CS can follow external power-setpoints that come from a grid operator, i.e., makes the EVs capable of providing services to the grid (e.g., primary and secondary frequency support, voltage control, congestion management), (ii) it takes into account the previous decisions issued by the scheduler and, (iii) it minimizes EV batteries-wear.

The scheduling of charging/discharging of EVs is a difficult task because the real arrivals, departures, user energy demands and bids, the production of stochastic renewables (e.g., PV or wind turbines), and the load consumption are uncertain, especially

for long scheduling-horizons. A method that tracks an aggregated signal is shown in [148], where EV charging and discharging powers are scheduled using model predictive control (MPC), assuming only three possible changing rates and perfect forecasts of an aggregated signal and EVs departures. However, such assumptions might be unrealistic. In order to achieve a power balance, P. Kou *et al.* in [149] developed an MPC control scheme for EVs charging coordination and wind generation. However, the economic benefits are not taken into account.

In this chapter, we use a scenario-based approach [150] for handling the uncertainty of the loads, stochastic generation, and EV user-behaviour. Indeed, a scenario-based MPC (e.g., [151, 152]) provides a powerful framework for scheduling under uncertainties. It can easily account for time correlations in the realizations of disturbances of, e.g., PV production. In contrast, this is considerably more complicated with other methods, such as chance-constrained optimization [153], where a probability of a succession of constraints over time is needed. In this context, we create several plausible scenarios based on the existing historical data for PV generation and load consumption and synthetic data representing users behavior. Our approach is to optimize the average performance over scenarios while satisfying all possible constraints of the problem. Thus, the scheduler is formulated as a scenario-based MPC to minimize the cost for the community and maximize the energy satisfaction. The scheduler has a long-term view and can anticipate or postpone the EV charge/discharge, depending on the available energy from the V2G EVs and the grid electricity price. Then, the real-time controller takes care of minimizing the battery wear by avoiding large power jumps, it follows the scheduler goals, and it reacts to the real-time behaviour of the uncertain variables.

The chapter is structured as follows. In Section 5.2, we state the main problem and the separation of concerns for the scheduler and the real-time controller. In Section 5.3, we describe all the details of the scheduling strategy. In Section 5.4, we formulate and solve the real-time control problem. We provide a numerical evaluation to validate our method in Section 5.5. Finally, in Section 5.6, we conclude the chapter.

5.2 Problem Statement

Without loss of generality and to help the reader to understand the ideas, we consider an energy community that is composed of a set of residential buildings, a PV plant, and a large CS. The CS has N charging slots that can serve both regular and V2G EVs (see Fig. 5.1). We assume that the buildings are inflexible, whereas the EVs can modify their charge and discharge rate, i.e., the CS power can be shifted in time to less expensive and less congested periods by properly dispatching charging and discharging powers of connected EVs. The community can obtain energy from the PV, from the main grid, or from V2G EVs. We assume that the community does not sell energy back to the

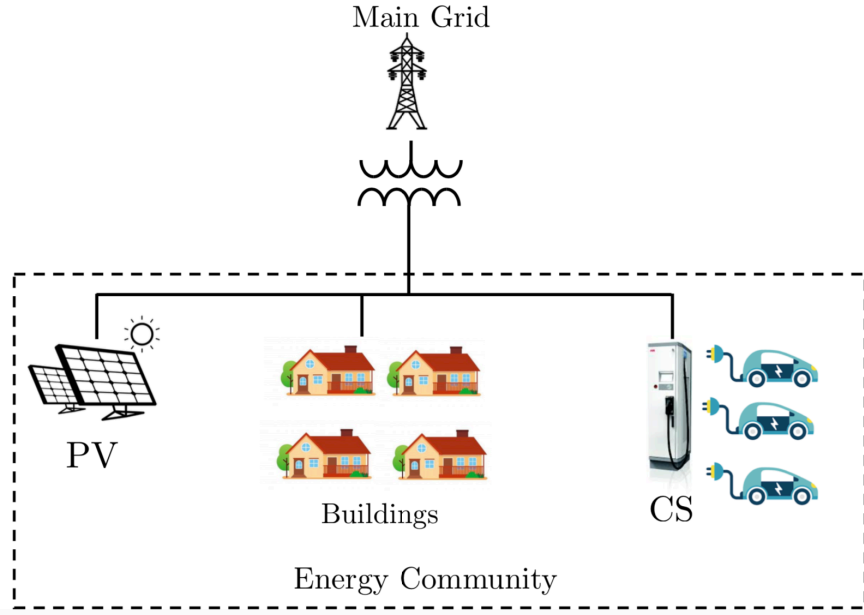


Figure 5.1 – Schematic representation of the energy community.

main grid. The main goal of the community is to minimize the energy expenses and to maximize the satisfaction of the EV goals. Every EV user willing to sell energy, commits an energy bid (i.e., amount, price, and expected staying time). With this information, and knowing the expected day-ahead electricity cost from the grid, the community can decide where (PV, V2G EVs, or grid) and when it is more convenient to buy energy and when it is more convenient to charge the charging EVs.

In this chapter, we assume that V2G users have economic incentives for discharging their EVs. For example, if the users get inexpensive and low-CO₂-content energy at their working place during the day (e.g., from renewable generation) and their battery is well charged, then it might be economically convenient to sell a fraction of this energy to the community in the evening. Furthermore, as one of the main goals of the method is to minimize the EV battery-wear, we enforce cycling avoidance. We consider that an EV user commits to the CS the desire to buy power from the community (be a consumer) or to sell energy to the community (be a producer) upon arrival. In particular, an EV will not be permitted to change from consumer to producer, or vice-versa, while it is connected. In brief, upon the arrival of an EV, we assume the following information is available: (i) charging-power bound P^{\max} , (ii) discharging-power bound P^{\min} , (iii) expected departure-time t^{dep} , (iv) energy demand E^{dem} (if consumer), or *energy bid*: energy that the user can sell E^{sell} and the price of this energy C (if producer).

With goals and available information already defined, we formulate the problem in two stages. First, in order to minimize the energy expenses of the community, the community operator (CO) *schedules* the power of all charging EVs, and all discharging EVs, and the power that the community buys from the main grid, from the current

period until the time horizon (see Section 5.3 for details). In order to solve the scheduling problem, the CO needs the forecasts of PV production, load consumption, and the following information about EVs: (i) future arrivals, (ii) future departures, (iii) future energy-demands of consuming EVs, (iv) future energy-bids for producing EVs. However, the real behaviour of the users, the real PV production, and the load consumption could be highly uncertain, especially for long time-horizons. To handle these uncertainties, we suggest using the approach based on the scenario-based model predictive control (MPC) because, as already mentioned, it can easily account for time correlations in the realizations of disturbances. In this sense, the MPC considers a finite number of possible scenarios. The result of this task is a sequence of EV charging and discharging powers, as well as the power exchanged with the main grid for every time interval (e.g., every 15 min) up to some horizon (e.g., 24 h). Only the EV charging and discharging powers of the first time interval are implemented and used as reference by the real-time controller. In Section 5.3, we formulate the scenario-based MPC and describe the scenario generator.

Second, due to the presence of stochastic resources, the forecasts of the state of the system might be inaccurate. As a result, the CS (as only controllable resource in the system) can adapt to these stochastic conditions while taking into account long-term objectives, given by the CO, to exploit the available energy. This is done by a grid controller that, very frequently (e.g., every 100 msec), computes aggregated power setpoints for the entire CS while keeping the grid in safe operating conditions [29]. Upon receiving an aggregated power-setpoint, the CS allocates the power, according to the setpoints obtained from the long-term scheduler, and minimizes the battery wear of each EV (see Fig. 5.2 for more details).

In summary, the objectives of the real-time controller are

1. track the aggregated setpoint from a grid controller,
2. track the long-term objectives of each EVs decided by the scheduler, and
3. minimize the wear of EV batteries.

The result of this task is a set of charging- and discharging-power setpoints that the CS instructs for all EVs to implement in real time. In Section 5.4, we formulate a quadratic optimization problem for this task.

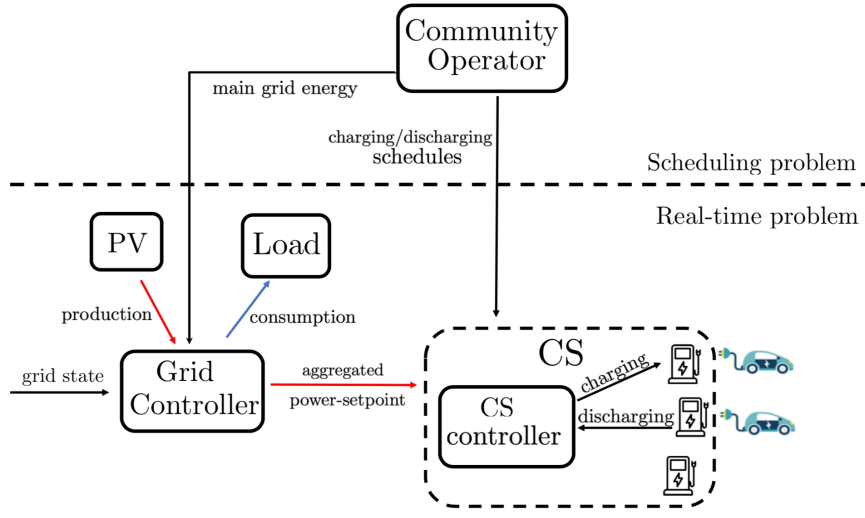


Figure 5.2 – Scheduling and real-time problems interaction.

5.3 Scheduling Problem

The objective of the scheduler is to determine, for all periods $t \in [1, H]$, where H is the time horizon, the power profiles of (i) the power bought from the grid \mathcal{P}_G , (ii) the power bought from (or sold by) V2G EVs (discharging profiles) \mathcal{P}^- , and (iii) the power consumed by EVs \mathcal{P}^+ (charging profiles).

5.3.1 Definitions

We assign to every EV, either charging or discharging, a unique identifier id . Each charging EV is associated with a tuple of size 3: $\{t_{id}^{arr}, t_{id}^{dep}, E_{id}^{trg}\}$. Whereas, each discharging EV is associated with a tuple of size 4: $\{t_{id}^{arr}, t_{id}^{dep}, E_{id}^{sell}, C_{id}\}$. t_{id}^{arr} and t_{id}^{dep} are the arrival and expected departure times of EV id , respectively. E_{id}^{trg} is the energy-goal upon departure, for EV id , defined by the user upon arrival. E_{id}^{sell} is the available energy that discharging EVs can sell before departing, and C_{id} is the cost of this energy; both are defined by the user upon arrival. We consider that each user is responsible for defining their own cost and assume that this is constant while the EV is connected. Hence, it is an input to our problem formulation. For example, one way to define this cost would be to consider three components: (i) the cost at which the energy was bought, (ii) an estimation of the degradation cost, specifically, it is expected that batteries that participate in this market are cycled more, thus reducing their lifetime; hence this has to be compensated¹ and (iii) a profit for participating in the market.

Furthermore, we assume that we have two maps of EV identifiers at period t : Ch_t - connected EVs that want to charge and Dh_t - connected EVs that want to discharge.

¹For example, the degradation cost could be estimated as $\frac{I}{E_{nom} FEC}$, where I is the investment in replacing the battery, FEC the amount of Full Equivalent Cycles, and E_{nom} the rated energy.

For example, for a discharging EV with $\text{id} = 1$, $\text{Dh}_t(1) = \{t_1^{\text{arr}}, t_1^{\text{dep}}, E_1^{\text{sell}}, C_1\}$.

5.3.2 Formulation

Let H be a control horizon and N the number of slots in the CS. We define the matrix \mathcal{I} of size $N \times H$ that stores the identifiers of connected EVs for the control horizon H , meaning $\mathcal{I}_{i,t}$ gives the identifier of the EV connected to slot i at period t . If no EV is connected to slot i at period t , then $\mathcal{I}_{i,t} = 0$. For example:

$$\mathcal{I} = \left(\begin{array}{c} \text{horizon } H \\ \begin{pmatrix} 1 & 1 & 1 & 5 & 5 & 0 \\ 0 & 4 & 4 & 4 & 4 & 0 \\ 2 & 2 & 0 & 6 & 6 & 6 \\ 3 & 3 & 3 & 0 & 1 & 1 \end{pmatrix} \end{array} \right) \left. \vphantom{\begin{pmatrix} 1 & 1 & 1 & 5 & 5 & 0 \\ 0 & 4 & 4 & 4 & 4 & 0 \\ 2 & 2 & 0 & 6 & 6 & 6 \\ 3 & 3 & 3 & 0 & 1 & 1 \end{pmatrix}} \right\} \text{slots } N$$

In order to handle uncertainties, we generate M possible scenarios. Each scenario $m = 1, \dots, M$ consists of forecasts of PV production PV_t^m , of load consumption PL_t^m , and of user behavior $\mathcal{I}^m, \text{Dh}_t^m, \text{Ch}_t^m, \forall t = 1, \dots, H$ (see Section 5.3.3 for the details on how these are generated). Let $\mathcal{P}_{\mathcal{I}_{i,t}^m, t}^{+,m}$ be the charging and $\mathcal{P}_{\mathcal{I}_{i,t}^m, t}^{-,m}$ the discharging power of the EV connected to the slot i with $\text{id} = \mathcal{I}_{i,t}^m$, and $\mathcal{P}_{G,t}^m$ the power that community buys from the main grid, for scenario m at time t . Also, let $E_{\mathcal{I}_{i,t}^m, t}^{\text{dep}}$ be an amount of energy that an EV buy or sell up to time t (initial value is 0). Finally, let $S_{G,t}$ be the price of the grid power at time t (same for all scenarios).

Given the multiplicity of scenarios, we formulate the scheduling problem by minimizing the weighted-average cost of all scenarios:

$$\begin{aligned} \text{(S)} \quad & \min_{\mathcal{P}^+, \mathcal{P}^-, \mathcal{P}_G} \sum_{m=1}^M w_m \sum_{t=1}^h \left(\sum_{i=1}^N C_{\mathcal{I}_{i,t}^m} \mathcal{P}_{\mathcal{I}_{i,t}^m, t}^{-,m} + S_{G,t}^m \mathcal{P}_{G,t}^m \right) \Delta t \\ & + \sigma \sum_{j \in \text{Ch}_t^m} \left(E_{\mathcal{I}_{i,t}^m, t}^{\text{dep}} - E_{\mathcal{I}_{j,k}^m}^{\text{trg}} \right)^2 \\ \text{s.t.} \quad & 0 \leq \mathcal{P}_{\mathcal{I}_{i,t}^m, t}^+ \leq P_{\mathcal{I}_{i,t}^m}^{\text{max}}, \forall \mathcal{I}_{i,t}^m \in \text{Ch}_t, \forall t \end{aligned} \tag{5.1}$$

$$- P_{\mathcal{I}_{i,t}^m}^{\text{min}} \leq \mathcal{P}_{\mathcal{I}_{i,t}^m, t}^- \leq 0, \mathcal{I}_{i,t}^m \in \text{Dh}_t, \forall t \tag{5.2}$$

$$\mathcal{P}_{G,t}^m \leq P_{\text{Tr}}, \forall t \tag{5.3}$$

$$E_{\mathcal{I}_{i,t}^m, t} \leq E_{\mathcal{I}_{i,t}^m}^{\text{sell}}, \forall \mathcal{I}_{i,t}^m \in \text{Dh}_t, \forall t \tag{5.4}$$

$$E_{\mathcal{I}_{i,t}^m, t+1} = E_{\mathcal{I}_{i,t}^m, t} + \eta^+ \mathcal{P}_{\mathcal{I}_{i,t}^m, t}^+ \Delta t, \tag{5.5}$$

$$\forall \mathcal{I}_{i,t}^m \in \text{Ch}_t, \forall t \leq t_{\mathcal{I}_{i,t}^m}^{\text{dep}}$$

$$E_{\mathcal{I}_{i,t}^m,t+1} = E_{\mathcal{I}_{i,t}^m,t} + \eta^- \mathcal{P}_{\mathcal{I}_{i,t}^m,t}^- \Delta t, \quad (5.6)$$

$$\begin{aligned} \forall \mathcal{I}_{i,t}^m \in \text{Dh}_t, \forall t \leq t_{\mathcal{I}_{i,t}^m}^{\text{dep}} \\ \text{PV}_t^m - \text{PL}_t^m = \sum_{\mathcal{I}_{i,t}^m \in \text{Ch}_t} \mathcal{P}_{\mathcal{I}_{i,t}^m,t}^+ \\ + \sum_{\mathcal{I}_{i,t}^m \in \text{Dh}_t} \mathcal{P}_{\mathcal{I}_{i,t}^m,t}^- + \mathcal{P}_{G,t}^m, \forall t \end{aligned} \quad (5.7)$$

$$\begin{aligned} \mathcal{P}_{\mathcal{I}_{i,1}^m}^{+,m} = \mathcal{P}_{\mathcal{I}_{i,1}^p}^{+,p}, \mathcal{P}_{\mathcal{I}_{i,1}^m}^{-,m} = \mathcal{P}_{\mathcal{I}_{i,1}^p}^{-,p}, \\ \mathcal{P}_{G,1}^m = \mathcal{P}_{G,1}^p, \forall m, p = 1, \dots, M \end{aligned} \quad (5.8)$$

\mathcal{P}^+ , \mathcal{P}^- , and \mathcal{P}_G are the collections of all control variables $\mathcal{P}_{\mathcal{I}_{i,t}^m,t}^{+,m}$, $\mathcal{P}_{\mathcal{I}_{i,t}^m,t}^{-,m}$, $\mathcal{P}_{G,t}^m$ for all slots $i = 1, \dots, N$, planning horizon $t = 1, \dots, H$, and scenarios $m = 1, \dots, M$. The first linear term in the objective function minimizes the overall cost of the operation, i.e., it buys the required energy from the less expensive source (either PV, the V2G EVs, or the grid), for every possible scenario. w_m is the weight of scenario m . The computation of these weights is explained in Section 5.3.3. The second quadratic term is a soft constraint on the target energy of charging EVs, which cannot be formulated as a hard constraint as some EVs might not reach their goal. Parameter $\sigma > 0$ is a weight to compare both objectives. Δt is the amount of time between two consecutive timesteps.

Constraints (5.1), (5.2) prevent discharging EVs from charging and prevent charging EVs from discharging, as discussed in Section 5.2. Constraint (5.3) limits the power at the grid connection-point (GCP) to the transformer rated power P_{Tr} . Constraint (5.4) fixes the availability of V2G EV to be sold, thus preventing over-discharging. Constraints (5.5) and (5.6) represent the model of EVs batteries with η^+ and η^- as charging and discharging efficiencies, respectively; we consider them constant, without loss of generality. The constraint (5.7) is the community power-balance equation. Constraint (5.8) ensures that, for every scenario m and every scenario p , the control decisions are identical for the first time step ($t = 1$), as these decisions are actually implemented, following the standard formulation of scenario-based MPC [152].

The result of problem (S) is the schedule of all EV powers and the power that the community buys from the grid. We define the result of this operation as \mathcal{P} . The scheduled power $\mathcal{P}_{G,1}$ is sent to the local grid controller, i.e., the local controller tracks this power at the GCP, whereas the powers $\mathcal{P}_{\mathcal{I}_{i,1}^m,1}^{+,m}$, $\mathcal{P}_{\mathcal{I}_{i,1}^m,1}^{-,m}$ are sent to the CS real-time controller. As (S) is formulated as a quadratic program with linear constraints, it has polynomial complexity, thus making it tractable.

5.3.3 Scenario Generation

In this subsection, we describe how the scenarios are generated. The scenario generator works in a rolling-horizon fashion, i.e., it generates scenarios at every time period t .

PV and Building Power

We describe the generation of traces for the PV production and load consumption. The method is similar to the one described in [154]. We assume that the scenario generator has historical data of the PV production and load consumption. For readability, we describe the generation of traces only for the load consumption (the PV traces are generated similarly).

First, we find the most similar days to the current calendar-day. This is done by computing the ℓ_2 -norm between the trace of the current day and the historical data of past days. Then, we take D closest days. Next, we take the corresponding horizon-ahead historical sequences. Second, for each sequence, we compute the mean values and use them to compute a new collection of zero-mean sequences. Then, using these zero-mean sequences, we construct the covariance matrix \mathcal{K} that accounts for the correlation between the load consumption at different time-steps. Third, using \mathcal{K} , we generate M zero-mean random samples using multivariate Gaussian distribution $\mathcal{N}(0, \mathcal{K})$. Finally, the traces of the load consumption are computed as the sum of the generated zero-mean samples and the mean values of the original sequences. As a result, we have L_1 traces for the load consumption. Similarly, using the method described above, we generate L_2 traces for the PV production.²

As an example of the output, Fig. 5.3 and Fig. 5.4 show the load and PV realization compared to the their lower/upper prediction traces (i.e., minimum and maximum values for all traces for each time-step). As scenarios are recomputed at every time period t , we show the snapshot of the traces at time 12:00.

EV User Model and Data

We describe the generation of traces for modelling the EV behaviour. Note that, contrary to PV and load, the uncertainty of these traces is higher as it is strongly related to human behaviour. Therefore, we treat the EV traces as conservative.

To generate traces for the EV behaviour, we need information about the behavior of EV users that are expected to arrive at the CS after the current time $t = 1$. Note

²In practice, an AI-based forecasting tool could be used to determine the horizon-ahead traces (e.g., [155]). Our proposed method is presented only as an alternative to generating the needed scenarios.

Chapter 5. Combined Grid-Aware Control and Optimal Scheduling of Electric Vehicle Charging Stations with V2G Capabilities

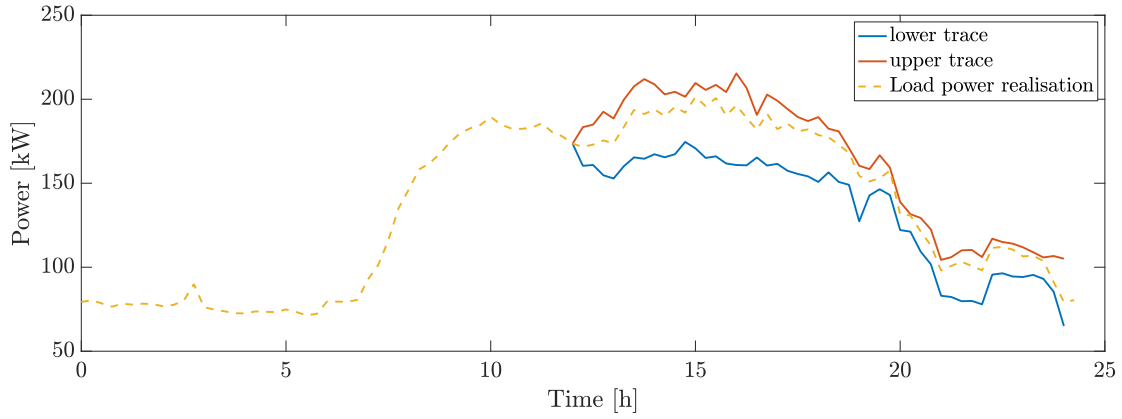


Figure 5.3 – Load consumption realisation vs upper and lower traces of all scenarios.

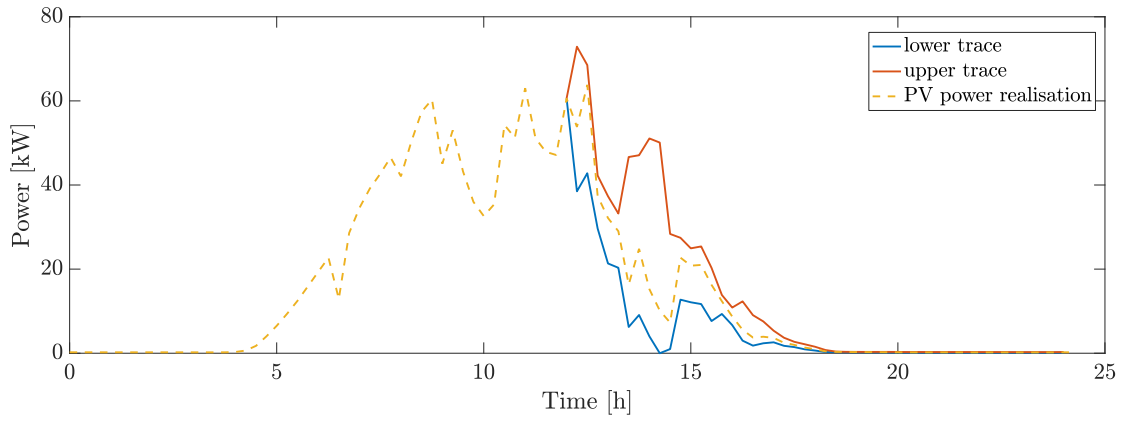


Figure 5.4 – PV production realisation vs upper and lower traces of all scenarios.

that the state of the CS at $t = 1$ is known, i.e., we know the following information about connected EVs: number of charging/discharging EVs, prices of energy and its available amount for discharging EVs, charging demand for charging EVs, and expected departure times. Therefore, it is necessary to emulate the behaviour of users at times $t = 2, \dots, H$ for the scheduling horizon. In this chapter, we assume that the scenario generator synthesizes scenarios, based on the following information:

1. arrivals of EVs,
2. the energy demand of charging EVs,
3. the staying time of both charging and discharging EVs,
4. for discharging EVs, the amount of energy that EV users would like to sell and the price of energy,
5. the average fraction of charging and discharging EVs connected to CS at every timestep.

The process for generating the EV traces is described in Alg. 3. The purpose of the algorithm is to generate traces that emulate: arrivals, departures, the amount of selling/buying energy and selling prices of different EV users for $t = 2, \dots, H$. First, it defines the number of arrivals A , at time t , using a pre-defined probability distribution (line 3). Then, we remove the departed EVs from maps Ch_t and Dh_t computed in previous iterations (line 5). For every arrival, we need to choose an available slot at CS. If there is no free slot, the iteration stops (lines 7-9). Then, we assign a unique id to the newly arrived EV, decide whether it is charging or discharging EV and generate its departure time (lines 10). If it charges, we generate the energy demand E_{id}^{trg} , create the corresponding 3-element tuple, and insert it into the map Ch_t (lines 11-13). Similarly, if it discharges, we generate the amount of energy that the user wants to sell E_{id}^{sell} , its price C_{id} , we create the corresponding 4-element tuple, and insert it into the map Dh_t (lines 14-16). Finally, we modify \mathcal{I} accordingly (line 18). We generate L_3 traces of EVs users behavior using Alg. 3.

Scenario Selection

We generate scenarios for the whole community behavior, i.e., we combine the PV, load, and the EVs traces, thus obtaining L possible scenarios ($L = L_1 \times L_2 \times L_3$). However, as L is expected to be large, it might be prohibitively expensive for the scheduler to provide results in reasonable time (i.e., before the next time-step). To cope with this issue, we propose to take the M most representative scenarios ($M \ll L$), by defining two metrics: (i) the *energy deficit*, defined as the difference between the energy that charging EVs and the load need to fully satisfy their demand and the energy that discharging EVs and the PV have available to sell, and (ii) the *total price of the available energy* from discharging EVs and the grid. Therefore, we select the scenarios using k -means clustering, according to the metrics presented above, thus creating M clusters. Then, for each cluster, we choose the scenario that is closest to the cluster centroid. Finally, we compute the weights w_m for $m = 1, \dots, M$ as the fraction of the number of scenarios in the cluster m and the total number of scenarios. The value of M is decided *ex-ante* as a function of the available computational power to solve (S).

Chapter 5. Combined Grid-Aware Control and Optimal Scheduling of Electric Vehicle Charging Stations with V2G Capabilities

Algorithm 3 Scenario generation

Input: the state of CS at $t = 1$: $\mathcal{I}, \text{Ch}_1, \text{Dh}_1$
Output: matrix \mathcal{I} and collections $\{\text{Ch}_t, \text{Dh}_t\}_{t=1}^H$

```

1: let  $t = 2$ 
2: while  $t < H$  do
3:   generate amount of arrivals  $A$ 
4:   initialize  $\text{Ch}_t = \text{Ch}_{t-1}, \text{Dh}_t = \text{Dh}_{t-1}$ 
5:   remove departed EVs from  $\text{Ch}_t$  and  $\text{Dh}_t$ 
6:   for each arrival  $a \in A$  do
7:     if no empty slots then
8:       break loop;
9:     end if
10:    assign available slot id and generate  $t_{\text{id}}^{\text{dep}}$ 
11:    if EV is charging then
12:      generate  $E_{\text{id}}^{\text{trg}}$ 
13:       $\text{Ch}_t(\text{id}) = \{t, t_{\text{id}}^{\text{dep}}, E_{\text{id}}^{\text{trg}}\}$ 
14:    else
15:      generate  $E_{\text{id}}^{\text{sell}}$  and  $C_{\text{id}}$ 
16:       $\text{Dh}_t(\text{id}) = \{t, t_{\text{id}}^{\text{dep}}, E_{\text{id}}^{\text{sell}}, C_{\text{id}}\}$ 
17:    end if
18:    insert id into matrix  $\mathcal{I}$ 
19:  end for
20: end while

```

5.4 Real-Time Problem

In this section, we describe the details of the real-time controller. We assume that the CS receives an aggregated power setpoint $P^{\text{req}}[k]$ from the grid controller at every time k , and it receives the collection \mathcal{P} from the scheduler at every period t (note that $\Delta t \gg \Delta k$). Contrary to the scheduling operation, where each slot i can have multiple EVs at different times, in the real-time operation every slot hosts a single EV at time k . Consequently, in this section we can interpret $P_i[k]$ as the power of slot i or EV i .

The CS computes setpoints $P_i[k]$ for all slot i where an EV is connected at time k . According to the objectives described in Section 5.2, the CS solves the following optimization problem:

$$\begin{aligned}
 (\text{RT}) \quad & \min_{\mathbf{P}[k]} \quad f_0(\mathbf{P}[k], P^{\text{req}}[k]) + c_1 f_1(\mathbf{P}[k], \hat{\mathbf{P}}[k]) \\
 & \quad + c_2 f_2(\mathbf{P}[k], \mathcal{P})
 \end{aligned} \tag{5.9}$$

$$\text{s.t.} \quad -P_i^{\min} \leq P_i[k] \leq P_i^{\max}, \forall i \in \mathbf{I}[k] \tag{5.10}$$

where

- $\Gamma[k]$ is the collection of EVs that are connected to the CS at time k ,
- $\mathbf{P}[k]$ is the collection of resulting setpoints $P_i[k]$ that will be issued to each slot i where there is a connected EV,
- P^{req} is the aggregated power-setpoint from the grid controller,
- $\hat{\mathbf{P}}[k]$ is the collection of measured powers $\hat{P}_i[k]$ for slots where there are connected EVs,
- $c_1, c_2 > 0$ are weights.

The first term in the objective function is responsible for tracking the aggregated power-setpoint P^{req} and can be expressed as

$$f_0(\mathbf{P}[k], P^{\text{req}}[k]) = \left(P^{\text{req}}[k] - \sum_{i \in \Gamma[k]} P_i[k] \right)^2 \quad (5.11)$$

The term f_1 minimizes the battery wear. As this is a real-time problem, the battery wear can be minimized by avoiding large power jumps from one time-step to the next one [123]. Therefore,

$$f_1(\mathbf{P}[k], \hat{\mathbf{P}}[k]) = \sum_{i \in \Gamma[k]} \left(P_i[k] - \hat{P}_i[k] \right)^2 \quad (5.12)$$

Finally, the term f_2 is responsible for following the long-term goals computed by the scheduler:

$$f_2(\mathbf{P}[k], \mathcal{P}) = \sum_{i \in \Gamma[k]} (P_i[k] - \mathcal{P}_i)^2 \quad (5.13)$$

Notice that according to the constraints (5.8), the long-term goals for all scenarios are equal for the first time step ($t = 1$), thus \mathcal{P} contains long-term goal of the first scenario for $t = 1$.

In summary, we formulate the real-time problem as a quadratic program with linear constraints.

5.5 Validation

5.5.1 Benchmarks

In order to benchmark the performance of our solution, we consider two standard heuristic algorithms: *Earliest Deadline First* (EDF) [58] and *Least Laxity First* (LLF) [59].

The EDF algorithm creates a priority list based on the departure times of EVs, in increasing order. The charging power is assigned to charging EVs, in real time, as the minimum between the power needed to satisfy the energy demand at departure time, and the maximum charging power, i.e., $\min\left(\frac{\Delta E[k]}{t^{\text{dep}}}, P^{\text{max}}\right)$, where $\Delta E[k] = E^{\text{trg}} - E[k]$. Hence, this algorithm enables the EVs with the latest deadlines to stay at low SoE, until there are enough resources to charge it. For a fair comparison, we adapt the EDF algorithm for discharging EVs, i.e., the EVs that depart earlier than others are discharged first. The discharging powers are computed similarly.

The LLF algorithm creates a list sorted by laxity ϕ in increasing order. The laxity is the amount of time needed to satisfy the energy demand at maximum charging power (see Eq. (5.14)). The laxity is computed at every timestep k as

$$\phi[k] = t^{\text{dep}} - k - \frac{\Delta E[k]}{P^{\text{max}}} \quad (5.14)$$

The resulting charging power per EV is computed in the same way as in the EDF algorithm, and it is assigned in order defined by laxity. Similarly to EDF, we adapt the algorithm for discharging such that the EVs with the smallest laxity are discharged first.

5.5.2 Performance Evaluation Metrics

We define the following metrics for the performance evaluation:

- *non-satisfied demand* – measures whether the expected energy demand, defined at arrival, was satisfied upon departure for a charging EV i

$$M_i^{\text{nsd}} = \Delta E_i[t_i^{\text{dep}}] / E^{\text{trg}}, \quad (5.15)$$

where $\Delta E_i[t_i^{\text{dep}}]$ is the energy that remains to be satisfied at departure time. Note that, $M_i^{\text{nsd}} \in [0, 1]$. If $M_i^{\text{nsd}} = 1$, then EV i did not charge. On the contrary, EV i is fully satisfied if $M_i^{\text{nsd}} = 0$.

- *battery-wear* – measures the changes of the charge power

$$M_i^{\text{bw}} = \frac{1}{2(P_i^{\text{max}})^2} \sum_{k=1}^K (P_i[k] - P_i[k-1])^2. \quad (5.16)$$

This metric shows the effect of the control scheme on the battery life. The closer M_i^{bw} is to 0, the less effect there is. If $M_i^{\text{bw}} < 1$, there would be no sharp jump of charging power from 0 to P_i^{max} and back.

5.5.3 Simulation Setup

To validate our method, we consider the following case: a 70 kWp PV plant and a 220 kW load are connected to the main grid, through a transformer rated $P_{\text{Tr}} = 250$ kVA. At the same point, a CS with 20 slots of 22 kW is connected. Commonly, such a configuration would be avoided as, in the worst case when there is no PV generation and the load and CS are consuming its rated power, the transformer protections would trip, thus limiting the CS rated power to 30 kW only. However, this is technically an excessively restrictive constraint as the power variations of PV and load could allow a much larger power for the CS.

To model the uncontrollable resources, the PV and load, we consider a series of historical measurements collected on the EPFL campus at 20 ms resolution [31]. The observations at 15-minute resolution are obtained by average down-sampling the original time-series. This information was used to create the scenarios described in Section 5.3.3.

5.5.4 EV-related Hypotheses

For the modelling of the EV arrivals, we consider that they follow a non-homogeneous Poisson process ($\text{Poisson}(\text{arr}(t))$) [156] with a day-dependent rate $\text{arr}(t)$. To concretize the example, we assume that from 18:00 to 22:00 the arrival rate is 8 arrivals/hour, otherwise it is 4 arrivals/hour. As discussed in [157, 158], usually EVs that arrive in the evening have energy demands and staying time larger than EVs that arrive during the day. Hence, we assume, for simulation purposes, that the energy demands of charging EVs that arrive from 18:00 to 22:00 is distributed normally with mean 80 kWh and standard deviation of 4 kWh ($\mathcal{N}(80, 4)$), and that the staying time (Δt) of these EVs is also distributed normally with mean 10 h with standard deviation of 1 h ($\mathcal{N}(10, 1)$). Consequently, EVs that arrive at other times of the day have energy demands distributed normally $\mathcal{N}(50, 2)$ and the staying time follows $\mathcal{N}(3, 1)$. For discharging EVs, we assume that the amount of energy that EV users would like to sell from 18:00 to 22:00 follows $\mathcal{N}(50, 4)$ and that the staying time follows $\mathcal{N}(10, 1)$. For discharging EVs that arrive at other times of the day, the amount of energy to sell follows $\mathcal{N}(15, 2)$ and

| Parameters / Time | from 18:00 to 22:00 | other time of the day |
|--------------------|----------------------|-----------------------|
| arr (arrivals/h) | 8 | 4 |
| E^{trg} (kWh) | $\mathcal{N}(80, 4)$ | $\mathcal{N}(50, 2)$ |
| E^{sell} (kWh) | $\mathcal{N}(50, 4)$ | $\mathcal{N}(15, 2)$ |
| Δt (h) | $\mathcal{N}(10, 1)$ | $\mathcal{N}(3, 1)$ |
| C (cents/kWh) | $\mathcal{U}(6, 15)$ | $\mathcal{U}(6, 15)$ |

Table 5.1 – Parameters of EV users behavior

the staying time follows $\mathcal{N}(3, 1)$. The energy prices of discharging EVs are assumed to be uniformly distributed between 6 and 15 cents/kWh. Finally, it is assumed that, upon arrival, there will be on average 60% of charging EVs and 40% of discharging EVs. See Table 5.1 for more details. The scenarios of EVs users behavior was created using these data, as explained in Section 5.3.3. We take $L_1 = 20$, $L_2 = 20$, $L_3 = 500$ and $M = 50$, as a trade-off between computational complexity and forecasting performance. In particular, we show that our method is robust even in case of unexpected situations when the forecasts are out of the realisation.

5.5.5 Real-Time Control Evaluation

To demonstrate the need of the real-time controller, we compare the behavior of our method, formulated as the combination of the scheduling problem (S) and the real-time problem (RT) with the scenario-based scheduler formulated in (S), without a real-time controller. We perform a 24-hour simulation for both cases and take the horizon $H = 10$ hours with step equal to 15 minutes.

Fig. 5.5 shows the PV and load power traces (same for both cases), the CS power traces, (one under the control of our method and the other only MPC), the transformer power trace, and the transformer active-power limit. We see that, during the day when the CS is controlled only by the MPC, there are violations of the transformer limit, regardless of constraint (5.3). This is due to the fact that the MPC does not see the inter-period power fluctuations. Fig. 5.6 shows the time window from 14:30 to 14:45 where we zoom in on one of the violation periods of the transformer power limit. We observe that, in this case, there is 10% violation of transformer limit.

An alternative to avoiding this problem, without real-time control, would be to have more conservative bounds in the scheduler. However, defining such large bounds depends on the maximum expected fluctuations of the uncontrollable resources. To show this, we show a specific case where we increase the PV size, hence we set it equal to the transformer's rated power (250 kW) and scale accordingly the PV production. To compare with the original case, Fig. 5.7 and Fig. 5.8 show the 24 h simulation and the time window from 14:30 to 14:45, respectively. Here, we see that violation reaches 32 % of the transformer rated power in the case when real-time control is disabled.

Conservative bounds in this case would significantly decrease the available flexibility of the CS, whereas real-time control solves this issue by fully exploiting the available flexibility.

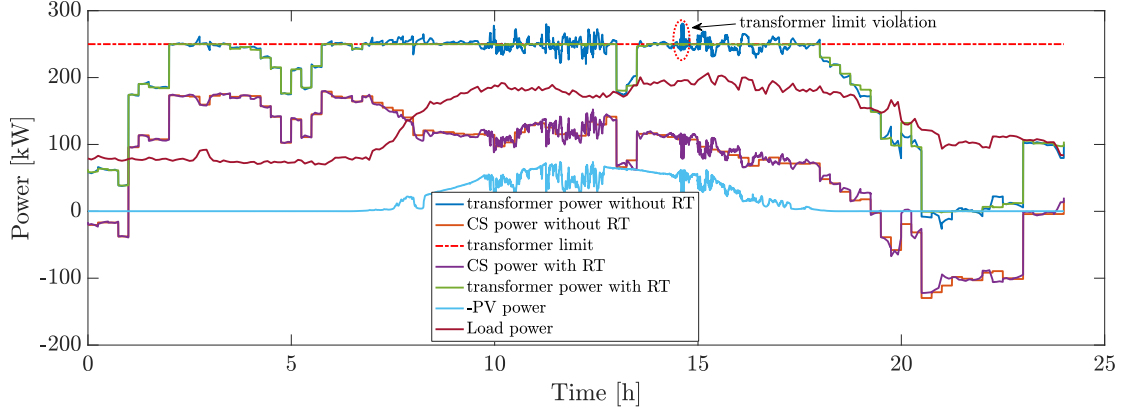


Figure 5.5 – Our method and scenario-based MPC without real-time control 24-hours simulation.

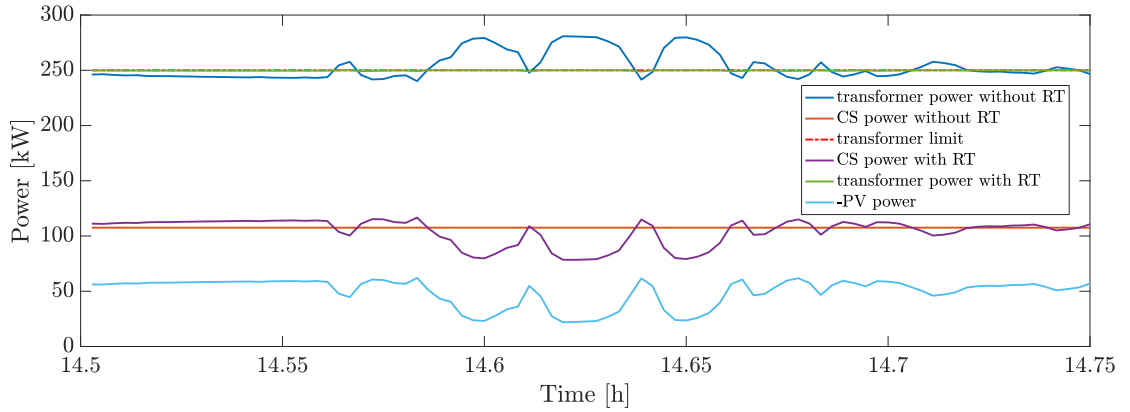


Figure 5.6 – Our method and scenario-based MPC without real-time control zoom on 15 minutes window.

5.5.6 Comparison against Benchmarks

In this subsection, we show the performance evaluation of our method and the state-of-the-art real-time control methods, EDF and LLF. We perform a 24-hour simulation for each method and take the horizon for the scenario-based MPC as $H = 10$ hours with step 15 minutes. Fig. 5.9 and Fig. 5.10 show the non-satisfied-demand and the battery-wear metrics, respectively, of EVs that charged and discharged from 13:00 to 21:00, when there was congestion in the transformer.

These results show that our method performs significantly better than the benchmark algorithms. Indeed, the mean of the non-satisfied-demand metric for our method

Chapter 5. Combined Grid-Aware Control and Optimal Scheduling of Electric Vehicle Charging Stations with V2G Capabilities

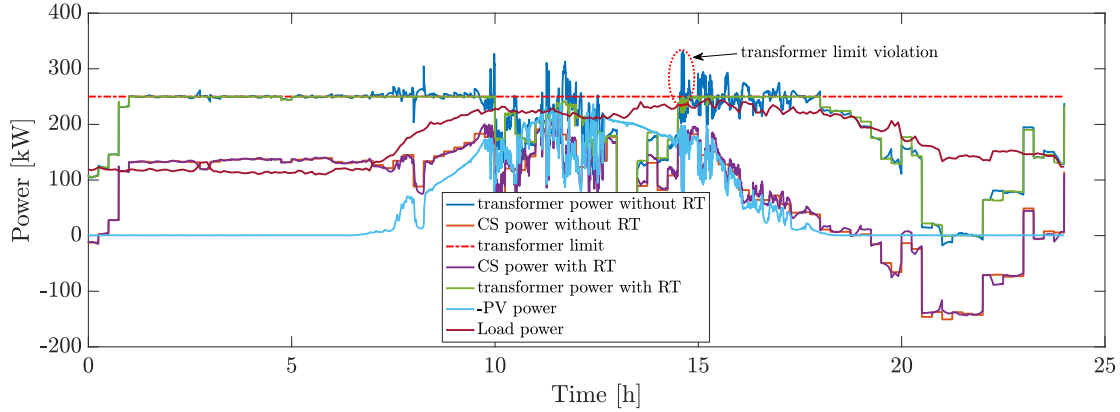


Figure 5.7 – Our method and scenario-based MPC without real-time control 24-hours simulation.

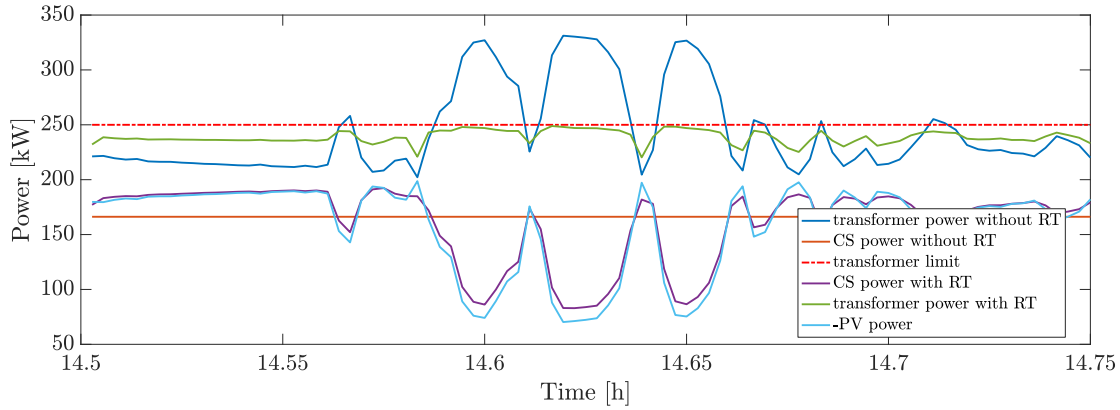


Figure 5.8 – Our method and scenario-based MPC without real-time control zoom on 15 minutes window.

is 0.01 and the whisker of the box that indicate the extreme value equal is to 0.08, hence most of EVs were fully satisfied. Whereas, the means of non-satisfied-demand metric are 0.28 and 0.22 with 0.69 and 0.23 extremes for EDF and LLF, respectively. Furthermore, the median of the battery-wear metric for our method is 0.18 with an extreme value of 0.64. The mean of the battery-wear metric for EDF and LLF is higher than in case of our method: 0.94 and 1, respectively. And more importantly, the top edge of our method is only 0.5, whereas for EDF it is 2.14 and for LLF 2.58, which means that some vehicles will see their batteries strongly affected by these algorithms.

Fig. 5.11 and Fig. 5.12 show the metrics for the EVs that were connected to the CS during the non-congested part of the day. In this case, we see that all methods fully charge the EVs (i.e., the non-satisfied-demand metric is close to 0), because there was a sufficient amount of energy from the different resources. Yet, the battery-wear metric is smaller with our method. In other words, the mean is 0.16 and the extreme value is 0.43, whereas the mean values for EDF it is 0.82 and for LLF is 0.83. Also, the extreme value of the non-satisfied-demand metric is 1.82 in the case of EDF and 1.67 in the case

of LLF. Therefore, as in the congested period of the day, our method shows a reduced battery wear.

We also evaluated, during the whole period, the total operational cost for the consumers (load and charging EVs). The total cost in our method is 767 dollars: 836 dollars for EDF, and 841 dollars for LLF. We observe that our method is more optimal also in terms of overall operational costs.

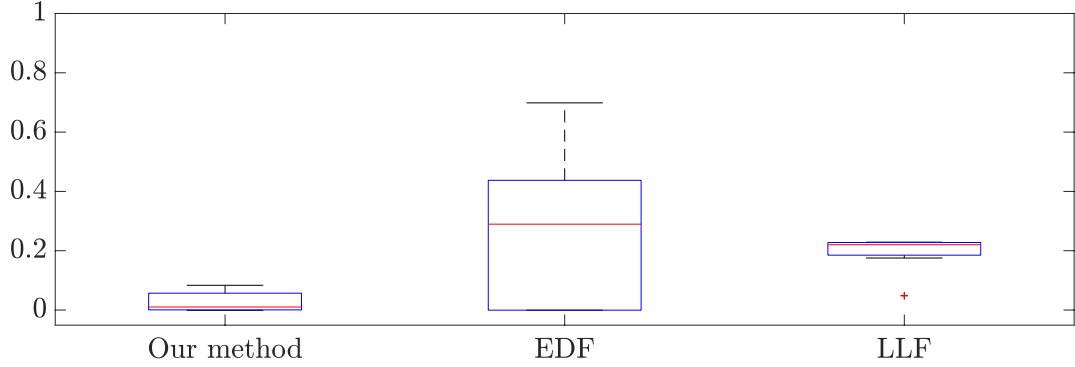


Figure 5.9 – Non-satisfied demand metric for our method, EDF and LLF during congested period.

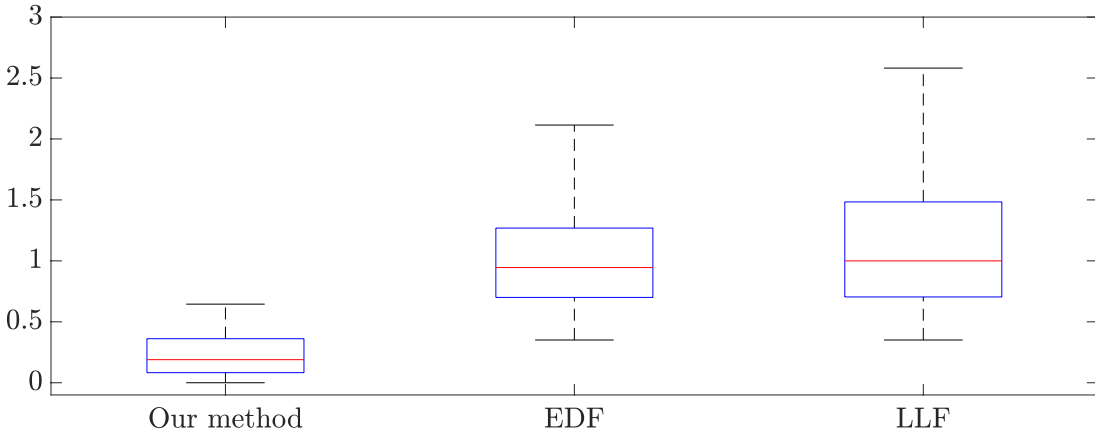


Figure 5.10 – Battery-wear metric for our method, EDF and LLF congested period.

5.5.7 Results for Different Grid-Price Traces

We next study the sensitivity of the proposed method against the grid price. For this, we create 3 different traces of the grid price such that we can see how our method performs with the increased overall price of the grid (See Fig. 5.13 for more details).

For the comparison, we compute separately the total amount of energy that the community buys from the main grid (E^G) and from the V2G EVs (E^{V2g}). We observe that, as expected, E^G decreases for larger grid prices, whereas E^{V2g} increases (see

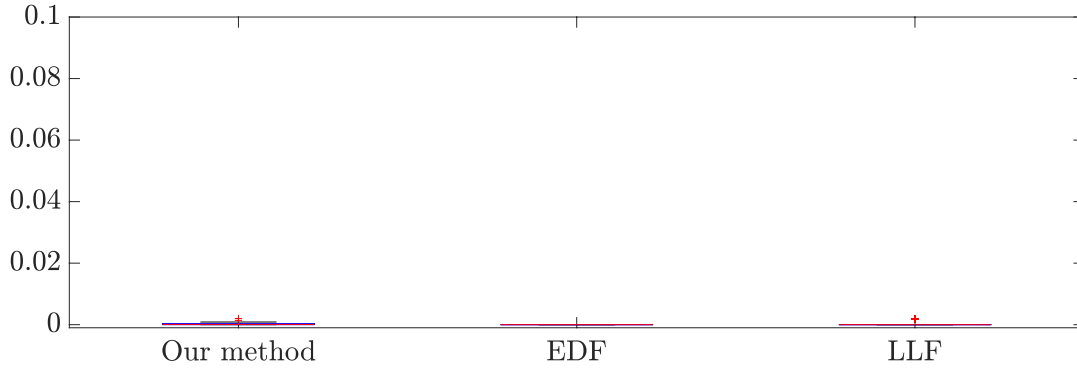


Figure 5.11 – Non-satisfied demand metric for our method, EDF and LLF non-congested period.

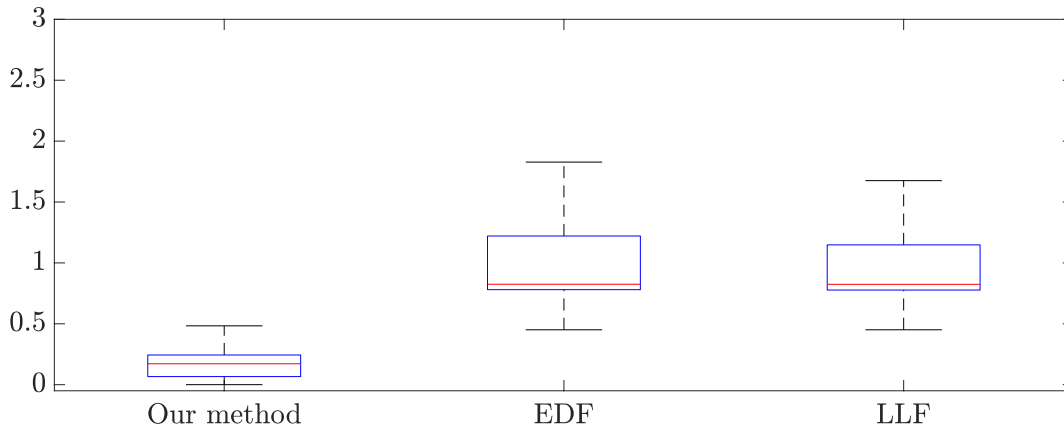


Figure 5.12 – Battery-wear metric for our method, EDF and LLF during non-congested period.

Table 5.2). Still, the overall system cost increases less than the grid prices, by taking advantage of the less expensive energy in the discharging EVs.

| Energy / Cases | case I | case II | case III |
|-----------------|--------|---------|----------|
| E^G (MWh) | 7.587 | 7.369 | 7.154 |
| E^{v2g} (MWh) | 1.153 | 1.384 | 1.608 |

Table 5.2 – Energy bought from the grid and from V2G EVs, for different price cases.

5.5.8 Robustness Evaluation

In this subsection, we study how our method behaves if the prediction scenarios are off the real behavior of the system. For this purpose, we create an unexpected increase of the EV demand during the day. We simulate the EV behavior, as in Section 5.5.4, but we assume that the EVs arriving from 12:00 to 16:00 have a larger energy demand,

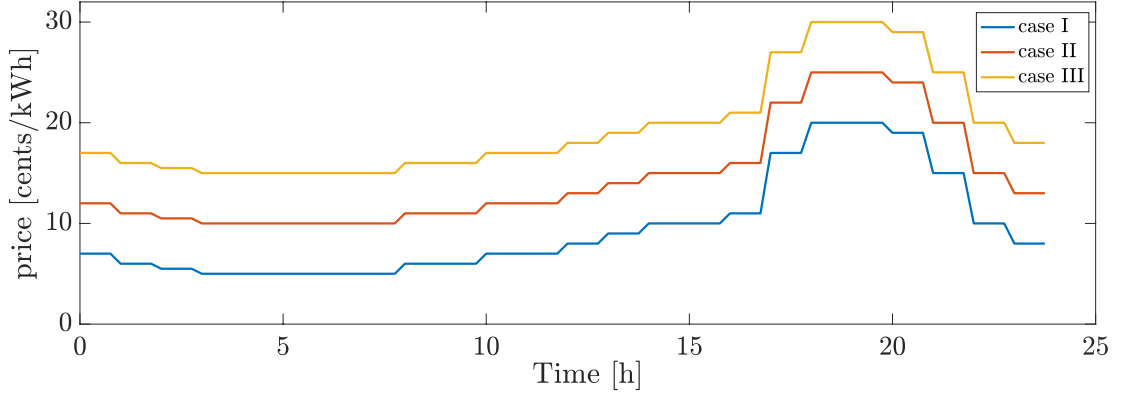


Figure 5.13 – Grid price traces for different cases.

following $\mathcal{N}(90, 2)$ (recall that before we considered $\mathcal{N}(50, 2)$ in this period). In this case, the scenarios generated using the parameters from Table 5.1 will not be able to cover the possible aggregated energy demand of CS.

To evaluate the performance of our method, we compare it with an oracle that perfectly knows the future. We perform two separated simulations for both methods. Fig. 5.14 and Fig. 5.15 show the non-satisfied-demand and battery-wear metrics of EVs during all the simulation periods for the oracle and our method. These results show that the performance of our method is close to that of the oracle for both metrics. The mean values of non-satisfied demand are both equal to 0.08, with upper extremes 0.33 and 0.37 for oracle and our method, respectively. The battery-wear mean values are 0.23 for the oracle and 0.27 for our method, with top edges equal to 0.52 and 0.57. We observe that, due to the fact that we combine MPC and real-time control, our method is robust: the MPC rolling-horizon adapts to the incorrect forecasts and maximises the EV energy-demand satisfaction, whereas the real-time control, in turn, avoids large power jumps to minimize the battery wear.

The total cost when using the oracle is of 767 dollars and 771 dollars for our method, which is less than a 1% difference.

Finally, we show in Fig. 5.16 power traces for the PV production, load consumption, CS controlled by our method, and the transformer power for the robustness evaluation. We see that the power at the transformer never exceeds the transformer limit, even though the forecasts are not correct. This is achieved by the real-time control that maintains the grid in safe operation and prevents transformer overloading.

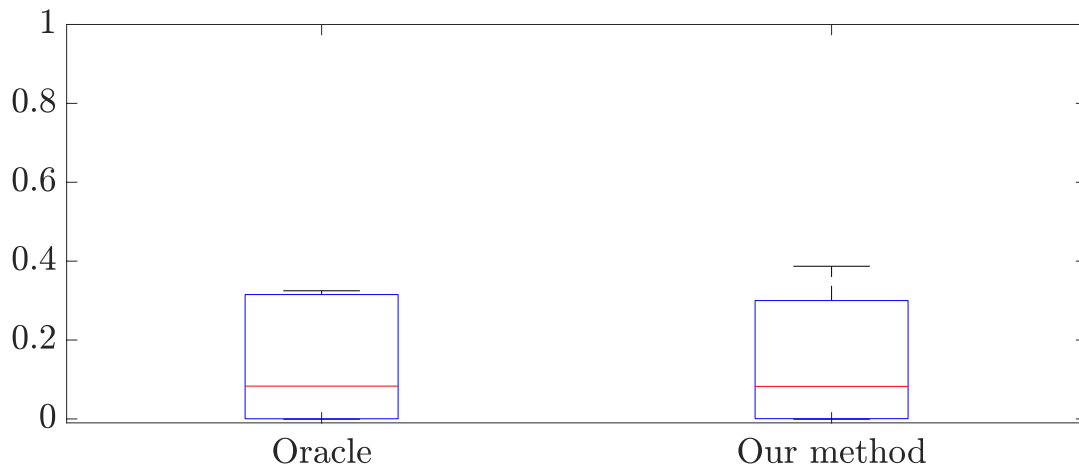


Figure 5.14 – Non-satisfied demand metric for the oracle and our method.

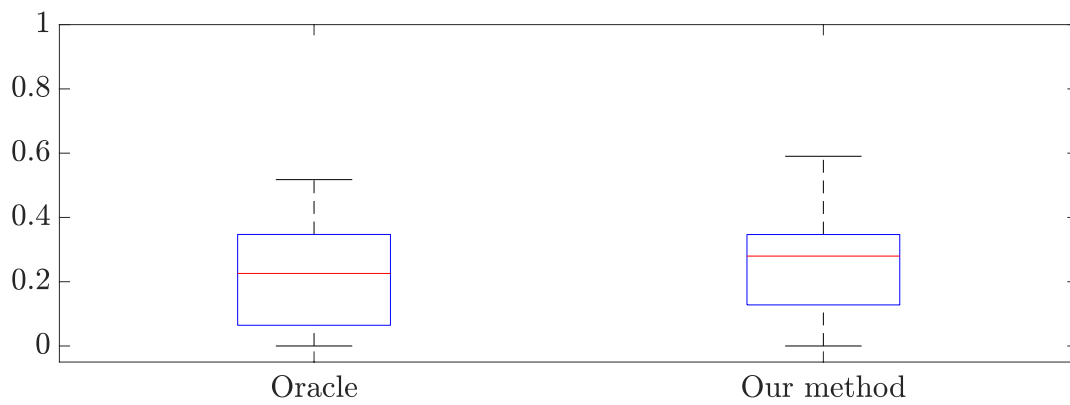


Figure 5.15 – Battery-wear metric for the oracle and our method.

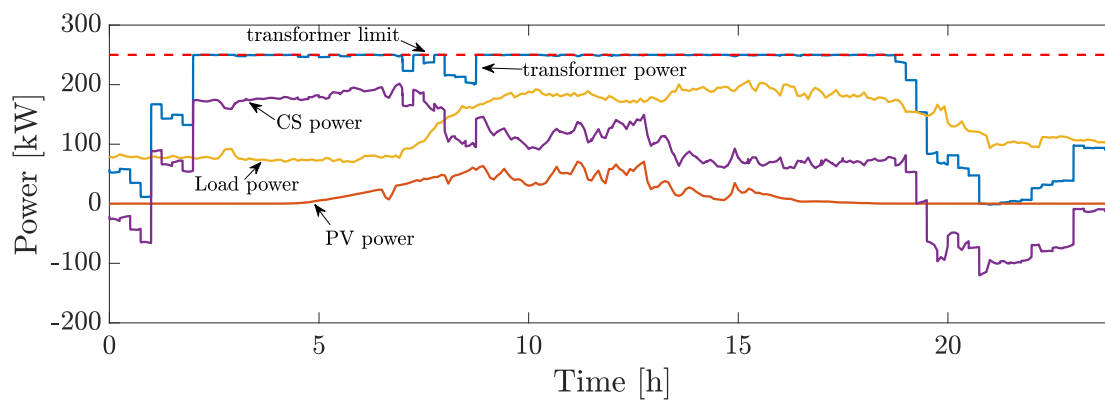


Figure 5.16 – Robustness simulation results.

5.6 Conclusions

In this chapter, we have proposed a method for taking advantage of the available flexibility of regular and V2G EVs in a community setting, by minimizing the community energy-cost and reducing the impact of modifying the charging and discharging powers in the battery wear. The method is proposed as a combination of a scheduling problem and a real-time problem. In this sense, the method is aware of the grid operation, while taking into account the decisions of the scheduler, satisfying the EV energy-needs and minimizing the EV battery-wear. With the proposed method, we show the importance of incorporating the real-time control by demonstrating that the scenario-based MPC on its own is not capable of accounting for the intra-period fluctuations, reducing the capability of the controller to take advantage of the available flexibility and, in consequence, the hosting capacity of EVs and distributed generation.

6 Handling Large Power Steps in Real-Time Microgrid Control via Explicit Power Setpoints

In this chapter, we focus on one of the issues of CS integration in grid-control system. As we mention in Chapter 1, CS itself is a controllable resource from the point of view of the grid controller. We consider a microgrid with real-time control using explicit power-setpoints. Sudden power-steps, such as load disconnections or load in-rushes, directly affect the decisions of the microgrid controller that aims at avoiding voltage or line-ampacity violations. When trying to completely avoid these violations, the microgrid operation may be too restricted, which may lead to large suboptimality. However, temporary violations of the steady-state bounds are allowed by grid standards and could enable the exploitation of the flexibility of other resources to better control the system's state. In this chapter, we propose a method by which such temporary violations are controlled so that they remain within the limits imposed by grid standards and safe operation. The method is experimentally tested and validated on a real microgrid.

6.1 Introduction

As was mentioned in Chapter 1, the number of high-power energy resources in distribution grids, such as electric vehicles (EV), is growing rapidly. These loads could represent the largest ones in microgrids, having a non-negligible impact on their operation. Indeed, the sudden connection or disconnection of such resources may heavily impact the operation of the electrical grid. Specifically, the two major challenges related to distribution systems operation are voltage control and lines congestion management. Possible solutions are grid reinforcement, advanced droop control or real-time agent

based control. In this chapter we are interested in the last solution.

As an example, consider a grid-tied microgrid, that contains local generation (PV or storage system) and electric vehicle charging stations. When an EV suddenly disconnects (e.g., by decision of the EV user) a large power step occurs, potentially leading to overvoltages or overcurrents¹ caused by the local generation that was absorbed by the EV before the step. With real-time agent-based controls, possible solutions might curtail local generation or reduce the EV charging power prior to the step, thus enabling the grid to be always prepared for the large power step.

However, hardly defined operational limits can be violated for short amounts of time with no harm to the grid. For instance, for voltage violations, electric standards (such as [53]) define time-dependent operational bounds. For maximum currents on power lines, line ampacities² are typically not violated. However, the actual operational constraint of a line is its conductor temperature [54]. The line can therefore be temporarily and safely overloaded³; the limit depends on *specific energy* characteristic [55].

In this chapter, we propose a method that allows a real-time grid controller to continuously provide optimal control by relaxing the pre-defined hard constraints and allowing temporary voltage and current violations. More precisely, we make use of the specific real-time control framework in COMMELEC [29] and modify the decision process of the grid controller (a.k.a grid agent), by defining state-dependent penalty functions in the optimization process. We evaluate our proposed solution using a real scale microgrid equipped with real loads, distributed generators and storage. To the best of our knowledge, this is the first attempt to design a real-time grid controller that accounts for temporary voltage and current violations according to electric standards.

The structure of this chapter is the following. Section 6.2 briefly describes the COMMELEC framework. In Section 6.3, we focus on the details of the proposed methodology. Finally, Section 6.4 provides the results of the experimental validation of the method on a real microgrid.

6.2 The Commelec Framework

COMMELEC is multi agent-based framework for real-time control of an electrical grid. The agents are responsible for an entire grid (Grid Agent - GA) or for single resources (Resource Agents - RA [159]).

The GA communicates with its RAs using a common, device-independent protocol for message exchange. More precisely, each RA advertises an abstract representation

¹In this chapter we do not consider electromagnetic transients.

²also known as Permanently Admissible Transmission Loading: PATL

³known as Temporarily Admissible Transmission Loading: TATL

of its internal state using the following format: (1) The *PQ profile* is the set in the (P, Q) plane (for active and reactive power) that the resource under the control of the RA can deploy. (2) The *virtual cost* $C(P, Q)$ is a function, that evaluates the preference of a system to stay in a particular zone of the *PQ profile*. (3) The *belief function* $BF(P, Q)$ is a set valued function that accounts for the uncertainty of the resource operation. Specifically, it returns a convex set that contains all possible set-points that the resource might implement when it is instructed to apply (P, Q) .

The main goal of the GA is to steer the electrical state of its grid in real-time by explicitly setting the power setpoints so that the grid is in a feasible state of operation, that is, the nodal voltage magnitudes and line currents are in safe bounds. To perform this, the GA first needs the advertisements from the resources and the estimation of the current electrical state of the grid. Then the GA computes optimal power setpoints, using a gradient-based method, and sends them to RAs. These process is repeated every 100ms. Thus, the GA has a software-based delay in the sense that it cannot control the grid between two consecutive time-steps. However, the GA makes sure that the state of the grid will be feasible during the next 100 ms by estimating the maximum variation of control using the belief functions. For instance, for EVs, which can be disconnected at any moment, the belief function should take into account the fact that the power consumption might be suddenly equal to zero. Therefore, the advertised belief function is equals to $BF(P) = [-P, 0]$ (assuming reactive power $Q = 0$).

6.3 Penalty Functions in the Grid Agent

As already mentioned, the main task of the GA is to compute setpoints for each RA. To do so, the GA attempts to minimize an objective function that integrates the virtual costs of the resources and a penalty term J that is used to keep voltages and currents between admissible bounds. Let us denote the penalty term for voltage as J_V and penalty term for current as J_I , so that $J = J_V + J_I$. In [29] these functions are chosen as follows (in the next subsection, we propose a suitable modification of these functions):

$$J_V = \sum_k J_{V,k}(V_k) \quad (6.1)$$

where

$$\begin{aligned} J_{V,k}(V_k) &\triangleq \frac{(V_k - V_k^{nom})^2}{\beta_k^2 - (V_k - V_k^{nom})^2} \\ &\quad \text{if } V_k \in [V_k^{nom} - \beta_k, V_k^{nom} + \beta_k] \\ &= \infty \text{ otherwise, and} \end{aligned} \quad (6.2)$$

$$J_I = \sum_l \frac{I_l^2}{(I_l^{max})^2 - I_l^2} \text{ if } I_l \leq I_l^{max}$$

$$= \infty \text{ otherwise.} \quad (6.3)$$

In the above β_k (typically 10% of the nominal voltage) and I_l^{max} are threshold variables, V_k is the voltage magnitude at bus k and V_k^{nom} its nominal value. I_l is the current magnitude at a line l . In other words, the original penalty functions introduce hard constraints on voltages and currents.

6.3.1 Modification to the Voltage Penalty-Function

The standard [53] claims that an undervoltage of 30% and an overvoltage of 20% of the nominal voltage are allowed for at most $T_v = 500\text{ms}$. We call T_v the *violation period*. To account for this, we first replace the hard constraints involving β_k in Eq. (6.2) by

$$V_k \in [V_k^{nom} - \gamma_k, V_k^{nom} + \bar{\gamma}_k] \quad (6.4)$$

where $\gamma_k, \bar{\gamma}_k > \beta_k$ represent the 20% overvoltage and 30% undervoltage bounds respectively. We also define the *relaxation period* T_r , as the time-window that should elapse between two-consecutive violations periods. Note that standards do not explicit such a period. However, in our understanding, a relaxation period of several minutes is necessary in order to avoid repetitive violations. In this work, we take $T_r = 3\text{min}$.

Second, we define four states, that indicate whether the bus is in relaxation or violation period, as defined below:

| States | I | II | III | IV |
|--------------------------------------|----|-----|-----|-----|
| in relaxation ($\tau_{r,k} < T_r$) | No | No | Yes | Yes |
| in violation ($\tau_{v,k} < T_v$) | No | Yes | Yes | No |

where timers $\tau_{r,k}$ and $\tau_{v,k}$ count the time that a bus k is in relaxation or violation period respectively. Fig. 6.1 shows the associated state-machine.

Third, the voltage penalty term depends on the state:

$$J_{V,k}(V_k) = \begin{cases} J_{A,k}(V_k) & \text{if bus } k \text{ in state I, II or III} \\ J_{B,k}(V_k) & \text{if bus } k \text{ in state IV,} \end{cases}$$

where $J_{A,k}$ and $J_{B,k}$ are defined next. $J_{A,k}$ enforces the hard constraint in Eq. (6.4), and has a fast increasing gradient outside the region $(V_k^{nom} - \beta_k + \epsilon, V_k^{nom} + \beta_k - \epsilon)$, where $\epsilon > 0$ is a safety margin. This has the effect that voltage remains in the safe region $(V_k^{nom} - \beta_k, V_k^{nom} + \beta_k)$ when there is no power step and an occasional excursion

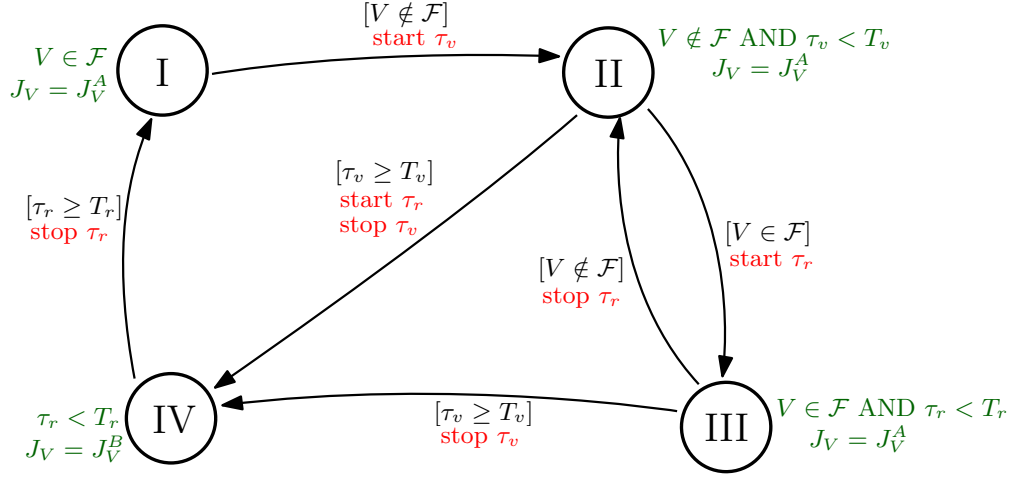


Figure 6.1 – States transitions per bus. $\mathcal{F} = [V^{nom} - \beta, V^{nom} + \beta]$ represents the voltage feasible state. In brackets we describe the condition under which the transition will occur. In red we describe the action associated with the transition. In green we describe the properties of the state.

outside the safe region is allowed when there is a power step. $J_{B,k}$ differs from $J_{A,k}$ in that it has a dramatically larger gradient outside the safe region, so that the voltage quickly returns to it (see Fig. 6.2).

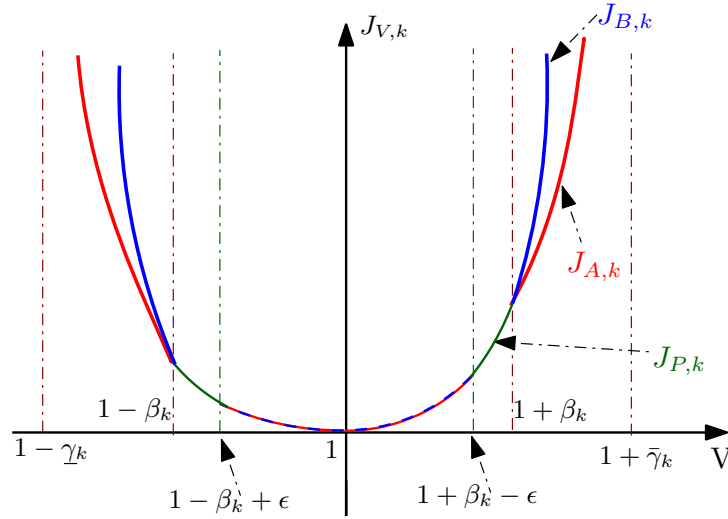


Figure 6.2 – Functions $J_{A,k}(V)$ and $J_{B,k}(V)$, $\alpha = 10^4$ and $V_k^{nom} = 1$.

We now give the description of $J_{A,k}$ and $J_{B,k}$. Note that we impose $J_{A,k}$ and $J_{B,k}$ to have continuous gradients in order to avoid oscillations, which explains some of the complexities of the definitions below.

Chapter 6. Handling Large Power Steps in Real-Time Microgrid Control via Explicit Power Setpoints

First, we define $F_k(V, \mu)$ by:

$$F_k(V, \mu) = \frac{(V - V_k^{nom})^2}{\mu^2 - (V - V_k^{nom})^2} \quad (6.5)$$

Note that F_k is the function that was used in the Eq. (2). Second, we define the function $J_{P,k}(V)$ by:

1. defined on $[V_k^{nom} + \beta_k - \epsilon, V_k^{nom} + \beta_k]$ as the unique quadratic function that satisfies

$$(a) \quad \nabla_V J_{P,k}(V_k^{nom} + \beta_k - \epsilon) = \nabla_V F_k(V_k^{nom} + \beta_k - \epsilon, \underline{\gamma}_k)$$

$$(b) \quad \nabla_V J_{P,k}(V_k^{nom} + \beta_k) = \alpha \nabla_V F_k(V_k^{nom} + \beta_k, \underline{\gamma}_k)$$

$$(c) \quad J_{P,k}(V_k^{nom} + \beta_k - \epsilon) = F_k(V_k^{nom} + \beta_k - \epsilon, \underline{\gamma}_k)$$

2. defined on $[V_k^{nom} - \beta_k, V_k^{nom} - \beta_k + \epsilon]$ as the unique quadratic function that satisfies

$$(a) \quad \nabla_V J_{P,k}(V_k^{nom} - \beta_k + \epsilon) = \nabla_V F_k(V_k^{nom} - \beta_k + \epsilon, \underline{\gamma}_k)$$

$$(b) \quad \nabla_V J_{P,k}(V_k^{nom} - \beta_k) = \alpha \nabla_V F_k(V_k^{nom} - \beta_k, \underline{\gamma}_k)$$

$$(c) \quad J_{P,k}(V_k^{nom} - \beta_k + \epsilon) = F_k(V_k^{nom} - \beta_k + \epsilon, \underline{\gamma}_k)$$

where α is a very large parameter ($= 10^4$ in our case).

Third we introduce the functions $C_{1,k}(V)$ and $C_{2,k}(V)$.

$C_{1,k}(V)$ is defined on $[V_k^{nom} + \beta_k, V_k^{nom} + \bar{\gamma}_k]$ as the unique linear function with the following properties:

1. $\nabla_V F_k(V_k^{nom} + \beta_k, \bar{\gamma}_k) + \nabla_V C_{1,k} = \nabla_V J_{P,k}(V_k^{nom} + \beta_k)$
2. $F_k(V_k^{nom} + \beta_k, \bar{\gamma}_k) + C_{1,k}(V_k^{nom} + \beta_k) = J_{P,k}(V_k^{nom} + \beta_k)$.

$C_{2,k}(V)$ is defined on $[V_k^{nom} - \bar{\gamma}_k, V_k^{nom} - \beta_k]$ as the unique linear function with the following properties:

1. $\nabla_V F_k(V_k^{nom} - \beta_k, \bar{\gamma}_k) + \nabla_V C_{2,k} = \nabla_V J_{P,k}(V_k^{nom} - \beta_k)$
2. $F_k(V_k^{nom} - \beta_k, \bar{\gamma}_k) + C_{2,k}(V_k^{nom} - \beta_k) = J_{P,k}(V_k^{nom} - \beta_k)$.

Now we can define $J_{A,k}$ as follows:

$$J_{A,k}(V) = \begin{cases} F_k(V, \bar{\gamma}_k) + C_{1,k}(V) & \text{if } V \in [V_k^{nom} + \beta_k, V_k^{nom} + \bar{\gamma}_k] \\ J_{P,k}(V) & \text{if } V \in [V_k^{nom} + \beta_k - \epsilon, V_k^{nom} + \beta_k] \\ F_k(V, \bar{\gamma}_k) & \text{if } V \in [V_k^{nom}, V_k^{nom} + \beta_k - \epsilon] \\ F_k(V, \underline{\gamma}_k) & \text{if } V \in [V_k^{nom} - \beta_k + \epsilon, V_k^{nom}] \\ J_{P,k}(V) & \text{if } V \in [V_k^{nom} - \beta_k, V_k^{nom} - \beta_k + \epsilon] \\ F_k(V, \underline{\gamma}_k) + C_{2,k}(V) & \text{if } V \in [V_k^{nom} - \underline{\gamma}_k, V_k^{nom} - \beta_k] \\ \infty & \text{otherwise.} \end{cases}$$

In other words, $J_{A,k}$ is given by the function F_k inside $(V_k^{nom} - \beta_k + \epsilon, V_k^{nom} + \beta_k - \epsilon)$, by the function F_k plus a large linear function outside the region $(V_k^{nom} - \beta_k, V_k^{nom} + \beta_k)$, and is patched between the two by means of $J_{P,k}$ such that it has a continuous derivative. Last, $J_{B,k}$ is defined by

$$J_{B,k}(V) = \begin{cases} \alpha J_{A,k}(V) - (\alpha - 1) J_{A,k}(V_k^{nom} + \beta_k) & \text{if } V \geq V_k^{nom} + \beta_k \\ J_{A,k}(V) & \text{if } V \in [V_k^{nom} - \beta_k, V_k^{nom} + \beta_k] \\ \alpha J_{A,k}(V) - (\alpha - 1) J_{A,k}(V_k^{nom} - \beta_k) & \text{if } V \leq V_k^{nom} - \beta_k. \end{cases}$$

We next show how the algorithm handles overvoltages. The idea is schematically illustrated on Fig. 6.3 for a possible voltage trajectory (with $\beta_k = 0.1$ and $\bar{\gamma}_k = 0.2$). The trajectory starts with no violation. Then, at time t_1 a violation of the $V_k^{nom} + \beta_k$ bound occurs, and $\tau_{v,k}$ starts counting; at time t_2 the voltage goes back below the bounds and $\tau_{r,k}$ starts counting. Note that, at this stage, the violation is still allowed, since $\tau_{v,k}$ has not elapsed. Finally, at time t_3 the violation period ends.

6.3.2 Modification to the Current Penalty-Function

In the case of the current penalty function, we propose a method to track the thermal limit I_l^{max} , and we propose a new definition for the current penalty-function. For the first, we rely on the fact that the operational limit of a conductor is its maximum temperature, which will be reached at different speed depending on the magnitude of the transferred current. We consider the energy balance equation of a conductor [160],

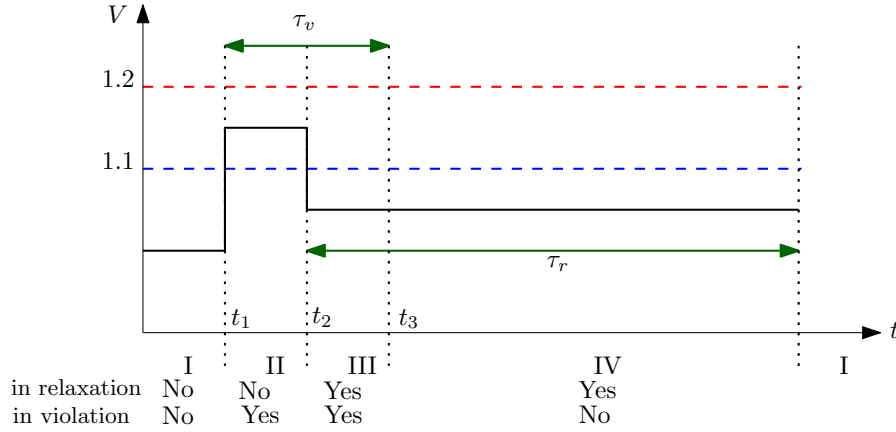


Figure 6.3 – Voltage trajectory with time period dynamics.

$$RI^2 = mc_p \dot{\theta}(t) + k_t S(\theta(t) - \theta_a), \quad (6.6)$$

where θ_a is the ambient temperature, I is the current magnitude and θ the conductor's temperature, while R , m , c_p , k_t and S are physical parameters of the conductor (the per-unit-length resistance of the conductor [Ω/m], the per-unit-length mass of the cable insulator [kg/m], the specific heat of the insulator [$\text{J}/(\text{kg}^\circ\text{C})$] and the global heat-exchange coefficient of the cable [$\text{W}/(\text{m}^2^\circ\text{C})$] respectively). The three elements of the equation represent: Joule losses, heat capacity and forced convection respectively. We assume that all other sources of heating or cooling are negligible (e.g. solar radiation, radiated heat, etc.). In practice, many of the parameters of Eq. (6.6) are difficult to find in datasheets and the temperature estimation through a model becomes an untractable problem.

Instead, we propose to re-write Eq. (6.6) as

$$(\theta_m - \theta_a)I/\bar{I} = H/\bar{I}^2 \dot{\theta}(t) + (\theta(t) - \theta_a), \quad (6.7)$$

where θ_m is the maximum temperature, \bar{I} is the ampacity and H is the *heat impulse*⁴ (in A^2s) of the conductor. These three parameters are typically found in cables datasheets.

In practice, Eq. (6.7) represents the time to reach the maximum temperature for a given current magnitude. Indeed, when the current magnitude is below the ampacity the conductor can operate forever since $\theta|_{t=\infty} < \theta_m$, while the time will be finite only for values above the ampacity. The current-dependent energy involved in this process is known as the *specific energy* (in A^2s). This suggests that, in general, the conductor has an energy *quota* that is only used for values larger than the ampacity. This definition follows the IEC standard [54], that bounds the loss of insulation life of the cable per overload. To account for this use, we continuously evaluate the *integral of Joule* i_J , that

⁴Where $H = \frac{mc_p}{R}(\theta_m - \theta_0)$, and θ_0 is the initial conductor-temperature.

represents a state, using

$$i_J[k] = \begin{cases} i_J[k-1] + I[k]^2 \Delta t & \text{if } I > \bar{I}, \\ i_J[k-1] e^{-\Delta t / \tau_I} & \text{if } I < (1 - \epsilon_I) \bar{I}, \\ i_J[k-1] & \text{otherwise,} \end{cases} \quad (6.8)$$

where I is the current magnitude, Δt the time spent between time-steps $k-1$ and k , $\epsilon_I > 0$ and $\tau_I = H/\bar{I}^2$ represents the decay time-constant of Eq. (6.7). Using this state, the maximum allowed current magnitude I^{max} is the solution of

$$I^2 \Delta \hat{t} = -H/\bar{I}^2 \ln(1 - (\bar{I}/I)^2) I^2 - i_J, \quad (6.9)$$

where $\Delta \hat{t}$ is the estimation of the time that current I will be implemented. The equation cannot be solved analytically. It is solvable, instead, numerically using a lookup-table approach, compatible with the real-time operation. In order to account for the temporal reduction of the maximum allowed current, we propose the following penalty function

$$J_I = \sum_l \frac{\left(\frac{I_l^*}{I_l^{max}}\right)^2 I_l^2}{(I_l^*)^2 - I_l^2},$$

where I_l^* is the maximum allowed current when $i_J = 0$ for $\Delta \hat{t}$, that is used as a hard constraint.

6.4 Validation

We evaluate the proposed method using both simulation and an implementation in a real-scale microgrid. In this chapter we give results obtained by simulation and results from the implementation in the real-scale microgrid (see Fig. 6.6).

6.4.1 Simulation Scenario

Our simulation setup consists of the following elements: a battery (B), an electric vehicle (EV) and a photovoltaic plant (PV). The PV is uncontrollable and is characterized by a rated power of 20kW. It is assumed that the PV injects only active power. The EV, assumed to behave as an uncontrollable load, constantly consumes 30kW (P_{max}). The battery in our case is considered as a fully controllable device and its rated power 25kW. We assume that the battery is almost charged (90%) at the beginning and has a long-term objective to get discharged. For both battery and PV plant the PQ profile, virtual cost and belief function are adopted from [159].

Our goal is to simulate a sudden disconnection of the EV. For that reason we assume that initially the EV active power is $-P_{max}$ and it suddenly goes to zero (at time t_2). As the resource cannot be controlled, we define the PQ profile as the actual measured active-power, the virtual cost equals to zero and the BF will express the power change uncertainty. At the beginning of the simulation, the EV agent advertises a small belief set $[-P_{max}, -P_{max} + \delta]^5$. At time t_1 , as the agent predicts that the EV may get disconnected, it will advertise the belief set $[-P_{max}, 0]$. In this specific scenario, we use small bounds for the voltage and current constraints, so that they are replicable in the real-scale microgrid.

6.4.2 Simulation Results: Voltage Violation

For the validation of the proposed method, we present two cases: *case 1* using the GA as described in [29] and *case 2* with the proposed method integrating the new voltage penalty. The simulation results are shown in Fig. 6.4, that shows the battery power and the voltage profile of the bus where the EV is connected. Note that, at the beginning of the simulation, the GA in both cases behaves similarly as expected. That is, the battery is allowed to provide the same amount of active power. However, at time t_1 the EV agent expands its belief function. The GA of case 1 will try to prevent the worst-possible scenario, namely, a large voltage-step caused by a sudden EV disconnection, before it happens. Since in our setup the only controllable device is the battery, the GA, in a conservative action, reduces the battery production. On the contrary, the GA of case 2 will continue allowing the battery to produce power. We also shown that, when the EV actually disconnects (at time t_2), the voltage does not exceed the smaller bound, in case 1. In case 2, the GA reduces the power production of the battery and brings the voltage back to the safe region after the allowed violation period ends at time t_3 .

6.4.3 Simulation Results: Current Violation

We present in Fig. 6.5 the evolution in time of the current in a congested line, the state variable i_J of the same line and the active power of the battery. Before t_2 , the power of the battery slightly decreases. When the EV is disconnected, the lines gets congested and i_J of the line of interest quickly increases. Consequently, the dynamic current limit I_l^{max} decreases, forcing the actual flowing current magnitude to decrease as well. When the current magnitude goes below $(1 - \epsilon_I)\bar{I}$, i_J decreases exponentially letting the battery to increase the power back⁶.

⁵Negative power indicates consumption. We take $\delta = 10\%$ of P_{max}

⁶We take $\epsilon_I = 0.1$.

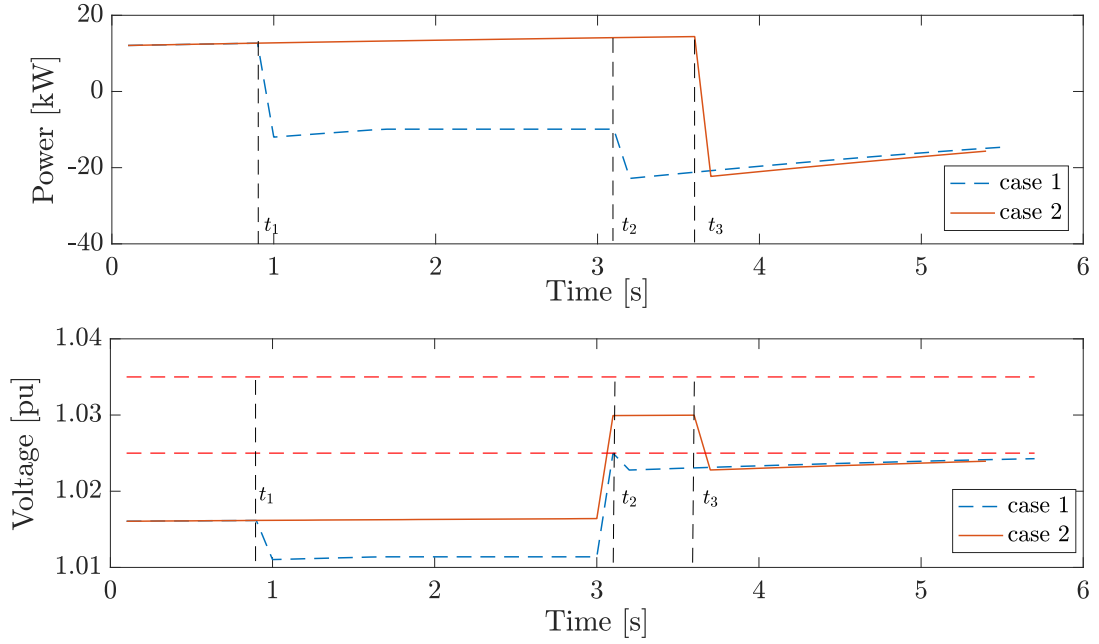


Figure 6.4 – Simulation results for the voltage violation case.

6.4.4 Experimental Setup

The results described in this section refer to the application of the proposed methodology to a real-scale microgrid, that represents at real-scale the CIGRÉ low-voltage (400V at 50Hz) microgrid benchmark defined in [57]. For simplicity, we only use a subset of the energy resources: a controllable resource (L1), a battery (B) and a photovoltaic plant (PV). L1 is a fully controllable 4-quadrants resource, that is used in this case for creating the power step.

The microgrid of Fig. 6.6 is connected to a 20 kV grid at bus B01 via a suitable transformer. The line that connects to the transformer, L01, has a current limit of 40 A, i.e. a power transfer limit of ca. 28 kVA.

6.4.5 Experimental Results: Voltage Violation

Since our experimental setup (see Fig. 6.6) does not have a real EV, we use the controllable resource L1 instead, in order to emulate a large power step. In this section, we present the behavior of the voltage at the node where L1 is located (B03) when a large power step of 30 kW is produced by L1.

At the beginning of the experiment, L1 consumes 15 kW. Then, we emulate the power step by producing 15 kW with it. This 30 kW power step causes a violation of $\beta = 4\%$ of the nominal voltage. In Fig. 6.7 we show how the GA reduces the power

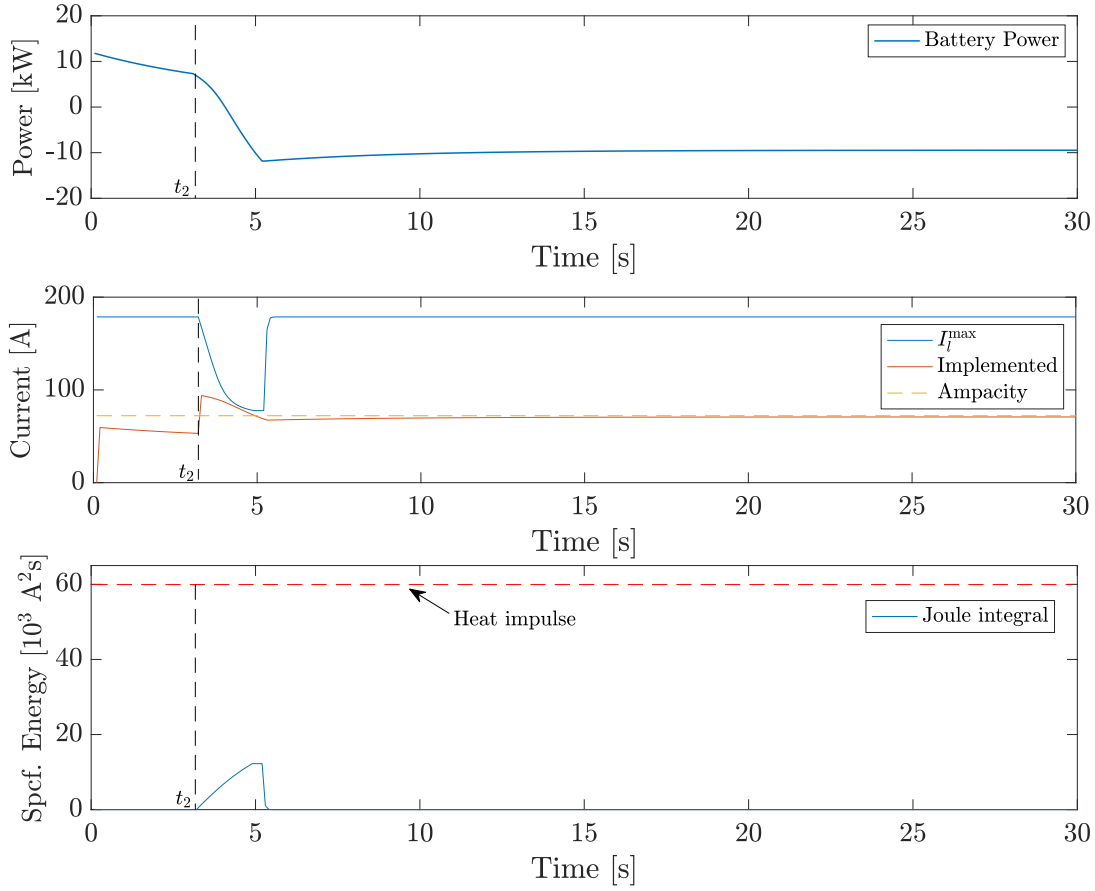


Figure 6.5 – Simulation results for the current violation case.

production of the battery and brings the voltage of node B03 back to the safe region after the allowed violation period ends. Also, it is interesting to see that due to the definition of J_P , the voltage stabilizes below its soft limit β .

6.4.6 Experimental Results: Current Violation

In this section, we focus on the behavior of the current of line L01 when a large power step of 20 kW is produced by the sudden increment of L1. The emulated load has a power factor of 0.9, thus the reactive power consumption also increases accordingly. In this specific scenario, we have considered that the PV is not injecting power into the microgrid and that the battery is being charged. In Figure 6.8 we show how the proposed methodology allows an initial current violation, that triggers the increment of the line's integral of Joule i_J . Consequently, after solving Eq. (6.9), the maximum allowed current I_l^{max} decreases, forcing the GA to quickly steer the battery power to reduce the current at L01. When the current magnitude reaches safe values, i_J smoothly decreases following Eq. (6.8). This smooth behavior permits that the current I_l stabilizes at safe values even when the perturbation is persistent.

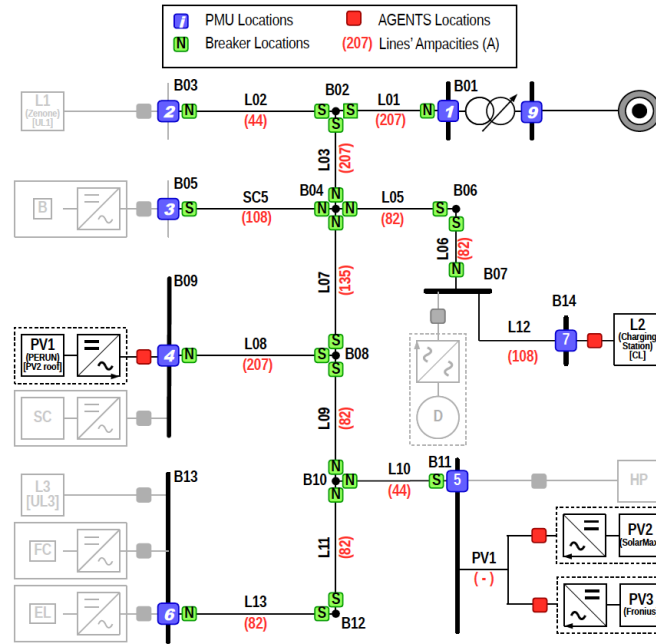


Figure 6.6 – The experimental microgrid. In black all elements participating in this work’s experiments. Location of measurement devices for state estimation (PMUs) are also indicated.

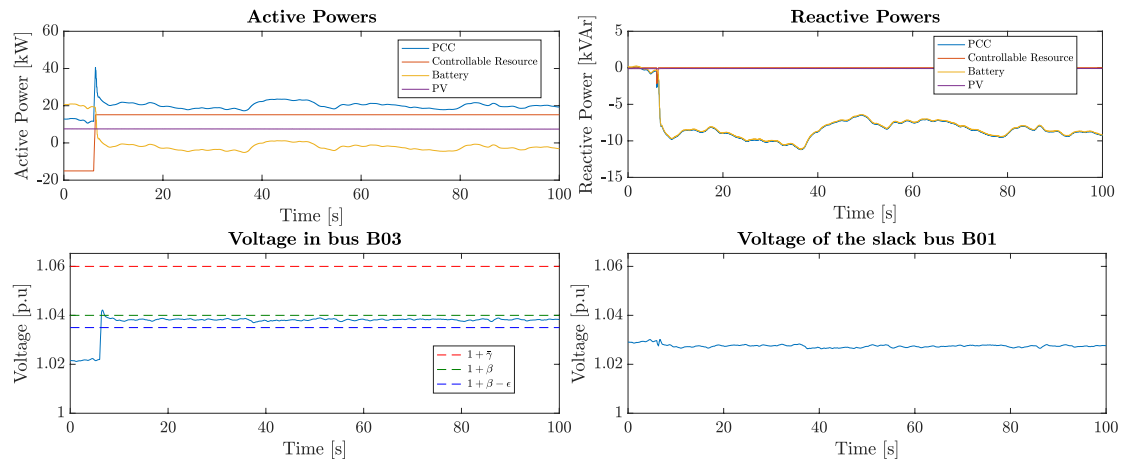


Figure 6.7 – Experimental results for the voltage violation case.

Chapter 6. Handling Large Power Steps in Real-Time Microgrid Control via Explicit Power Setpoints

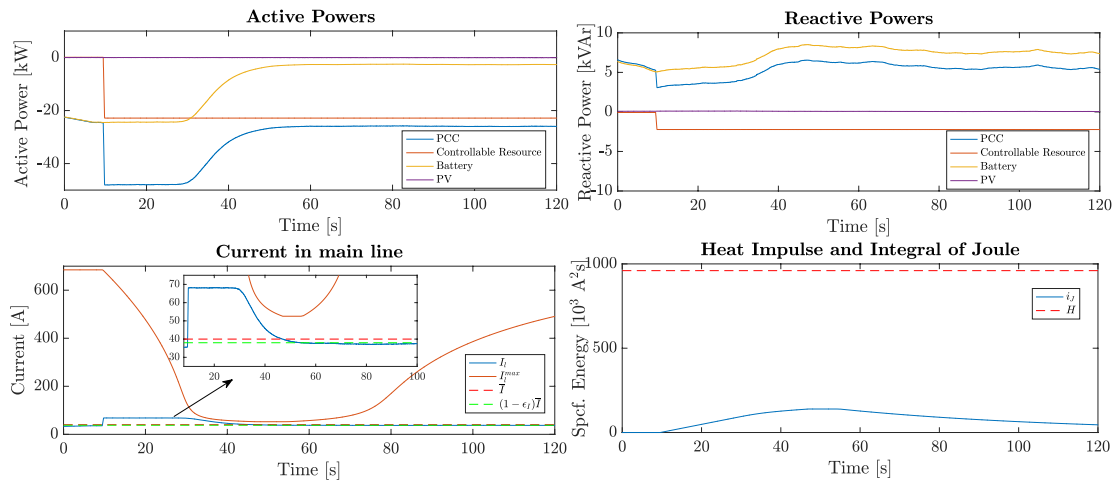


Figure 6.8 – Experimental results for the current violation case. The plots in the lower part refer to line L01 of Fig.6.6.

6.5 Conclusions

In this chapter we have proposed a method by which a grid real-time control can handle large power steps by allowing and controlling temporary voltage and current violations so that they remain within the limits imposed by standards and safe operation. This brings more flexibility to the grid operation, which can lead to better operational results such as increased self-consumption or higher EV charging rates. The proposed methodology has been validated both with simulations and experimentally.

7 Robust Real-Time Control of Power Grids in the Presence of Communication Network Non-Idealities

In this chapter, we discuss the issue of message losses caused by the inherent uncertainties and non-idealities of communication networks and processes in the context of real-time power grid control. More precisely, we consider a hierarchical power grid controller that monitors and controls resources in real-time. The resources send *advertisements* that contain information about their state, and an estimation of their behavior in the time horizon when the control action is expected to be implemented. The controller uses this information to compute and issue setpoints that are thus only valid for this time horizon. An occasional loss of one or more advertisements might render the controller incapable of issuing valid setpoints. We introduce advertisements with a longer-term prediction interval, which are constantly sent along with the short-term ones, and can be used by the controller when it is missing information from some or all resources. We show the advantages of using such an approach on a controller that, by exploiting local resources flexibilities, performs frequency support on the CIGRÉ benchmark low-voltage microgrid.

7.1 Introduction

7.1.1 Background

The trend in power distribution-grid control is to aggregate in real-time the network flexibilities in order to achieve local and global objectives. Controllers that implement real-time (sub-second) functionalities, will occasionally experience communication network non-idealities during deployment, such as message losses and delays. This

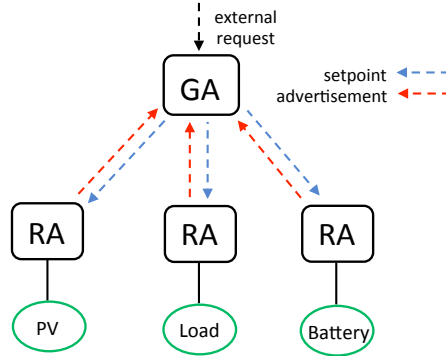


Figure 7.1 – COMMELEC Architecture

increases the uncertainty in the operation of the controller, and limits its ability to maintain a feasible control over the grid resources. Given the mission-critical nature of power grid control, and the possible consequences that might arise in case of failure [161], it is essential for power grid controllers to be robust in the presence of such uncertainties.

Several controller designs presented in literature assume an ideal communication network [29, 162, 163] since, as they are designed for real-time, they can quickly counteract an occasional missing package. However, despite advances in improving the resiliency and reliability of communication networks in power grids [164, 165, 166], non-idealities cannot be eliminated due to the stochastic nature of wide-spread communication networks. This is especially true for real-time applications, in which low latencies are required.

As an example, in this work we consider the COMMELEC framework [29], initially designed with the assumption of ideal communication, and we propose a method that makes it robust to message losses and delays. COMMELEC is a multi-agent framework for real-time control of distribution power grids using explicit power setpoints. However, the method presented in this chapter is not limited to this framework and can be applied to any application with real-time decisions.

Such a method complements the traditional redundancy approach in achieving a higher degree of reliability [167, 168].

The COMMELEC architecture is shown in Figure 7.1. It consists of a main controller, henceforth the *Grid Agent* (GA), and several local controllers, each in charge of a specific resource, henceforth the *Resource Agents* (RAs). An RA captures the inner state of its resource and sends it as an *advertisement* to the GA. The GA uses the received advertisements to compute and issue explicit power *setpoints* that the RAs will instruct their resources to implement. The setpoints are computed such that their implementation: (1) maintains the grid in a feasible state (i.e. within voltage and current bounds), (2) tracks an upper-level request, such as dispatching a power profile

or providing frequency support, and (3) tries to yield to the desired operation of the resources.

The advertisements sent by the RAs consist of, among other entries, the following two fields. (1) A *PQ profile* which represents the feasibility region of the resource, the region in the PQ -plane (for active and reactive power) in which the resource can be instructed to operate. (2) A *Belief function* $\mathcal{B}(u)$, which captures the uncertainty of the resource. It maps every point $u = (P, Q)$ in the PQ profile to a set of points in the PQ -plane, which the resource might implement if instructed to implement u . The above fields are constructed by RAs such that they are only valid for a short-horizon ϑ , i.e. they need to be updated in the next setpoint implementation.

Under ideal communication network conditions (i.e. in the absence of messages losses and delays), the GA receives the latest advertisement from each RA, and performs the setpoint computation. For each resource, the GA determines a power setpoint from its PQ profile, such that the set of power setpoints for all resources results in a feasible grid state and maximizes the tracking of the requested external signal. This computation relies on the prediction in the advertisement, which is only valid for the horizon ϑ . An occasional lost or delayed advertisement from a resource might render the GA incapable of computing setpoints that satisfy the mentioned constraints. In principle, the GA waits until the advertisement is received, causing a loss of control for that period.

As an example, consider a grid-tied microgrid, as shown in Figure 7.1, that consists of a battery, a PV, and a load. Let us suppose that the GA has the objective of providing primary frequency support to the main grid by controlling the battery power flow injection/absorption. It also needs to ensure that the bus-voltage and line-current magnitudes are within the safety limits, despite the stochastic profile of the PV injections and load consumption. A quick change in the frequency signal, PV production, or load consumption, coupled with a loss of advertisements, renders the GA unaware of the present and future state of the grid resources, and thus incapable of computing valid setpoints in the next cycle.

7.1.2 Contributions

In this chapter, we propose a method that augments the RA advertisement, enabling the GA to become robust to communication network non-idealities. More precisely, we introduce two fields into the advertisements, constituting long-term information valid for a period greater than ϑ . We modify the GA in order to store the latest received advertisement, and make use of the long-term fields in the stored advertisement when the present advertisement is lost from some resource. The newly added fields are constructed in a way that ensures the safety of the grid, when they are used in a

setpoint computation.

We validate our method and compare it to alternative methods, using a virtual commissioning tool that simulates the CIGRÉ benchmark low-voltage microgrid [57] consisting of a battery, a PV plant, and a load. This tool enables us to emulate non-ideal network conditions and study the behavior of the actual COMMELEC implementations under such conditions.

The structure of this chapter is as follows. Section 7.2 focuses on the details of our proposed methodology, highlighting the properties of the newly added fields. In Section 7.3, we describe the setup under study. Section 7.4 provides the results of the validation and comparative experiments. Finally, we conclude the chapter and discuss future work in Section 7.5.

7.2 Method

We augment the COMMELEC advertisements to include two new fields: (1) a long-term PQ profile (\mathcal{A}_l), and (2) a long-term Belief function (\mathcal{B}_l). The original PQ profile (\mathcal{A}) and Belief function (\mathcal{B}) are henceforth referred to as *short-term fields*. As mentioned earlier, the short-term fields estimate the behavior of the resource in the horizon that the control action is expected to be implemented, ϑ . This horizon should be short enough to allow the main controller to cope with the fastest dynamics in the system. On the other hand, long-term fields must be valid for a longer horizon Λ , taking into account all possible control actions and internal/external changes that might occur during this time. In practice, Λ should be chosen to ensure that a setpoint will be received during that horizon even in the presence of communication network non-idealities.

In general, the choice of a time horizon (ϑ or Λ) is a trade-off between several factors. A shorter horizon requires less time to compute, provides a more accurate prediction, and exports less uncertainty to the GA. However, as the horizon is shorter, the GA is not robust to losses. Therefore, sending both short-term and long-term fields allows us to take advantage of the accuracy of the short-term prediction, and the robustness of having a longer-term time horizon.¹

Note that since the PQ profile and the Belief function have a time horizon in which they are valid, they implicitly contain a time argument that represents their construction time, i.e. the time from which they are valid. This argument is made explicit in the rest of this section.

¹Note that, the proposed method is independent of the choice of ϑ and Λ .

7.2.1 Properties of Long-term Fields of an Advertisement

Formally, the following properties must hold for the long-term fields of an advertisement.

Property 7.1 (Long-term PQ profile).

$$\forall t' \in [t, t + \Lambda], \mathcal{A}_l(t) \subseteq \mathcal{A}(t')$$

In other words, the long-term PQ profile should be a subset of all short-term PQ profiles that lie within its horizon. This ensures that any setpoint in \mathcal{A}_l lies within the flexibility region of the resource for the entire long-term horizon. Therefore, if the GA chooses a setpoint from $\mathcal{A}_l(t)$, the implementation of this setpoint at the RA is guaranteed to be feasible if it is received at a time $t' \leq t + \Lambda$.

Property 7.2 (Long-term Belief function).

$$\forall t' \in [t, t + \Lambda], \forall u \in \mathcal{A}_l(t), \mathcal{B}(t')(u) \subseteq \mathcal{B}_l(t)(u)$$

As the belief function encapsulates the uncertainty of the resource when instructed to implement a setpoint $u = (P, Q)$, the long-term belief set of a setpoint should contain all the short-term belief sets of that setpoint in the long-term horizon. This ensures that any actual implementation lies within the long-term belief set of the issued setpoint. Therefore, if the GA computes a setpoint that is valid when considering the uncertainty advertised in $\mathcal{B}_l(t)$, then it is valid in the actual uncertainty $\mathcal{B}(t')$, for $t' \leq t + \Lambda$.

Note that the condition in Property 7.2 must hold for all u in $\mathcal{A}_l(t)$. Given that the domain of $\mathcal{B}_l(t)$ is $\mathcal{A}_l(t)$ and the domain of $\mathcal{B}(t')$ is $\mathcal{A}(t')$, then Property 7.1 guarantees that all the elements of $\mathcal{A}_l(t)$ are in the domain of $\mathcal{B}(t')$ as well.

7.2.2 Constructing Long-term Fields

Here, we define how the long-term fields can be constructed for the three types of resources of our case study, namely a battery, an uncontrollable PV, and an uncontrollable load. The method presented builds on the method defined in [159] for constructing the original COMMELEC advertisement (containing only the short-term fields).

Batteries

To compute the short-term fields, the battery agent makes use of the battery model proposed in [169]. Note that, assuming that the batteries are fully controllable, there is no uncertainty to deploy a setpoint. Thus, only the PQ profile needs to be continuously updated but not the Belief function. In particular, only the minimum and maximum active power, P_{min} and P_{max} (that depend on the state-of-charge of the battery, for details see [159]), need to be estimated. In general, the battery advertisement is defined by:

$$\begin{aligned}\mathcal{A} &= \{(P, Q) \in \mathbb{R}^2 | P_{min} \leq P \leq P_{max}, \sqrt{P^2 + Q^2} \leq S_r\}, \\ \mathcal{B}(P, Q) &= \{(P, Q)\},\end{aligned}\tag{7.1}$$

where S_r represents the rated power of the battery converter.

Now, assuming that the state-of-charge (SoC) of the battery changes little in a ϑ -horizon, the battery agent is able to compute P_{min}^ϑ and P_{max}^ϑ , which represent the power limits that can be applied at horizon ϑ . Note that, this computation depends on the last implemented setpoint P . The pseudo-algorithm of this process is detailed in Algorithm 4.

Algorithm 4 Compute Power Bounds for the ϑ -horizon

Function: getShortTermBounds(P, ϑ, SoC)

- 1: Get the corresponding DC power p from the setpoint P implemented at t , using a converter model
 - 2: Use p and SoC to compute the SoC^ϑ : the state of the battery at $t + \vartheta$
 - 3: Compute the DC short-term power bounds ([159]), $p_{min}^\vartheta, p_{max}^\vartheta$, that respect the DC voltage and current limits
 - 4: Use the converter model to get $P_{min}^\vartheta, P_{max}^\vartheta$ **return** $P_{min}^\vartheta, P_{max}^\vartheta, \text{SoC}^\vartheta$
-

In order to compute the PQ profile at the horizon Λ , we use Algorithm 4, $2(n-1)+1$ times, with:

$$n = \left\lceil \frac{\Lambda}{\vartheta} \right\rceil\tag{7.2}$$

In other words, after computing the short-term power bounds, we use them as inputs for the computation of the bounds at the next ϑ -horizon (since they are valid). Note that, this is a worst-case analysis since the actual implemented power will always respect the pre-computed bounds. We repeat the same until reaching the $n\vartheta$ -horizon, using the $P_{min}^{i\vartheta}$ as input for computing the $P_{min}^{(i+1)\vartheta}$ bound (and similarly for P_{max}). In

general, the computed power bounds are not monotonic with time, hence we take:

$$\begin{aligned} P_{min}^\Lambda &= \max_{i \in [1, n]} P_{min}^{i\vartheta}, \\ P_{max}^\Lambda &= \min_{i \in [1, n]} P_{max}^{i\vartheta} \end{aligned} \quad (7.3)$$

This will ensure that $\mathcal{A}_l \subseteq \mathcal{A}$, satisfying Property 7.1 from Section 7.2.1. We summarise this process in Algorithm 5.

Algorithm 5 Compute Power Bounds for the Λ -horizon

Function: getLongTermBounds(P, ϑ, Λ)

```

1: Compute  $n = \lceil \Lambda / \vartheta \rceil$ 
2:  $[P_{min}^\vartheta, P_{max}^\vartheta, \text{SoC}^\vartheta] = \text{getShortTermBounds}(P, \vartheta, \text{SoC})$ 
3:  $\underline{\text{SoC}}^\vartheta = \overline{\text{SoC}}^\vartheta = \text{SoC}^\vartheta$ 
4: for all  $i \in [1, n - 1]$  do
5:    $[P_{min}^{(i+1)\vartheta}, -, \underline{\text{SoC}}^{(i+1)\vartheta}] =$ 
6:      $\text{getShortTermBounds}(P_{min}^{i\vartheta}, \vartheta, \underline{\text{SoC}}^{i\vartheta})$ 
7:    $[-, P_{max}^{(i+1)\vartheta}, \overline{\text{SoC}}^{(i+1)\vartheta}] =$ 
8:      $\text{getShortTermBounds}(P_{max}^{i\vartheta}, \vartheta, \overline{\text{SoC}}^{i\vartheta})$ 
9: end for
10:  $P_{min}^\Lambda = \max_{i \in [1, n]} P_{min}^{i\vartheta}$ 
11:  $P_{max}^\Lambda = \min_{i \in [1, n]} P_{max}^{i\vartheta}$  return  $P_{min}^\Lambda, P_{max}^\Lambda$ 
    
```

Uncontrollable PV

In the case of an uncontrollable resource, the GA does not count on the flexibility to request a setpoint different to what the resource is able to do. Thus, the short- and long-term PQ profiles will be same and equal to the forecasted power injection (P_f, Q_f) . In general, the uncontrollable-PV advertisement is defined by:

$$\begin{aligned} \mathcal{A} &= \{(P_f, Q_f)\}, \\ \mathcal{B}(P_f, Q_f) &= \{(P, Q) \in \mathbb{R}^2 \mid P_{min} \leq P \leq P_{max}, \\ &\quad Q_{min} \leq Q \leq Q_{max}\} \end{aligned} \quad (7.4)$$

For computing the long-term Belief function we use the same method as the one used for the short-term one, as proposed in [170]. This method predicts the interval where the injected power will lie in a given time-horizon. It consists of a training stage where it learns from past data, sampled at the desired horizon. Then, in an on-line stage, it uses the results of the training stage and the current measured value to

estimate a prediction interval for the pre-defined horizon. As in practice longer term PV dynamics are larger than short-term ones, this method ensures that $\mathcal{B} \subseteq \mathcal{B}_l$ by the use of historical data in the training stage, satisfying Property 7.2 of Section 7.2.1. Finally, we deploy two parallel predictions for both the short- and the long-term horizons.

Uncontrollable Load

As in the previous case, this agent only needs to update the Belief function. Likewise, the advertisement can be defined as in Eq. (7.4).

In order to have control on the validity of the advertisements, we use in this case a simple predictor for both short- and long-term fields. This is, we use the persistence method as a point predictor for both horizons and we compute the power bounds (in this case for both active and reactive power) using:

$$\begin{aligned} P_{min}(t + \vartheta) &= (1 - \alpha_P^\vartheta) \hat{P}(t), \\ P_{max}(t + \vartheta) &= (1 + \alpha_P^\vartheta) \hat{P}(t), \\ Q_{min}(t + \vartheta) &= (1 - \alpha_Q^\vartheta) \hat{Q}(t), \\ Q_{max}(t + \vartheta) &= (1 + \alpha_Q^\vartheta) \hat{Q}(t), \end{aligned} \tag{7.5}$$

where $(\hat{P}(t), \hat{Q}(t))$ is the measured power at time t , and the parameters $\alpha_P^\vartheta, \alpha_Q^\vartheta \in (0, 1]$. The same definition can be used for Λ , and in order to guarantee Property 7.2 of Section 7.2.1, $\alpha^\Lambda \geq \alpha^\vartheta$ must hold for both P and Q .

7.3 Experimental Setup

We test our method on the CIGRÉ benchmark low-voltage microgrid [57], shown in Figure 7.2. The microgrid is connected to the main grid, and consists of a 25 kW uncontrollable PV, a 30 kW / 90 kWh battery, and a 5 kW uncontrollable load. The GA is instructed to provide frequency support to the main grid, in addition to tracking a pre-determined power profile.

In our setup, we compare four different implementations of the COMMELEC GA. (1) The *Normal* GA, which is the original implementation that keeps requesting advertisements until it receives them from all RAs. (2) The *Robust* GA, which is our proposed methodology with short- and long-term fields in the advertisement. This GA replaces any missing short-term advertisement with valid long-term fields from that resource, if available. (3) The *Only-long* GA, which is a variation of the Robust GA, in that it only uses long-term fields throughout its operation (i.e. just by replacing ϑ by Λ in the *Normal* GA). This decreases the size of an advertisement and simplifies the design of the GA. (4) The *Previous-short* GA, which replaces any missing advertisement with

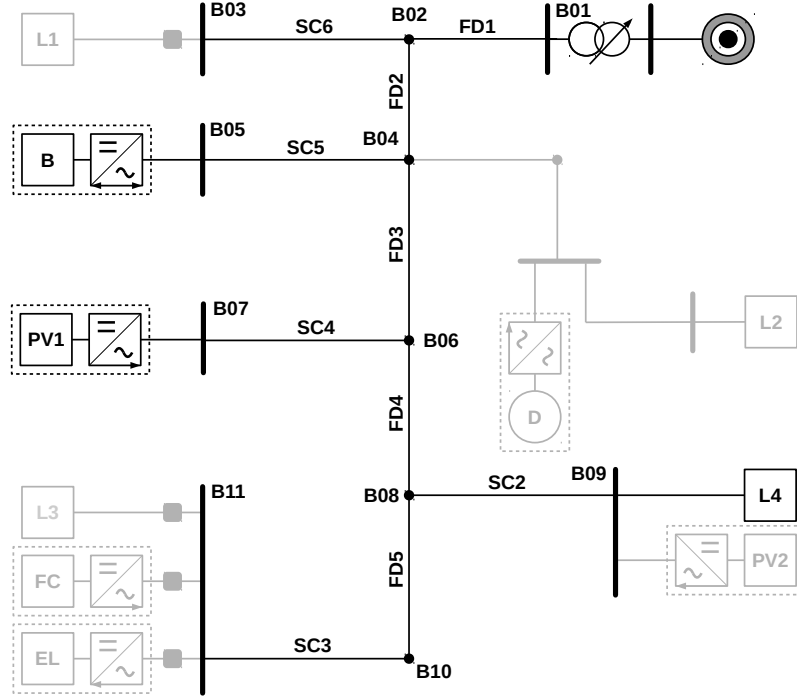


Figure 7.2 – CIGRÉ low-voltage benchmark microgrid. The resources not used for our experiments are greyed-out.

the latest previously received advertisement from that RA. This eliminates the need to construct, send, or handle long-term fields. In this work, we consider $\vartheta = 100$ ms and $\Lambda = 1$ s.

We use T-RECS [171], a virtual commissioning tool, to perform our tests on a simulated version of the grid. T-RECS enables us to use the actual GA and RA code, a simulated version of the resources, and the messages are exchanged over an emulated communication network. The topology consists of one router, with each software agent (GA and RAs) on a different subnet. Resources are on the same host machine as the RAs. With T-RECS, we are able to vary the link loss rate, and we analyze different values between 0% and 20%.

We use the root mean square error (RMSE) as a metric to measure the performance of the different GA implementations. The RMSE is calculated between the measured power at the slack and the frequency support signal (or dispatch plan signal). This shows how well each implementation can track the signal, and how robust each is to message losses.

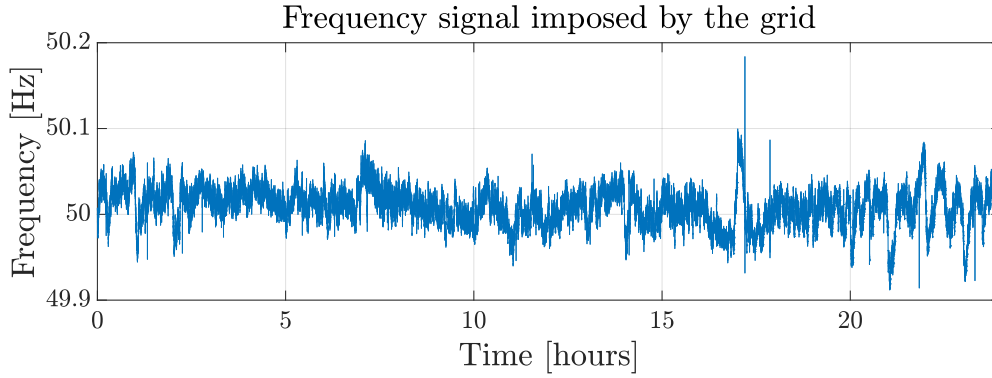


Figure 7.3 – Frequency signal imposed by the main grid used to provide frequency support.

| Method / Loss rate | 0% | 5% | 10% | 15% | 20% |
|--------------------|--------|--------|--------|--------|---------|
| Normal | 121.65 | 198.95 | 317.48 | 541.52 | 1442.98 |
| Robust | 120.44 | 129.03 | 147.25 | 150.55 | 188.12 |
| Only-long | 121.65 | 130.36 | 153.84 | 154.99 | 178.85 |
| Previous-short | 121.65 | 122.18 | 139.40 | 154.77 | 451.17 |

Table 7.1 – Root mean square error (in Watts) between the real power at the slack bus and the requested tracking signal, for a 10-minute interval

7.4 Results

In this section, we illustrate the performance of the proposed method of handling communication network non-idealities under different conditions, and compare the results for the four different GAs described in Section 7.3. Several scenarios are considered in order to highlight the conditions under which each method performs well.

7.4.1 Frequency Support with Non-binding Grid Constraints

We first study the performance of the methods when the grid state is far from the operational limits in terms of bus voltages and line currents. The GA is instructed to provide frequency support to the main grid, based on the frequency signal of Figure 7.3, which represents quick dynamics. As we are interested in studying the effects of the losses in the network, we vary the link loss rate between the GA and the RAs in the range [0%, 20%].

Table 7.1 and Figure 7.4 show the resulting RMSE for the different methods across the different link loss rates, for an interval of 10 minutes. The RMSE is calculated between the actual power at the slack, and the result of $S = -\sigma(f - f_0)$, where S is the expected power at the PCC when providing frequency support, computed by multiplying the droop parameter σ with the divergence of the grid frequency f from

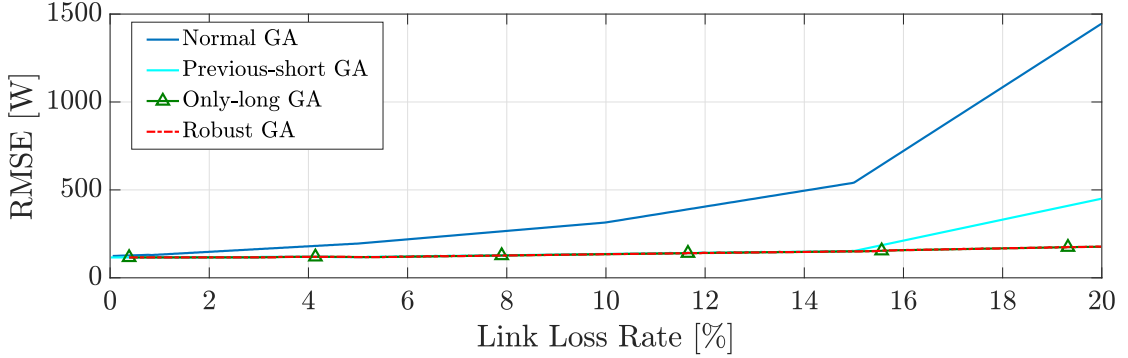


Figure 7.4 – Root mean square error (in Watts) between the real power at the slack bus and the requested tracking signal, for a 10-minute interval

the reference frequency $f_0 = 50$ Hz.²

We observe that the performance of the *Normal* GA rapidly deteriorates as the link loss rate increases. This follows directly from the fact that it is extremely sensitive to the amount of available information, and fails to follow the request in our quick dynamic scenario. The *Previous-short* GA maintains a good level of tracking until the loss rate is too high. This is expected as the information it uses in case of a loss (the previous advertisements) is invalid, and as the loss rate increases, tracking the quick frequency changes becomes increasingly unlikely.

The *Robust* and *Only-long* GA manage to provide frequency support even under 20% link loss rate, although the *Only-long* GA obtains worse performance throughout, especially for lower loss rates. This stems from the fact that its computations are always conservative, as they all use advertisements with a long-term horizon Λ . The effects of this are not drastic in such a scenario, but will appear when the grid conditions are binding, as presented in the next section.

7.4.2 Tracking a Power Profile with Binding Grid Constraints

In order to study the behavior of the *Robust* and *Only-long* GA under binding grid conditions, we consider a scenario in which the GA is instructed to follow a pre-computed dispatch plan. The slower dynamics in this experiment allow us to better visualize the tracking performance. Moreover, we artificially limit the ampacity of the line connecting the microgrid to the main grid (FD1) to 16 A, i.e. a power limit of c.a. 11 kVA.

Figures 7.5 and 7.6 show the tracking results of *Only-long* GA and *Robust* GA, respectively, when the link loss rate is 2%. We observe that, although both manage to track the 10 kW request fully (as it results in a current far away from the ampacity limit

²We take $\sigma = 100$ kW/Hz in our experiments.

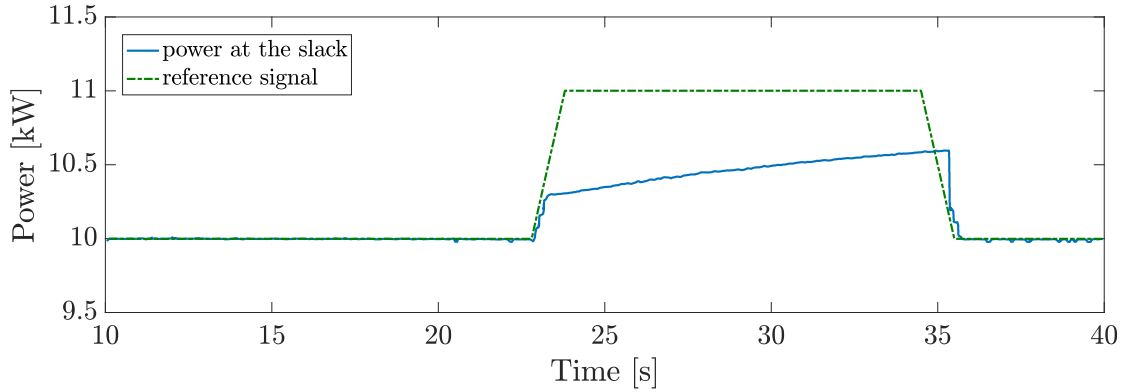


Figure 7.5 – Tracking experiment of *Only-long* GA with binding grid conditions and a 2% loss rate

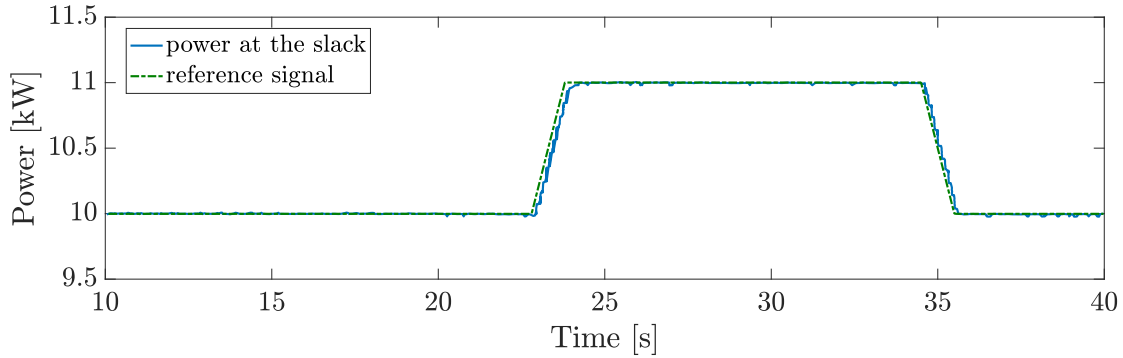


Figure 7.6 – Tracking experiment of *Robust* GA with binding grid conditions and a 2% loss rate

of line FD1), only the *Robust* GA manages to track the 11 kW signal. The *Only-long* GA uses advertisements with larger uncertainty, and is thus conservative in order to avoid current violations. The *Robust* GA maintains tracking as it can safely do so without risking violation, due to the accuracy of the short-term advertisements it uses.

The conservative nature of the *Only-long* GA is highlighted in such binding grid constraints. Similar results are observed for frequency support experiments.

The *Previous-short* GA is not conservative, and thus maintains tracking (under low loss rates) even in binding grid conditions. However, as it uses invalid information, it might cause voltage and/or current violations.

7.4.3 Validation

Finally, we validate the *Robust* method via a 24-hour frequency support experiment with a 2% link loss rate. The 24-hour simulation, with the profiles of the PV and the load taken from an actual experimental run, enables us to see the performance under

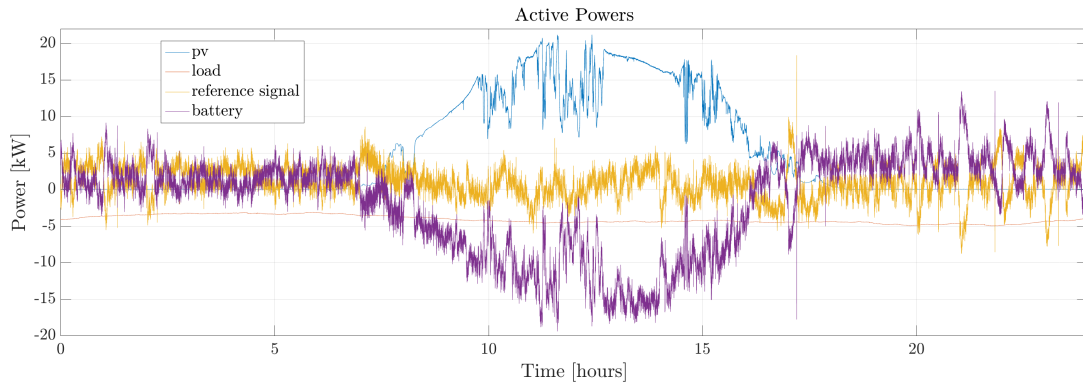


Figure 7.7 – 24-hour frequency support *Robust* experiment with a 2% link loss rate. The power at the slack is not visible since it is below the reference (tracking).

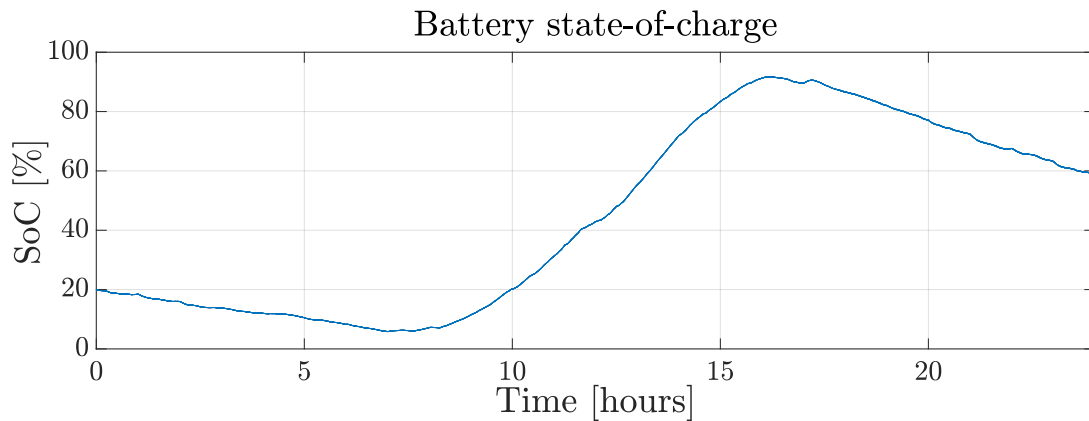


Figure 7.8 – Battery state-of-charge (SoC) during the 24-hour experiment

different and realistic grid conditions. In this particular case, the battery power is used as the slack variable compensate for the PV power-variations and adapting to the frequency signal to provide frequency support. The initial state of charge of the battery (20%) is pre-defined by the forecasted PV and load powers the day before.

Figure 7.7 shows the results of the tracking, in addition to the power at the buses of the battery, the PV, and the load. Although the comparison between the reference signal and the measured power is not visible in the graph, the computed RMSE is 145.67 W for the entire day. We also measure the RMSE over a rolling window of 20 minutes, and the resulting average and the maximum RMSE are 142.40 W and 263.53 W, respectively. This shows the robustness of our method throughout the daily cycle. Furthermore, the state-of-charge of the battery during the experiment is shown in Figure 7.8, showing the capabilities of the battery to provide such an ancillary service to the main grid.

7.5 Conclusions

We present a method for real-time power grid control that is robust in non-ideal network conditions. We take an example of a state-of-the-art framework for power grid control, and augment it such that it maintains its performance in spite of communication failures that lead to losses or delays of messages from the resources to the controller. This is done by having the resources send information about their state that is valid for a longer time horizon, in addition to the short-term information originally sent. The long-term information can be used to compute valid setpoints in cases when the short-term messages are lost due to a non-ideal network.

We show that our method guarantees grid safety, by construction. We also show a validation of our method over a 24-hour period, and provide a comparative analysis with alternative methods. We observe that the *Robust* GA is able to track the requested frequency signal better than alternative methods, under both binding and non-binding grid conditions.

For scenarios in which the dynamics are not as quick, such as power profile tracking, and under non-binding grid conditions, we find that the *Only-long* GA alternative is comparable with the proposed *Robust* method, but still performs worse. Our proposed methodology comes at no additional expense, and provides significant advantages in deployment conditions.

Here, we address losses of advertisements, and our proposed methodology focuses on dealing with communication failures that affect these messages, without explicitly dealing with the dual issue of lost setpoints. However, our experimental setup was designed to test for random communication failures, with the RAs maintaining the previous setpoint until a new one is issued. This problem will be studied further in future research.

8 Conclusions and Directions for Future Work

In this thesis, we have studied the problems of designing grid-aware real-time optimal control for the charging/discharging of EVs.

First, in Chapter 3, we focus on grid-aware real-time charging control of an EVs. We developed a method that, on one side, helps the grid to keep its state in safe operating conditions by exploiting EVs flexibility and, on the other side, minimizes the EVs-battery wear and keeps the charging balance between EVs connected to a CS. More precisely, the CS follows an aggregated power-setpoint issued by a grid-control system. By following an aggregated power-setpoint, a CS participates in the control of the grid and helps the controller to keep a grid in safe operation conditions and to provide services to an upper-level grid. The grid control sees a CS as a single controllable resource, i.e., all connected EVs are not visible for the grid control, instead it has abstract aggregated information about their flexibility, implementation uncertainty, and preferences to implement power-setpoints. A CS, in turn, should allocate an aggregated power-setpoint among EVs. The allocation among EVs has the following features: it keeps the charging balance between connected EVs and it minimizes the battery wear of EVs. Although the state of the art assumes that EV charging behavior is ideal, we consider the impact of non-idealities on both the EV and the grid operations. We implement a number of features that account for the realistic behaviour of EVs by incorporating the results of the measurements on real-field deployment. In particular, our method considers a non-ideal response, due to the internal reaction and implementation delays, of an EV to a charging power change. Furthermore, EVs have a non-zero minimum charging power, i.e., an EV can be either switched off and consume no power, or can charge at a power that lies between non-zero bounds, where the minimum charging-power cannot be arbitrarily small. Consequently, the CS should decide which EVs should be switched on and which should be switched off. This leads to mixed-integer variables in the optimization problem. In order to solve this efficiently in real time, we have proposed a heuristic that limits the number of integer variables and that enables us to solve the optimization problem in real time. In Chapter 4, the

Chapter 8. Conclusions and Directions for Future Work

method has been deployed and validated in real field on a real-scale microgrid with real commercial EVs.

Second, we have studied the real-time grid-aware V2G control of EVs. The main difference in this case is the decision regarding the discharging of EVs. Compared to charging only EVs, where EVs are used as flexible loads, V2G EVs can be used as energy storage and discharge their batteries when it is needed. However to do so, the control method should take into account users' incentives as V2G operations accelerate the degradation of the EVs batteries. These decisions are long-term, meaning that in order to decide when to discharge an EV, the future such as arrivals/departure of an EV, the energy demands of charging the EV, staying times, amount of energy that V2G could provide, and the PV production and consumption of loads (e.g., domestic buildings) should be taken into account. We have suggested using a scenario-based MPC technique for performing the scheduling of charging/discharging of EVs. However, MPC becomes highly computationally complicated and difficult if we add grid constraints. Alternatively, we have proposed using a two-layer approach by using real-time grid-aware control that keeps the grid operating safely and takes into account the decisions of the scheduling. We have shown that the real-time control method is crucial in order to handle intra-period fluctuations, because a scheduling layer is blind to them. Using this method, the controller can take advantage of the available flexibility of EVs while handling the incentives of the users' behavior and reacting to the fluctuations of renewable generation in order to keep the grid in safe operating conditions.

Finally, we have addressed the issues related to the integration of CSs into a grid-control system. In Chapter 6 we have proposed a method that handles sudden unexpected power-steps, such as load disconnections. These events can cause voltage or line-ampacity violations. The traditional approach, i.e., avoid violations by incorporating hard predefined safety bounds, could be too restricted, which leads to large sub-optimality of the grid operation. Our method permits temporary violations of the steady-state bounds allowed by grid standards and could enable the exploitation of the flexibility of other resources to better control the system's state.

In Chapter 7, we have focused on non-idealities of communication communication networks and processes and their influence on real-time control of a power grid. We have presented a method for a real-time power grid-control that is robust in non-ideal network conditions. We have achieved robustness by expanding the original short-term message that resources send to the grid controller. Short-term messages are valid for the next control period, additional information provides the estimation of the resource state for longer time-horizons. This information is stored by the grid controller and used in case of message loss.

Based on the work done in this thesis, there are several directions for further research on V2G. First, in our method, we schedule each EV individually, which can be

computationally heavy with the increasing number of EVs. However, we can improve our solution by aggregating separately charging and discharging EVs and by having only two variables to schedule. This would require the method to aggregate a charging demands of charging only EVs defined by its users and a method to aggregate energy bids (amount of energy that an EV is planning to sell and its price) for discharging EVs. Then, at the real-time control level, we need a technique to disaggregate the scheduled powers among charging and discharging EVs. Second, we currently assume that EVs can either charge or discharge. In this direction, we can expand our solution to handle the charging-discharging operations of EVs while they are plugged-in to CSs. This will require defining the pricing policy of EVs that are selling their energy to the grid, because the selling energy price will now depend on the selling and buying operations of an EV. Also, in this setting, the user can have its own strategy of selling/buying energy from the grid. These strategies are also the directions of further investigation.

Bibliography

- [1] A. Y. Saber and G. K. Venayagamoorthy, "Plug-in vehicles and renewable energy sources for cost and emission reductions," *IEEE Transactions on Industrial Electronics*, vol. 58, no. 4, pp. 1229–1238, 2011.
- [2] N. Rietmann, B. Hügler, and T. Lieven, "Forecasting the trajectory of electric vehicle sales and the consequences for worldwide CO₂ emissions," *Journal of Cleaner Production*, vol. 261, 2020.
- [3] D. Block, J. Harrison, and P. Brooker, "Electric vehicle sales for 2014 and future projections," *Florida Solar Energy Center*, 2015.
- [4] D. Pevec, J. Babic, and V. Podobnik, "Electric vehicles: A data science perspective review," *Electronics*, vol. 8, no. 10, p. 1190, 2019.
- [5] K. Clement, E. Haesen, and J. Driesen, "Coordinated charging of multiple plug-in hybrid electric vehicles in residential distribution grids," in *2009 IEEE/PES Power Systems Conference and Exposition*, 2009, pp. 1–7.
- [6] J. A. P. Lopes, F. J. Soares, and P. M. R. Almeida, "Integration of electric vehicles in the electric power system," *Proceedings of the IEEE*, vol. 99, no. 1, pp. 168–183, 2011.
- [7] G. A. Putrus, P. Suwanapongkarn, D. Johnston, E. C. Bentley, and M. Narayana, "Impact of electric vehicles on power distribution networks," *IEEE Vehicle Power and Propulsion Conference*, 2009.
- [8] P. B. Evans, S. Kuloor, and B. Kroposki, "Impacts of plug-in vehicles and distributed storage on electric power delivery networks," *IEEE Vehicle Power and Propulsion Conference*, 2009.
- [9] C. Dharmakeerthi, N. Mithulananthan, and T. Saha, "Impact of electric vehicle fast charging on power system voltage stability," *Electrical Power and Energy Systems*, vol. 57, pp. 241–249, 2014.
- [10] J. Pillai and B. Bak-Jensen, "Impacts of electric vehicle loads on power distribution systems," *IEEE Vehicle Power and Propulsion Conference*, 2010.

Bibliography

- [11] L. Fernández, T. San Roman, R. Cossent, C. Domingo, and P. Frias, "Assessment of the impact of plug-in electric vehicles on distribution networks," *IEEE Trans. on Power Sys.*, vol. 26, no. 1, pp. 206–213, 2011.
- [12] S. Acha, T. Green, and N. Shah, "Effects of optimised plug-in hybrid vehicle charging strategies on electric distribution network losses," *IEEE PES T&D 2010*, 2010.
- [13] E. Veldman and R. A. Verzijlbergh, "Distribution grid impacts of smart electric vehicle charging from different perspectives," *IEEE Transactions on Smart Grid*, vol. 6, no. 1, pp. 333–342, 2015.
- [14] S. Shao, M. Pipattanasomporn, and S. Rahman, "Challenges of phev penetration to the residential distribution network," in *2009 IEEE Power Energy Society General Meeting*, 2009, pp. 1–8.
- [15] E. Veldman and R. A. Verzijlbergh, "Distribution grid impacts of smart electric vehicle charging from different perspectives," *IEEE Transactions on Smart Grid*, vol. 6, no. 1, pp. 333–342, 2015.
- [16] N. B. G. Brinkel, I. Lampropoulos, and W. AlSkaif, T.A. van Sark, "Should we reinforce the grid? Cost and emission optimization of electric vehicle charging under different transformer limits," *Applied Energy*, vol. 276, 2020.
- [17] A. Soares, H. Melo, C. H. Antunes, J. P. Trovao, A. Gomes, and H. Jorge, "Integration of the electric vehicle as a manageable load in a residential energy management system," in *2015 IEEE Vehicle Power and Propulsion Conference (VPPC)*, 2015, pp. 1–6.
- [18] J. Hu, S. You, M. Lind, and J. Østergaard, "Coordinated charging of electric vehicles for congestion prevention in the distribution grid," *IEEE Transactions on Smart Grid*, vol. 5, no. 2, pp. 703–711, 2014.
- [19] O. Sundstrom and C. Binding, "Flexible charging optimization for electric vehicles considering distribution grid constraints," *IEEE Transactions on Smart Grid*, vol. 3, no. 1, pp. 26–37, 2012.
- [20] V. Sharma, S. M. Aziz, M. H. Haque, and T. Kauschke, "Effects of high solar photovoltaic penetration on distribution feeders and the economic impact," *Renewable and Sustainable Energy Reviews*, vol. 131, p. 110021, 2020.
- [21] M. Q. Duong, N. T. Nam Tran, G. N. Sava, and M. Scripcariu, "The impacts of distributed generation penetration into the power system," in *2017 International Conference on Electromechanical and Power Systems (SIELMEN)*, 2017, pp. 295–301.

-
- [22] J. Stiasny, T. Zufferey, G. Pareschi, D. Toffanin, G. Hug, and K. Boulouchos, "Sensitivity analysis of electric vehicle impact on low-voltage distribution grids," *Electric Power Systems Research*, vol. 191, p. 106696, 2021.
 - [23] Q. Dang, "Electric vehicle (ev) charging management and relieve impacts in grids," in *2018 9th IEEE International Symposium on Power Electronics for Distributed Generation Systems (PEDG)*, 2018, pp. 1–5.
 - [24] E. Akhavan-Rezai, M. F. Shaaban, E. F. El-Saadany, and A. Zidan, "Uncoordinated charging impacts of electric vehicles on electric distribution grids: Normal and fast charging comparison," in *2012 IEEE Power and Energy Society General Meeting*, 2012, pp. 1–7.
 - [25] F. Shahnia, A. Ghosh, G. Ledwich, and F. Zare, "Voltage unbalance sensitivity analysis of plug-in electric vehicles in distribution networks," in *AUPEC 2011*, 2011, pp. 1–6.
 - [26] J. Meyer, S. Hähle, P. Schegner, and C. Wald, "Impact of electrical car charging on unbalance in public low voltage grids," in *11th International Conference on Electrical Power Quality and Utilisation*, 2011, pp. 1–6.
 - [27] E. Scolari, D. Torregrossa, J.-Y. Le Boudec, and M. Paolone, "Ultra-short-term prediction intervals of photovoltaic AC active power," *International Conf. on Prob. Methods Applied to Power Systems*, 2016.
 - [28] J. Soares, H. Morais, T. Sousa, Z. Vale, and P. Faria, "Day-ahead resource scheduling including demand response for electric vehicles," *IEEE Transactions on Smart Grid*, vol. 4, no. 1, pp. 596–605, 2013.
 - [29] A. Bernstein, L. Reyes-Chamorro, J.-Y. Le Boudec, and M. Paolone, "A composable method for real-time control of active distribution networks with explicit power set points. Part I: Framework," *Electric Power Systems Research*, vol. 6, no. August, pp. 254–264, 2015.
 - [30] L. Zanni, S. Sarri, M. Pignati, R. Cherkaoui, and M. Paolone, "Probabilistic assessment of the process-noise covariance matrix of discrete Kalman filter state estimation of active distribution networks," in *2014 International Conference on Probabilistic Methods Applied to Power Systems (PMAPS)*, 2014, pp. 1–6.
 - [31] M. Pignati, M. Popovic, S. Barreto, R. Cherkaoui, G. Dario Flores, J.-Y. Le Boudec, M. Mohiuddin, M. Paolone, P. Romano, S. Sarri, T. Tesfay, D.-C. Tomozei, and L. Zanni, "Real-time state estimation of the epfl-campus medium-voltage grid by using PMUs," in *2015 IEEE Power Energy Society Innovative Smart Grid Technologies Conference (ISGT)*, 2015, pp. 1–5.
 - [32] S. Sarri, M. Paolone, R. Cherkaoui, A. Borghetti, F. Napolitano, and C. Nucci, "State estimation of active distribution networks: Comparison between wls and

Bibliography

- iterated kalman-filter algorithm integrating pmus,” in *2012 3rd IEEE PES Innovative Smart Grid Technologies Europe (ISGT Europe)*, 2012, pp. 1–8.
- [33] G. Cavraro, E. Dall’Anese, and A. Bernstein, “Dynamic power network state estimation with asynchronous measurements,” in *2019 IEEE Global Conference on Signal and Information Processing (GlobalSIP)*, 2019, pp. 1–5.
- [34] S. Fan, J. Liu, Q. Wu, M. Cui, H. Zhou, and G. He, “Optimal coordination of virtual power plant with photovoltaics and electric vehicles: A temporally coupled distributed online algorithm,” *Applied Energy*, vol. 277, p. 115583, 2020.
- [35] N. Kariminejad, S. A. Taher, M. Shahidehpour, and K. Khateri, “A hierarchical governor/turbine and electric vehicles optimal control framework for primary frequency support in power systems,” *IEEE Transactions on Smart Grid*, vol. 9, no. 6, pp. 6702–6712, 2018.
- [36] S. Falahati, S. A. Taher, and M. Shahidehpour, “Grid secondary frequency control by optimized fuzzy control of electric vehicles,” *IEEE Transactions on Smart Grid*, vol. 9, no. 6, pp. 5613–5621, 2018.
- [37] F. Hoffart, “Proper care extends li-ion battery life,” *Power Electronics*, vol. 25, 2008.
- [38] J. D. Bishop, C. J. Axon, D. Bonilla, T. Martino, D. Banister, and M. D. McCulloch, “Evaluating the impact of V2G services on the degradation of batteries in PHEV and EV,” *Applied Energy*, vol. 111, pp. 206–218, 2013.
- [39] X. Dong, Y. Mu, X. Xu, H. Jia, J. Wu, X. Yu, and Y. Qi, “A charging pricing strategy of electric vehicle fast charging stations for the voltage control of electricity distribution networks,” *Applied Energy*, vol. 225, pp. 857–868, 2018.
- [40] Y. Dai, Y. Qi, L. Li, B. Wang, and H. Gao, “A dynamic pricing scheme for electric vehicle in photovoltaic charging station based on stackelberg game considering user satisfaction,” *Computers & Industrial Engineering*, vol. 154, p. 107117, 2021.
- [41] B. Radunovic and J.-Y. Le Boudec, “A unified framework for max-min and min-max fairness with applications,” *IEEE/ACM Transactions on Networking*, vol. 15, no. October, pp. 1073–1083, 2007.
- [42] T. Bonald, L. Massoulié, A. Proutière, and J. Virtamo, “A queueing analysis of max-min fairness, proportional fairness and balanced fairness,” *Queueing Systems*, vol. 53, no. 1, pp. 65–84, 2006.
- [43] “Electric vehicle database,” <https://ev-database.org/>, [Online].
- [44] W. Kempton and J. Tomić, “Vehicle-to-grid power fundamentals: calculating capacity and net revenue,” *Journal of Power Sources*, vol. 144, no. 1, pp. 268–279, 2005.

- [45] —, “Vehicle-to-grid power implementation: from stabilizing the grid to supporting large-scale renewable energy,” *Journal of Power Sources*, vol. 144, no. 1, pp. 280–294, 2005.
- [46] P. Mitra and G. Venayagamoorthy, “Wide area control for improving stability of a power system with plug-in electric vehicles,” *IET Generation, Transmission and Distribution*, vol. 4, no. 10, pp. 1151–1163, 2010.
- [47] M. Yilmaz and P. Krein, “Review of the impact of vehicle-to-grid technologies on distribution systems and utility interfaces,” *IEEE Transactions on Power Electron.*, vol. 28, no. 12, pp. 5673–5689, 2013.
- [48] D. Dallinger, D. Krampe, and M. Wietschel, “Vehicle-to-grid regulation reserves based on a dynamic simulation of mobility behavior,” *IEEE Transactions on Smart Grid*, vol. 2, no. 2, pp. 302–313, 2011.
- [49] R. Gupta, F. Sossan, and M. Paolone, “Countrywide pv hosting capacity and energy storage requirements for distribution networks: The case of switzerland,” *Applied Energy*, vol. 281, p. 116010, 2021.
- [50] J. Geske and D. Schumann, “Willing to participate in vehicle-to-grid (V2G)? Why not!” *Energy Policy*, vol. 120, pp. 392–401, 2018.
- [51] Y. Preger, H. M. Barkholtz, A. Fresquez, D. L. Campbell, B. W. Juba, J. RomÃ n Kustas, S. R. Ferreira, and B. Chalamala, “Degradation of commercial lithium-ion cells as a function of chemistry and cycling conditions,” *Journal of The Electrochemical Society*, vol. 167, no. 12, 2020.
- [52] Y. Huang, H. Wang, A. Khajepour, H. He, and J. Ji, “Model predictive control power management strategies for hevs: A review,” *Journal of Power Sources*, vol. 341, pp. 91–106, 2017.
- [53] IEEE Power and Energy Society, “IEEE Guide for Voltage Sag Indices,” 2014.
- [54] International Electrotechnical Commission, “International Standard: Electric cables – calculation of the current rating,” 2007.
- [55] IEEE Power Engineering Society, “IEEE Standard for Calculating the Current-Temperature of Bare Overhead Conductors,” 2006.
- [56] J. Postel, “Transmission Control Protocol,” Internet Requests for Comments, RFC Editor, STD 7, September 1981. [Online]. Available: <http://www.rfc-editor.org/rfc/rfc793.txt>
- [57] Taskforce C6.04.02, “Benchmark Systems for Network Integration of Renewable and Distributed Energy Resources,” CIGRÉ, Tech. Rep., 2010.

Bibliography

- [58] C. Liu and J. W. Layland, "Scheduling algorithms for multiprogramming in a hard-real-time environment," *Journal of the ACM*, vol. 20, no. 1, pp. 46–61, Jan. 1973.
- [59] M. Dertouzos, "Control robotics: The procedural control of physical processes," *Proceedings IFIP Congress*, pp. 807–813, 1974.
- [60] M. Roux, M. Apperley, and M. Booyens, "Comfort, peak load and energy: Centralised control of water heaters for demand-driven prioritisation," *Energy for Sustainable Development*, vol. 44, pp. 78–86, 2018.
- [61] S. Karagiannopoulos, P. Aristidou, and G. Hug, "A centralised control method for tackling unbalances in active distribution grids," in *2018 Power Systems Computation Conference (PSCC)*, 2018, pp. 1–7.
- [62] L. Bakule, "Decentralized control: An overview," *Annual Reviews in Control*, vol. 32, no. 1, pp. 87–98, 2008.
- [63] M. Moschella, M. A. A. Murad, E. Crisostomi, and F. Milano, "Decentralized charging of plug-in electric vehicles and impact on transmission system dynamics," *IEEE Transactions on Smart Grid*, vol. 12, no. 2, pp. 1772–1781, 2021.
- [64] N. I. Nimalsiri, C. P. Mediwaththe, E. L. Ratnam, M. Shaw, D. B. Smith, and S. K. Halgamuge, "A survey of algorithms for distributed charging control of electric vehicles in smart grid," *IEEE Transactions on Intelligent Transportation Systems*, vol. 21, no. 11, pp. 4497–4515, 2020.
- [65] P. Q. A. Guide, "Voltage disturbances, standard en 50160," 2004.
- [66] M. Eremia and M. Shahidehpour, *Handbook of electrical power system dynamics: modeling, stability, and control*. John Wiley & Sons, 2013, vol. 92.
- [67] K. Christakou, D.-C. Tomozei, J.-Y. Le Boudec, and M. Paolone, "GECN: Primary voltage control for active distribution networks via real-time demand-response," *IEEE Transactions on Smart Grid*, vol. 5, no. 2, pp. 622–631, 2014.
- [68] G. Cavraro, M. K. Singh, and A. Bernstein, "Emergency voltage regulation in power systems via ripple-type control," National Renewable Energy Lab.(NREL), Golden, CO (United States), Tech. Rep., 2021.
- [69] S. Deilami, A. Masoum, P. Moses, and M. A. S. Masoum, "Real-time coordination of plug-in electric vehicle charging in smart grids to minimize power losses and improve voltage profile," *IEEE Transactions on Smart Grid*, vol. 2, no. 3, pp. 456–467, 2011.
- [70] D. Oliveira, A. Zambroni de Souza, and L. Delboni, "Optimal plug-in hybrid electric vehicles recharge in distribution power systems," *Electric Power Systems Research*, vol. 98, pp. 77–85, 2013.

-
- [71] T. Sousa, H. Morais, Z. Vale, and R. Castro, "A multi-objective optimization of the active and reactive resource scheduling at a distribution level in a smart grid context," *Energy*, vol. 85, pp. 236–250, 2015.
 - [72] J. E. Cardona, J. C. López, and M. J. Rider, "Decentralized electric vehicles charging coordination using only local voltage magnitude measurements," *Electric Power Systems Research*, vol. 161, pp. 139–151, 2018.
 - [73] P. García-Triviño, J. P. Torreglosa, L. M. Fernández-Ramírez, and F. Jurado, "Decentralized fuzzy logic control of microgrid for electric vehicle charging station," *IEEE Journal of Emerging and Selected Topics in Power Electronics*, vol. 6, no. 2, pp. 726–737, 2018.
 - [74] M. Liu, P. K. Phanivong, Y. Shi, and D. S. Callaway, "Decentralized charging control of electric vehicles in residential distribution networks," *IEEE Transactions on Control Systems Technology*, vol. 27, no. 1, pp. 266–281, 2019.
 - [75] X. Huo and M. Liu, "Decentralized electric vehicle charging control via a novel shrunk primal-multi-dual subgradient (SPMDS) algorithm," in *2020 59th IEEE Conference on Decision and Control (CDC)*, 2020, pp. 1367–1373.
 - [76] S. Martinenas, K. Knezovic, and M. Marinelli, "Management of power quality issues in low voltage networks using electric vehicles: experimental validation," *IEEE Transactions on Power Delivery*, vol. 32, pp. 971–979, 2017.
 - [77] N. Leemput, F. Geth, J. Van Roy, A. Delnooz, J. Büscher, and J. Driesen, "Impact of electric vehicle on-board single-phase charging strategies on a Flemish residential grid," *IEEE Transactions on Smart Grid*, vol. 5, no. 4, pp. 1815–1822, 2014.
 - [78] S. Mocci, N. Natale, F. Pilo, and S. Ruggeri, "Demand side integration in LV smart grids with multi-agent control system," *Electric Power Systems Research*, vol. 125, pp. 23–33, 2015.
 - [79] R. Carli and M. Dotoli, "A decentralized control strategy for optimal charging of electric vehicle fleets with congestion management," in *2017 IEEE International Conference on Service Operations and Logistics, and Informatics (SOLI)*, 2017, pp. 63–67.
 - [80] J. de Hoog, T. Alpcan, M. Brazil, D. A. Thomas, and I. Mareels, "Optimal charging of electric vehicles taking distribution network constraints into account," *IEEE Transactions on Power Systems*, vol. 30, no. 1, pp. 365–375, 2015.
 - [81] S. Hajforoosh, M. A. Masoum, and S. M. Islam, "Online optimal variable charge-rate coordination of plug-in electric vehicles to maximize customer satisfaction and improve grid performance," *Electric Power Systems Research*, vol. 141, pp. 407–420, 2016.

Bibliography

- [82] J. Hu, S. You, M. Lind, and J. Østergaard, "Coordinated charging of electric vehicles for congestion prevention in the distribution grid," *IEEE Transactions on Smart Grid*, vol. 5, no. 2, pp. 703–711, 2014.
- [83] J. Hu, H. Morais, T. Sousa, S. You, and R. Dâhulst, "Integration of electric vehicles into the power distribution network with a modified capacity allocation mechanism," *Energies*, vol. 10, no. 2, 2017.
- [84] J. Hu, A. Saleem, S. You, L. Nordström, M. Lind, and J. Østergaard, "A multi-agent system for distribution grid congestion management with electric vehicles," *Engineering Applications of Artificial Intelligence*, vol. 38, pp. 45–58, 2015.
- [85] E. L. Karfopoulos and N. D. Hatziaargyriou, "Distributed coordination of electric vehicles providing V2G services," *IEEE Transactions on Power Systems*, vol. 31, no. 1, pp. 329–338, 2016.
- [86] H. Saadat, "Power system analysis,(2nd)," *McGraw-Hill Higher Education*, 2009.
- [87] M. Kashem, A. Le, M. Negnevitsky, and G. Ledwich, "Distributed generation for minimization of power losses in distribution systems," in *2006 IEEE Power Engineering Society General Meeting*, 2006, pp. 8 pp.–.
- [88] E. Sortomme, M. M. Hindi, S. D. J. MacPherson, and S. S. Venkata, "Coordinated charging of plug-in hybrid electric vehicles to minimize distribution system losses," *IEEE Transactions on Smart Grid*, vol. 2, no. 1, pp. 198–205, 2011.
- [89] L. Jian, X. Zhu, Z. Shao, S. Niu, and C. Chan, "A scenario of vehicle-to-grid implementation and its double-layer optimal charging strategy for minimizing load variance within regional smart grids," *Energy Conversion and Management*, vol. 78, pp. 508–517, 2014.
- [90] N. B. Arias, J. F. Franco, M. Lavorato, and R. Romero, "Metaheuristic optimization algorithms for the optimal coordination of plug-in electric vehicle charging in distribution systems with distributed generation," *Electric Power Systems Research*, vol. 142, pp. 351–361, 2017.
- [91] Y. Xu, "Optimal distributed charging rate control of plug-in electric vehicles for demand management," *IEEE Transactions on Power Systems*, vol. 30, no. 3, pp. 1536–1545, 2015.
- [92] T. Zhao and Z. Ding, "Distributed initialization-free cost-optimal charging control of plug-in electric vehicles for demand management," *IEEE Transactions on Industrial Informatics*, vol. 13, no. 6, pp. 2791–2801, 2017.
- [93] J. A. P. Lopes, A. G. Madureira, and C. C. L. M. Moreira, "A view of microgrids," *Wiley Interdisciplinary Reviews: Energy and Environment*, vol. 2, no. 1, pp. 86–103, 2013.

-
- [94] C. Gouveia, C. L. Moreira, J. A. P. Lopes, D. Varajao, and R. E. Araujo, "Microgrid service restoration: The role of plugged-in electric vehicles," *IEEE Industrial Electronics Magazine*, vol. 7, no. 4, pp. 26–41, 2013.
 - [95] M. Vahedipour-Dahraie, H. Rashidizaheh-Kermani, H. R. Najafi, A. Anvari-Moghaddam, and J. M. Guerrero, "Coordination of evs participation for load frequency control in isolated microgrids," *Applied Sciences*, vol. 7, no. 6, p. 539, 2017.
 - [96] Z. Yuan, A. Zecchino, R. Cherkaoui, and M. Paolone, "Real-time control of battery energy storage systems to provide ancillary services considering voltage-dependent capability of dc-ac converters," *IEEE Transactions on Smart Grid*, vol. 12, no. 5, pp. 4164–4175, 2021.
 - [97] E. Namor, F. Sossan, R. Cherkaoui, and M. Paolone, "Control of battery storage systems for the simultaneous provision of multiple services," *IEEE Transactions on Smart Grid*, vol. 10, no. 3, pp. 2799–2808, 2019.
 - [98] Z. Li, M. Chowdhury, P. Bhavsar, and Y. He, "Optimizing the performance of vehicle-to-grid (V2G) enabled battery electric vehicles through a smart charge scheduling model," *International Journal of Automotive Technology*, vol. 16, no. 5, pp. 827–837, 2015.
 - [99] H. Liu, Z. Hu, Y. Song, and J. Lin, "Decentralized vehicle-to-grid control for primary frequency regulation considering charging demands," *IEEE Transactions on Power Systems*, vol. 28, no. 3, pp. 3480–3489, 2013.
 - [100] S. Han, S. Han, and K. Sezaki, "Development of an optimal vehicle-to-grid aggregator for frequency regulation," *IEEE Transactions on smart grid*, vol. 1, no. 1, pp. 65–72, 2010.
 - [101] J. Kang, S. J. Duncan, and D. N. Mavris, "Real-time scheduling techniques for electric vehicle charging in support of frequency regulation," *Procedia Computer Science*, vol. 16, pp. 767–775, 2013.
 - [102] E. Sortomme and M. A. El-Sharkawi, "Optimal scheduling of vehicle-to-grid energy and ancillary services," *IEEE Transactions on Smart Grid*, vol. 3, no. 1, pp. 351–359, 2012.
 - [103] J. Tan and L. Wang, "Enabling reliability-differentiated service in residential distribution networks with phev: A hierarchical game approach," *IEEE Transactions on Smart Grid*, vol. 7, no. 2, pp. 684–694, 2016.
 - [104] C.-K. Wen, J.-C. Chen, J.-H. Teng, and P. Ting, "Decentralized plug-in electric vehicle charging selection algorithm in power systems," *IEEE Transactions on Smart Grid*, vol. 3, no. 4, pp. 1779–1789, 2012.

Bibliography

- [105] —, “Decentralized energy management system for charging and discharging of plug-in electric vehicles,” in *2012 International Conference on Wireless Communications and Signal Processing (WCSP)*. IEEE, 2012, pp. 1–6.
- [106] S. Vandael, N. Boucké, T. Holvoet, and G. Deconinck, “Decentralized demand side management of plug-in hybrid vehicles in a smart grid,” in *Proceedings of the first international workshop on agent technologies for energy systems (ATES 2010)*, 2010, pp. 67–74.
- [107] K. De Craemer, S. Vandael, B. Claessens, and G. Deconinck, “An event-driven dual coordination mechanism for demand side management of PHEVs,” *IEEE Transactions on Smart Grid*, vol. 5, no. 2, pp. 751–760, 2014.
- [108] M. Liu, P. K. Phanivong, and D. S. Callaway, “Electric vehicle charging control in residential distribution network: A decentralized event-driven realization,” in *2017 IEEE 56th Annual Conference on Decision and Control (CDC)*, 2017, pp. 214–219.
- [109] Y. Xu, F. Pan, and L. Tong, “Dynamic scheduling for charging electric vehicles: A priority rule,” *IEEE Transactions on Automatic Control*, vol. 61, no. 12, pp. 4094–4099, 2016.
- [110] Y. Liu, R. Deng, and H. Liang, “A stochastic game approach for pev charging station operation in smart grid,” *IEEE Transactions on Industrial Informatics*, vol. 14, no. 3, pp. 969–979, 2018.
- [111] R. Wang, Y. Li, P. Wang, and D. Niyato, “Design of a v2g aggregator to optimize phev charging and frequency regulation control,” in *2013 IEEE International Conference on Smart Grid Communications (SmartGridComm)*, 2013, pp. 127–132.
- [112] S. Vandael, B. Claessens, M. Hommelberg, T. Holvoet, and G. Deconinck, “A scalable three-step approach for demand side management of plug-in hybrid vehicles,” *IEEE Transactions on Smart Grid*, vol. 4, no. 2, pp. 720–728, 2013.
- [113] M. A. Ortega-Vazquez, F. Bouffard, and V. Silva, “Electric vehicle aggregator/system operator coordination for charging scheduling and services procurement,” *IEEE Transactions on Power Systems*, vol. 28, no. 2, pp. 1806–1815, 2013.
- [114] Y. Li, L. Li, C. Peng, and J. Zou, “An MPC based optimized control approach for ev-based voltage regulation in distribution grid,” *Electric Power Systems Research*, vol. 172, pp. 152–160, 2019.
- [115] B.-R. Choi, W.-P. Lee, and D.-J. Won, “Optimal charging strategy based on model predictive control in electric vehicle parking lots considering voltage stability,” *Energies*, vol. 11, no. 7, p. 1812, 2018.

-
- [116] P. Asmus, "Microgrids, virtual power plants and our distributed energy future," *The Electricity Journal*, vol. 23, no. 10, pp. 72–82, 2010.
- [117] T. L. Vandoorn, B. Zwaenepoel, J. D. M. De Kooning, B. Meersman, and L. Vandevelde, "Smart microgrids and virtual power plants in a hierarchical control structure," in *2011 2nd IEEE PES International Conference and Exhibition on Innovative Smart Grid Technologies*, 2011, pp. 1–7.
- [118] Q. Zhao, Y. Shen, and M. Li, "Control and bidding strategy for virtual power plants with renewable generation and inelastic demand in electricity markets," *IEEE Transactions on Sustainable Energy*, vol. 7, no. 2, pp. 562–575, 2016.
- [119] B. Zhou, K. Zhang, K. W. Chan, C. Li, X. Lu, S. Bu, and X. Gao, "Optimal coordination of electric vehicles for virtual power plants with dynamic communication spectrum allocation," *IEEE Transactions on Industrial Informatics*, vol. 17, no. 1, pp. 450–462, 2021.
- [120] M. Vasirani, R. Kota, R. L. Cavalcante, S. Ossowski, and N. R. Jennings, "An agent-based approach to virtual power plants of wind power generators and electric vehicles," *IEEE Transactions on Smart Grid*, vol. 4, no. 3, pp. 1314–1322, 2013.
- [121] M. Liu, P. McNamara, and S. McLoone, "Fair charging strategies for EVs connected to a low-voltage distribution network," *IEEE PES ISGT Europe*, 2013.
- [122] S. Xie, W. Zhong, K. Xie, R. Yu, and Y. Zhang, "Fair energy scheduling for vehicle-to-grid networks using adaptive dynamic programming," *IEEE Transactions on Neural Networks and Learning Systems*, vol. 27, no. 8, pp. 1697–1707, 2016.
- [123] Y. Leehter, W. H. Lim, and T. S. Tsai, "A real-time charging scheme for demand response in electric vehicle parking station," *IEEE Transactions on Smart Grid*, vol. 8, no. 1, pp. 52–62, 2017.
- [124] Z. Ma, D. Callaway, and I. Hiskens, "Decentralized charging control of large populations of plug-in electric vehicles," *IEEE Transactions on Control Systems Technology*, vol. 21, no. 1, pp. 67–78, 2013.
- [125] Y. He, B. Venkatesh, and L. Guan, "Optimal scheduling for charging and discharging of electric vehicles," *IEEE Transactions on Smart Grid*, vol. 3, no. 3, pp. 1095–1105, 2012.
- [126] Q. Yan, B. H. Zhang, and M. Kezunovic, "Optimized operational cost reduction for an EV charging station integrated with battery energy storage and PV generation," *IEEE Transactions on Smart Grid*, vol. 10, no. 2, pp. 2096–2106, 2019.
- [127] L. Gan, U. Topcu, and S. Low, "Optimal decentralized protocol for electric vehicle charging," *IEEE Transactions on Power Systems*, vol. 28, no. 2, pp. 940–951, 2013.

Bibliography

- [128] Y. Mou, H. Xing, Z. Lin, and M. Fu, “Decentralized optimal demand-side management for PHEV charging in a smart grid,” *IEEE Transactions on Smart Grid*, vol. 6, no. 2, pp. 726–736, 2015.
- [129] M. Liu, S. McLoone, S. Studli, R. Middleton, R. Shorten, and J. Braslavs, “On-off based charging strategies for EVs connected to a low voltage distribution network,” *IEEE PES APPEEC*, 2013.
- [130] F. S. Hillier and G. J. Lieberman, *Introduction to Operations Research*. McGraw-Hill, 2010.
- [131] O. E. Gouda, G. M. Amer, and W. A. A. Salem, “Predicting transformer temperature rise and loss of life in the presence of harmonic load currents,” *Ain Shams Engineering Journal*, vol. 3, no. 2, pp. 113–121, 2012.
- [132] D. Susa, M. Lehtonen, and H. Nordman, “Dynamic thermal modelling of power transformers,” *IEEE Transactions on Power Delivery*, vol. 20, no. 1, pp. 197–204, 2005.
- [133] G. Wenzel, M. Negrete-Pincetic, D. E. Olivares, J. MacDonald, and D. S. Callaway, “Real-time charging strategies for an electric vehicle aggregator to provide ancillary services,” *IEEE Transactions on Smart Grid*, vol. 9, no. 5, pp. 5141–5151, 2018.
- [134] J. Quirós-Tortós, L. F. Ochoa, and B. Lees, “A statistical analysis of EV charging behavior in the UK,” in *2015 IEEE PES Innovative Smart Grid Technologies Latin America (ISGT LATAM)*, 2015, pp. 445–449.
- [135] E. L. Karfopoulos and N. D. Hatziargyriou, “A multi-agent system for controlled charging of a large population of electric vehicles,” *IEEE Transactions on Power Systems*, vol. 28, pp. 1196–1204, 2013.
- [136] M. Marinelli, S. Martinenas, K. Knezovic, and P. B. Andersen, “Validating a centralized approach to primary frequency control with series-produced electric vehicles,” *Journal of Energy Storage*, vol. 7, pp. 63–73, 2016.
- [137] K. Knezovic, S. Martinenas, P. B. Andersen, A. Zecchino, and M. Marinelli, “Enhancing the role of electric vehicles in the power grid: field validation of multiple ancillary services,” *IEEE Transactions on Transportation Electrification*, vol. 3, pp. 201–209, 2017.
- [138] R. Rudnik, C. Wang, J. Reyes-Chamorro, Lorenzo Achara, J.-Y. Le Boudec, and M. Paolone, “Real-time control of an electric-vehicle charging station while tracking an aggregated power-setpoint,” *IEEE Trans. on Industry Applications*, vol. 56, no. 5, pp. 5750 – 5761, 2020.

-
- [139] D. Torregrossa, J.-Y. Le Boudec, and M. Paolone, "Model-free computation of ultra-short-term prediction intervals of solar irradiance," *Solar Energy*, vol. 124, pp. 57–67, 2016.
 - [140] D. Goldfarb and I. A., "A numerically stable dual method for solving strictly convex quadratic programs." *Mathematical Programming*, no. 27, pp. 1–33, 1983.
 - [141] IEC 61851-1, "International standard."
 - [142] J.-Y. Le Boudec, *Performance Evaluation of Computer and Communication Systems*. EPFL Press, Lausanne, Switzerland, 2010.
 - [143] R. Kanamori, T. Yoshimura, S. Kawaguchi, and T. Ito, "Evaluation of community-based electric power market with agent-based simulation," in *2013 IEEE/WIC/ACM International Joint Conferences on Web Intelligence (WI) and Intelligent Agent Technologies (IAT)*, vol. 2, 2013, pp. 108–113.
 - [144] R. A. Lopes, J. Martins, D. Aelenei, and C. P. Lima, "Receding horizon control," *Renewable Energy*, vol. 93, pp. 1–13, 2016.
 - [145] P. Richardson, D. Flynn, and A. Keane, "Optimal charging of electric vehicles in low-voltage distribution systems," *IEEE Transactions on Power Systems*, vol. 27, no. 1, pp. 268–279, 2012.
 - [146] F. Erden, M. C. Kisacikoglu, and N. Erdogan, "Adaptive V2G peak shaving and smart charging control for grid integration of PEVs," *Electric Power Components and Systems*, vol. 46, no. 13, pp. 1494–1508, 2018.
 - [147] H. Liu, Z. Hu, Y. Song, J. Wang, and X. Xie, "Vehicle-to-grid control for supplementary frequency regulation considering charging demands," *IEEE Transactions Power Systems*, vol. 30, no. 6, pp. 3110–3119, 2015.
 - [148] C. L. Floch, C. K. Emre, and S. Moura, "PDE modeling and control of electric vehicle fleets for ancillary services: a discrete charging case," *Applied Energy*, vol. 9, no. 2, pp. 573–581, 2018.
 - [149] P. Kou, D. Liang, L. Gao, and F. Gao, "Stochastic coordination of plug-in electric vehicles and wind turbines in microgrid: a model predictive control approach," *IEEE Transactions on Smart Grid*, vol. 7, no. 3, pp. 1537–1551, 2016.
 - [150] M. C. Campi and G. Calafiore, "Decision making in an uncertain environment: the scenario-based optimization approach," *Working paper, Universita di Brescia, Brescia, Italy*, 2004.
 - [151] J. Mattingley, Y. Wang, and S. Boyd, "Receding horizon control," *IEEE Control Systems Magazine*, vol. 31, no. 3, pp. 52–65, 2011.

Bibliography

- [152] M. Wytock, N. Moehle, and S. Boyd, “Dynamic energy management with scenario-based robust MPC,” *American Control Conference (ACC)*, 2017.
- [153] H. Wu, M. Shahidehpour, Z. Li, and W. Tian, “Chance-constrained day-ahead scheduling in stochastic power system operation,” *IEEE Transactions on Power Systems*, vol. 29, no. 4, pp. 1583–1591, 2014.
- [154] R. Gupta, F. Sossan, and M. Paolone, “Grid-aware distributed model predictive control of heterogeneous resources in a distribution network: Theory and experimental validation,” *IEEE Transactions on Energy Conversion*, vol. 36, no. 2, pp. 1392–1402, 2021.
- [155] “Solar radiation data,” <http://www.soda-pro.com/soda-products/ai-forecast>, [Online].
- [156] L. E. Bremermann, M. Matos, J. A. P. Lopes, and M. Rosa, “Electric vehicle models for evaluating the security of supply,” *Electric Power Systems Research*, vol. 111, pp. 32–39, 2014.
- [157] M. Lahariya, D. Benoit, and C. Develder, “Defining a synthetic data generator for realistic electric vehicle charging sessions,” in *Proceedings of the Eleventh ACM International Conference on Future Energy Systems*. Association for Computing Machinery, 2020, pp. 406–407.
- [158] —, “Synthetic data generator for electric vehicle charging sessions: Modeling and evaluation using real-world data,” *Energies*, vol. 13, no. 16, p. 4211, 2020.
- [159] L. Reyes-Chamorro, A. Bernstein, J.-Y. Le Boudec, and M. Paolone, “A composable method for real-time control of active distribution networks with explicit power set points. Part II: Implementation and validation,” *Electric Power Systems Research*, vol. 125, pp. 265–280, 2015.
- [160] J. Snajdr, J. Sedláček, and Z. Vostracký, “Application of a line ampacity model and its use in transmission line operations,” *Journal of Electrical Engineering*, vol. 65, no. 4, pp. 221–227, 2014.
- [161] G. Andersson, P. Donalek, R. Farmer, N. Hatziaargyriou *et al.*, “Causes of the 2003 major grid blackouts in North America and Europe, and recommended means to improve system dynamic performance,” *IEEE Transactions Power Systems*, vol. 20, no. 4, pp. 1922–1928, Nov 2005.
- [162] A. Lucas and S. Chondrogiannis, “Smart Grid Energy Storage Controller for Frequency Regulation and Peak Shaving, Using a Vanadium Redox Flow Battery,” *International Journal of Electrical Power & Energy Systems*, vol. 80, pp. 26–36, 2016.

-
- [163] S. J. Crocker and J. L. Mathieu, "Adaptive State Estimation and Control of Thermostatic Loads for Real-Time Energy Balancing," in *American Control Conference (ACC)*, 2016. IEEE, 2016, pp. 3557–3563.
 - [164] M. Popovic, M. Mohiuddin, D.-C. Tomozei, and J.-Y. Le Boudec, "iPRP – The Parallel Redundancy Protocol for IP Networks: Protocol Design and Operation," *IEEE Transaction on Industrial Informatics*, vol. 12, no. 5, pp. 1842–1854, 2016.
 - [165] E. Piatkowska, L. P. Bayarri, L. A. Garcia, K. Mavrogenou, K. Tsatsakis, M. Sanduleac, and P. Smith, "Enabling Novel Smart Grid Energy Services with the Nobel Grid Architecture," in *2017 IEEE Manchester PowerTech*, June 2017, pp. 1–6.
 - [166] Y. Wu, J. Wei, and B. M. Hodge, "A Distributed Middleware Architecture for Attack-Resilient Communications in Smart Grids," in *2017 IEEE International Conference on Communications (ICC)*, May 2017, pp. 1–7.
 - [167] M. Mohiuddin, W. Saab, S. Bliudze, and J.-Y. Le Boudec, "Axo: Masking Delay Faults in Real-Time Control Systems," in *Industrial Electronics Society, IECON 2016-42nd Annual Conference of the IEEE*. IEEE, 2016, pp. 4933–4940.
 - [168] W. Saab, M. Mohiuddin, S. Bliudze, and J.-Y. Le Boudec, "Quarts: Quick Agreement for Real-Time Control Systems," in *22nd IEEE International Conference on Emerging Technologies And Factory Automation*. IEEE, 2017.
 - [169] M. Bahramipanah, D. Torregrossa, R. Cherkaoui, and M. Paolone, "Enhanced Equivalent Electrical Circuit Model of Lithium-Based Batteries Accounting for Charge Redistribution, State-of-Health, and Temperature Effects," *IEEE Transactions Transportation Electrification*, vol. 3, no. 3, pp. 589–599, 2017.
 - [170] E. Scolari, F. Sossan, and M. Paolone, "Irradiance Prediction Intervals for PV Stochastic Generation in Microgrid Applications," *Solar Energy*, vol. 139, no. Supplement C, pp. 116 – 129, 2016.
 - [171] J. Achara, M. Mohiuddin, W. Saab, R. Rudnik, and J.-Y. Le Boudec, "T-RECS: A Software Testbed for Multi-Agent Real-Time Control of Electric Grids," in *22nd IEEE International Conference on Emerging Technologies And Factory Automation*. IEEE, 2017.

List of Publications

Following is the list of all my publications written as a PhD student at EPFL.

1. **R. Rudnik**, L.E Reyes-Chamorro, J.-Y. Le Boudec, M. Paolone. Combined Grid-Aware Control and Optimal Scheduling of Electric Vehicle Charging Stations with V2G Capabilities, *IEEE Transactions on Smart Grids*, under review.
2. **R. Rudnik**, S. Fahmy, J.-Y. Le Boudec, M. Paolone. Experimental Validation of the Real-Time Control of an Electric-Vehicle Charging Station, *IEEE PowerTech*, 2021 Madrid.
3. **R. Rudnik**, C. Wang, L.E Reyes-Chamorro, J.P. Achara, J.-Y. Le Boudec, M. Paolone. Real-Time Control of an Electric-Vehicle Charging Station While Tracking an Aggregated Power-Setpoint, *IEEE Transactions on Industry Applications*, 2020.
4. L.E. Reyes-Chamorro, W. Saab, **R. Rudnik**, A.M. Kettner, M. Paolone, J.-Y. Le Boudec. Slack Selection for Unintentional Islanding: Practical Validation in a Benchmark Microgrid, *Power Systems Computation Conference (PSCC)*, 2018.
5. W. Saab, **R. Rudnik**, L.E. Reyes-Chamorro, J.-Y. Le Boudec, M. Paolone. Robust Real-Time Control of Power Grids in the Presence of Communication Network Non-Idealities, *IEEE International Conference on Probabilistic Methods Applied to Power Systems (PMAPS)*, 2018 Dublin.
6. J.P. Achara, M.M. Maaz, W. Saab, **R. Rudnik**, J.-Y. Le Boudec. T-RECS: A Software Testbed for Multi-Agent Real-Time Control of Electric Grids, *IEEE International Conference on Emerging Technologies and Factory Automation (ETFA)*, 2017.
7. **R. Rudnik**, J.-Y. Le Boudec, A Bernstein, L. Reyes-Chamorro, M. Paolone. Handling large power steps in real-time microgrid control via explicit power setpoints, *IEEE PowerTech*, 2017 Manchester.
8. K. Christakou, M. Pignati, **R. Rudnik**, S. Sarri, J.-Y. Le Boudec, M. Paolone. Hardware-in-the-Loop validation of the Grid Explicit Congestion Notification mechanism for primary voltage control in Active Distribution Networks, *Power Systems Computation Conference (PSCC)*, 2016 Genoa.

Roman Rudnik

Prilly, Switzerland
☎ +41 78 956 32 69
✉ rudnroma@gmail.com
📄 bit.ly/2Zkrzgo



Work experience

Feb 2016 – **Doctoral Assistant**, *EPFL*, Lausanne, Switzerland.

present ○ Research activities

- Developed a novel real-time charging control mechanism for electric vehicles (EVs). The mechanism enables fair power allocation and minimizing the battery degradation of each EV while following a certain aggregated consumption.
 - Implemented the proposed mechanism in Matlab/C++ and deployed in a real-world setting (a smart grid with EVs and charging station).
 - Proposed several solutions for robust real-time control of electrical grids; implemented in C++; field-deployed these solutions in several smart grids in Switzerland.
 - Proposed a real-time islanding protocol; implemented in C++.
- Teaching activities
- Assisted in TCP/IP Networking, Smart Grid Technologies and Industrial Automation courses.
 - Successfully supervised several student semester projects.

Jun 2015 – **Research Intern**, *EPFL*, Lausanne, Switzerland.

- Jan 2016 ○ Developed a hardware-in-the-loop test platform for the real-time validation of the grid control mechanisms.
- Validated a method for real-time primary voltage control of the active distribution networks.
 - The results were published at the Power System Computational Conference (PSCC) 2016.

May 2013 – **Software Engineer**, *Samsung Research Center*, Moscow, Russia.

- May 2015 As a part of Mobile Software Group, I contributed to mobile development tools and technologies for Samsung's Tizen OS, allowing developers to easily port (convert) applications from iOS to Tizen OS with no additional code.
- Implemented intermediary UI libraries automating the application conversion.
 - Proposed performance and power consumption improvements in mobile applications of Tizen mobile platform (performance improved up to 10%).
 - Performed a regular profiling of the new mobile OS Tizen for searching bottlenecks.

Education

Feb 2016 – **Ecole Polytechnique Fédérale de Lausanne (EPFL)**, Lausanne, Switzerland.

present Computer Communications and Applications Laboratory 2 (LCA2)

PhD in Computer Science & Communication Systems.

Topic: Grid-aware real-time control of electric vehicles.

Supervisor: Prof. Jean-Yves Le Boudec

Sep 2008 – **Lomonosov Moscow State University**, Moscow, Russia.

Jun 2013 Specialist (equivalent to MSc) of Science in Mathematics.

Major: Computational Mathematics, GPA: 4.6 / 5

Thesis topic: The investigation of a difference scheme for non-stationary motion of viscous gas.

Awards

- Basil C. Papadias best paper award - third prize (Powertech, 2021)
- Merit-based scholarship at Moscow State University (2013)

Technical expertise

Languages C/C++ (experienced), Matlab/Simulink (experienced), SQL (basic), Python (basic)
Tools Git, Visual Studio, Eclipse, Xcode, CMake, LaTeX
Miscellaneous TCP/IP, Optimization, Real-time Control

Spoken Languages

English (fluent), Russian (native), French (basic)

Hobbies

Skiing, Hiking, Swimming, Cycling